



Department of Precision and Microsystems Engineering

**Polymer Stencil Printing for
High-Throughput Fabrication of Metamaterials**

C.C.H. Otte

Report no : 2022.024
Coach : dr. ir. M. Tichem
Professor : dr. ir. M. Tichem
Specialisation : Micro and Nano Engineering
Type of report : Master Thesis
Date : July 7, 2022

Polymer Stencil Printing for High-Throughput Fabrication of Metamaterials

by

C.C.H. Otte

to obtain the degree of Master of Science
at the Delft University of Technology,
to be defended publicly on Thursday July 7, 2022 at 12:30 PM.

Student number: 4488407
Project duration: June 6, 2021 – July 7, 2022
Thesis committee: Dr. ir. M. Tichem, TU Delft, supervisor
Dr. ir. J. F. L. Goosen, TU Delft
Dr. A. Hunt, TU Delft
H. M. Bilyalova MSc., TU Delft

An electronic version of this thesis is available at <http://repository.tudelft.nl/>.

Preface

Dear reader,

Before you lies the result of more than a year of hard work which marks the end of an era for me. My time as a student in Delft, starting in 2015, has eventually come to an end. This thesis was sparked by my fascination with all things small. The simplicity that is needed for mechanical engineering at such a scale is where the fun lies for me. The topic of this thesis is therefore a seamless fit to my interest. I did research spanning from reading literature about all the different kinds of metamaterial designs and micrometre-level fabrication techniques that exist, a breakdown of metamaterials to their fundamental elements to experimentally validating the opportunities for stencil printing of polymers.

I want to thank multiple people for helping me throughout this thesis journey. First and foremost, Marcel Tichem for providing me with lots of feedback and insight during our weekly meetings. Guiding me along the way to becoming a truly independent researcher. My beloved Taylor board members for all the fun, banter and (sometimes much-needed) seriousness during our year in the cosy office and beyond. All those coffee breaks at PME together certainly sparked interesting discussions and brought new insights to my work! The PME Lab support staff for brainstorming about my experimental set-ups and all the practical issues that are overlooked by us students. Finally, my roommates, friends and family for enduring me when I couldn't let go of all my thesis thoughts after a hard day's work.

Enjoy!

*C.C.H. Otte
Delft, June 22, 2022*

Abstract

In this thesis report, the potential for high-throughput fabrication of micromechanical metamaterials is studied. Metamaterials are structures typically consisting of repetitive micrometre-sized features that introduce new and extraordinary ‘material’ properties. However, up to now these structures are predominantly fabricated with slow 3D-print fabrication techniques. In this work, a range of micromechanical metamaterial designs are closely studied for their design aspects, alongside an investigation towards the high-throughput opportunities of mechanical contact-based fabrication techniques like nano imprint lithography and micro-transfer moulding. What is missing from current research, is the connection between the design attributes of micromechanical metamaterials and the capabilities of high-throughput micrometre-level fabrication techniques.

Here I show that micromechanical metamaterials can be broken down into geometric elements and eventually elementary material transformations that can be directly linked to fabrication techniques with high-throughput potential. These material transformations can be used to form several fabrication process flows. During this breakdown, stencil printing emerged as a compelling fabrication technique for high-throughput fabrication of thin intricate 2½D features. At this moment little is known about the prospects for stencil printing with polymeric materials because stencil printing has its origins in printed circuit board (PCB) fabrication. By performing experiments on the most influential parameters of ordinary PCB stencil printing found in literature and applying these parameters to polymer stencil printing, an understanding of the operating mechanisms is obtained. It is exhibited that by tweaking parameters such as viscosity, wettability, stencil design and substrate temperature, stencil printing with polymers like polydimethylsiloxane (PDMS) can be transformed from an ill-defined mess to a successful replication of the designed laser-cut stencil. The achieved stencil print shows good replication with a mean line width of 638 µm with a standard deviation of 20.8 µm against a 585 µm line width of the laser-cut stencil. The key to this rewarding transformation is the mixing of polytetrafluoroethylene (PTFE) into the PDMS matrix in a 50/50 wt% mixing ratio.

Contents

List of Figures	IX
List of Tables	XI
1 Introduction	1
1.1 Context	1
1.2 Literature Survey	2
1.2.1 Metamaterials	2
1.2.2 Fabrication Techniques	3
1.3 Research Questions	7
2 Global Fabrication Process for Micromechanical Metamaterials	9
2.1 Test Vehicle	9
2.2 Breakdown of the Metamaterial Test Vehicle Design	10
2.2.1 Generic Metamaterial Features	10
2.2.2 Basic Material Transformations	11
2.2.3 Coupling of Design and Fabrication	12
2.3 Fabrication Process Flow of an Entire Metamaterial.	12
2.4 Stencil Printing: Fabrication Technique with Untapped Potential	15
3 Stencil Printing of Polymeric Structures	17
3.1 Basics of Stencil Printing	17
3.2 Experimental Set-up	17
3.3 Influential Parameters	19
3.3.1 Viscosity	19
3.3.2 Wettability	23
3.3.3 Shear-Thinning & Thixotropy	24
3.3.4 Stencil Design	25
3.3.5 Snap-off Printing.	28
3.3.6 Number of Squeegee Pulls	29
3.3.7 Elasticity of the Substrate	30
3.3.8 Functionalising the Substrate Surface	30
3.4 Successful Polymer Stencil Printing	31
4 Conclusion & Future work	33
4.1 Conclusion	33
4.2 Future Work.	35
A Micromechanical Metamaterial Designs	37
B Initial Prints	41
C Spreading Behaviour	43
D PTFE-PDMS Composite Prints	45
E Viscosity Measurements	49
F Stencil Pictures	55
G Technical Drawings	59
H Matlab Code	71
H.1 Viscosity of PDMS PTFE Mixtures	71
H.2 Temperature Influence	72

H.3 Influence of Snap-off Height and Number of Squeegee Passes	73
H.4 Stencil Geometry	74
Bibliography	77

List of Figures

1.1	DWL techniques: (a) μ SL & (b) 2PP [1].	1
1.2	Division of the mechanical metamaterial classes.	2
1.3	Planar Fabrication techniques	3
1.4	Working principles of discussed planar fabrication techniques	5
2.1	(a) unit cell design of the selected acoustic metamaterial, which consists of a cube (grey) with a big void inside, (b) cut in half top view, (c) cut in half side view. <i>Solidworks</i> CAD drawing based on [2].	10
2.2	Coupling of metamaterial features and material transformations.	13
2.3	Potential generic feature combinations in fabrication process flows.	14
3.1	Stencil print set-up	18
3.2	viscosity characteristics.	20
3.3	Parameters of importance to achieve a high-precision stencil printing process	20
3.4	Spreading behaviour of 5 μ L droplets.	21
3.5	Contact angle	21
3.6	Effect of different PTFE-PDMS mixing ratios [3].	22
3.7	Viscosity measurements of different PDMS-PTFE composites	23
3.8	PTFE-PDMS (50/50wt%) stencil prints with zero snap-off height	23
3.9	Relation between contact angle and bond strength [4].	24
3.10	Viscosity behaviour of PTFE-PDMS mixtures [3]	25
3.11	stencil print deposition characteristics [5]	26
3.12	Amount of solder transfer with respect to aperture orientation [6]	26
3.13	Aperture dimension defined ratios by <i>MATLAB</i>	27
3.14	Test stencils for stencil geometry experiments	28
3.15	Stencil prints with 50/50 wt% PTFE-PDMS composite and in-contact printing	29
3.16	Details of PTFE-PDMS prints with test stencils	30
3.17	PTFE-PDMS composite stencil print with snap-off height	31
3.18	Line width of PTFE-PDMS composite (50/50 wt%)	31
3.19	elasticity of PDMS for different mixing ratios and curing temperatures [7].	31
A.1	Multiple auxetic metamaterials	37
A.2	Octet truss unit cell [8].	38
A.3	metamaterials with bistability.	38
A.4	Acoustic metamaterials.	38
A.5	Pentamode metamaterial	39
A.6	Metamaterial that twists under a compressive load [9].	39
B.1	Initial stencil prints, with a curing temperature of 70 °C	42
C.1	Spreading behaviour of 5 μ L droplets	44
D.1	PTFE-PDMS (50/50wt%) 1 stroke snap off, line width measured	45
D.2	PTFE-PDMS (50/50wt%) 1 stroke no snap off, line width measured	45
D.3	PTFE-PDMS (50/50wt%) multiple strokes snap off, line width measured	45
D.4	Stencil print of test stencil 1	46
D.4	Stencil print of test stencil 1 (cont.)	47
D.5	Stencil print of test stencil 2	47
D.5	Stencil print of test stencil 2 (cont.)	48

E1	Stencil with main design, laser-cut by IWS 3ME	55
E2	First test stencil, laser-cut on <i>Lasea</i> laser-cutter at the PME lab	56
E3	Second test stencil, laser-cut on <i>Lasea</i> laser-cutter at the PME lab	57

List of Tables

2.1	Generic metamaterial features	11
2.2	Basic material transformations and their fabrication techniques	12
3.1	Important parameters for material deposition in stencil printing.	25
A.1	Attributes of the presented metamaterial designs	39
A.2	Attributes of the fabrication techniques	40
E.1	Viscosity measurement data for native PDMS	50
E.2	Viscosity measurement data for 40/60 wt% PTFE-PDMS composite	51
E.3	Viscosity measurement data for 50/50 wt% PTFE-PDMS composite	52
E.4	Viscosity measurement data for 60/40 wt% PTFE-PDMS composite	53

Abbreviations

Abbreviation	Full name
PCB	printed circuit board
PDMS	polydimethylsiloxane
PTFE	polytetrafluoroethylene
DWL	direct write laser lithography
2PP	two-photon polymerisation
μ SL	micro-stereolithography
UV	ultraviolet
NIL	nano imprint lithography
μ TM	micro-transfer molding
MIMIC	micro-moulding in capillaries
μ CP	micro-contact printing
IJP	ink jet printing
WAD	wet-and-drag
CAD	computer aided design
AR	aspect ratio
AAR	area aspect ratio

Introduction

The goal of this chapter is to establish the basis on which this thesis has been conducted. Firstly, the context of this research will be explained in section 1.1, followed by a summary of the literature survey in section 1.2 that was performed to establish the knowledge gap that inspired this thesis. Finally, the goal of this research project is defined in section 1.3 and the questions to be answered in this thesis project will be posed.

1.1. Context

Metamaterials are cleverly designed structures that show extraordinary and unusual properties that are normally not found in naturally occurring materials (meta in Greek means “beyond”) [10]. Originally, metamaterials mainly dealt with electromagnetic properties [11] and consisted of negative index materials, which display a negative refractive index, such as split ring resonators [12], perfect lenses and cloaking devices [13, 14]. More recently the field of metamaterials has expanded to include materials with enhanced mechanical, thermal, electronic, and transport properties [10]. The behaviour of a metamaterial is defined by its unit cell, which is the smallest repetitive element in a structure. Therefore, the unit cell is the most studied part of a metamaterial design.

In mechanical metamaterials, the coordinated behaviour of a system of combined unit cells is similar to a mechanical continuum but exhibits the desired extraordinary functionalities. The unit cells consist of complex high aspect ratio elements to create tailored behaviour such as deformations like folding or rotating elements [10].

Up to now, most metamaterials have been manufactured with additive fabrication techniques. On a micrometre level, this means that direct write laser-lithography (DWL) techniques such as Two-Photon Polymerisation (2PP) and Microstereolithography (μ SL) are used. The two DWL techniques can be seen in Figure 1.1. These two fabrication techniques polymerise a liquid prepolymer through photon absorption with ultraviolet (UV) light [1]. However, fabrication for high-throughput, while keeping high precision, presents a challenge [15].

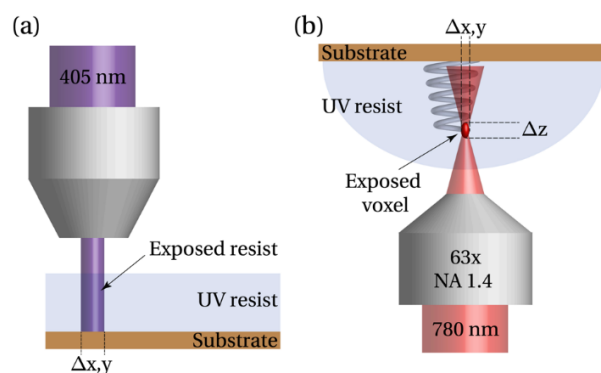


Figure 1.1: DWL techniques: (a) μ SL & (b) 2PP [1].

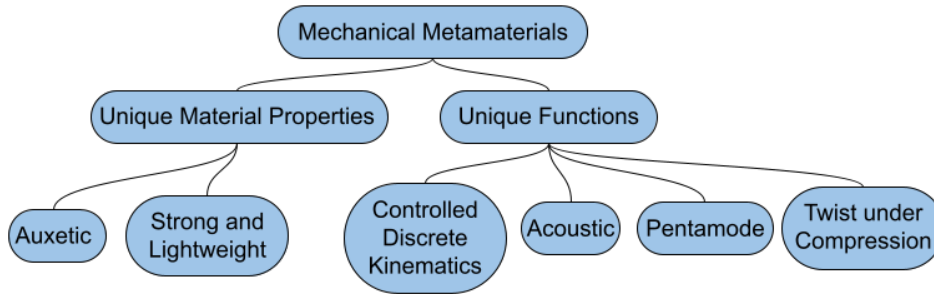


Figure 1.2: Division of the mechanical metamaterial classes.

1.2. Literature Survey

In this section, the main takeaways from the literature survey that was performed at the start of this thesis project [16] will be summarised. Firstly, metamaterials will be discussed in subsection 1.2.1, followed by the potential fabrication techniques for these metamaterials that are addressed in subsection 1.2.2. Several additional fabrication techniques that will be used later in this thesis are introduced here as well.

1.2.1. Metamaterials

This thesis has a specific focus on micromechanical metamaterials, meaning that attention is mostly aimed at metamaterials where the typical minimum feature size is between $1\ \mu\text{m}$ to $1000\ \mu\text{m}$ and the unique properties and functions that these metamaterials bring to the table are all of the mechanical kind. During the literature research, the first step was to get a clear idea of all the different kinds of micromechanical metamaterials that exist. Six different classes of micromechanical metamaterials have been distinguished and can be seen in Figure 1.2.

The first and largest class of mechanical metamaterials are auxetic metamaterials (Figure A.1). These metamaterials have a negative Poisson's ratio, meaning that they will simultaneously elongate in the stretched and non-stretched direction under uni-axial tension [11, 17–23]. The second class is metamaterials which are designed to be extremely stiff while being exceptionally lightweight at the same time (Figure A.2) [8]. Next, the third class of metamaterials shows controlled discrete kinematics (Figure A.3). These metamaterials rely on bistability for their extraordinary properties and can be divided into two branches whose first branch uses bistability to create metamaterials with negative stiffness, which occurs when the elastic moduli are non positive-definite and whose second branch uses bistability to realise snap-through structures so energy can be absorbed via buckling [24–26]. Acoustic metamaterials (Figure A.4) are another class of metamaterials that use a poroelastic microstructure which efficiently dissipates energy through the air flowing in and out of the pores at high frequencies [2]. The next class of metamaterials consists of pentamode materials (Figure A.5) which behave like a fluid, meaning that they do not resist shear and only resist volumetric deformations [19, 22, 23, 27]. Finally, there is a class of metamaterials that will twist under compression (Figure A.6). By careful unit cell design, a compressive force can be turned into a rotating movement [9].

After analysing design examples for each of these six classes of micromechanical metamaterials concerning their fabrication, a list of attributes has been established to define what kind of fabrication process would be suitable to fabricate such micromechanical metamaterials. The list of attributes is as follows:

1. Minimum feature size of the micromechanical metamaterial; small ($<10\ \mu\text{m}$), medium ($10\ \mu\text{m}$ to $100\ \mu\text{m}$) or large ($>100\ \mu\text{m}$)
2. Range of feature sizes present in the metamaterial
3. Multiple identical layers
4. Extruded 2D or 3D features in a layer
5. Usage of one or multiple materials
6. Spatial arrangement of the second material: global or local
7. Typical geometry: truss or plate

8. Variety of the unit cell geometry throughout the metamaterial

A couple of these attributes deserve an extra explanation to make clear what is meant by them. Attribute three deals with the fact whether the metamaterial consists of multiple identical layers and if these layers are equal to each other. Attribute four deals with the design within a layer. Is the design within a layer a 2D geometry that was extruded to a certain height or is it a true 3D design? The final attribute deals with the fact if there is a gradient present in the unit cell throughout the metamaterial. If this list of attributes is applied to the design examples that are found for each of the classes discussed above, each design example has a unique combination of the chosen attributes as can be seen in Table A.1. Therefore, it can be concluded that the attributes are a good measure to search for suitable fabrication techniques.

Apart from these attributes that are useful in distinguishing suitable fabrication techniques, there are multiple design characteristics that the several metamaterial designs have in common. Most designs share the repetitiveness of a unit cell that is present throughout the material and consist of one or multiple identical layers. Another peculiarity of micromechanical metamaterials is the large amount of empty space that is present. Consequently, a planar fabrication technique is promising as a solution to achieve high-throughput fabrication. With this list of attributes formulated, the search for suitable fabrication techniques can get started.

1.2.2. Fabrication Techniques

In this section, a summary will be given about the fabrication techniques for micromechanical metamaterials and what limits their design could pose on the fabrication technique choice. The choice for the best fabrication technique depends on which geometries are combined to form a structure and what the other techniques are in the fabrication process flow. As was concluded in subsection 1.2.1, techniques that work globally and create planar structures show the most potential. The common factor between these several different techniques is the mechanical contact of the stamp or mould with the resin. As a result of this mechanical contact, the resulting structure is 2D or 2½D, i.e. the third dimension does not consist of free-standing features, at best. Here the disadvantage of these kinds of fabrication techniques becomes apparent because true 3D structures are rather difficult to manufacture with contact-based techniques since a mould or stamp has to be in contact with printing material, and in some cases also with the substrate, during fabrication and thus a closed structure cannot be made in a single fabrication step. As was mentioned before, the metamaterial mainly exists out of identical 2D planar layers. Nevertheless, different possibilities exist to create true 3D materials. One way to accomplish this is by stacking multiple 2D layers on top of each other. These layers can be either equal or different to achieve a gradient in one of the parameters of the unit cell. 3D materials can also be obtained in other ways, with post-processing steps or smart design choices.

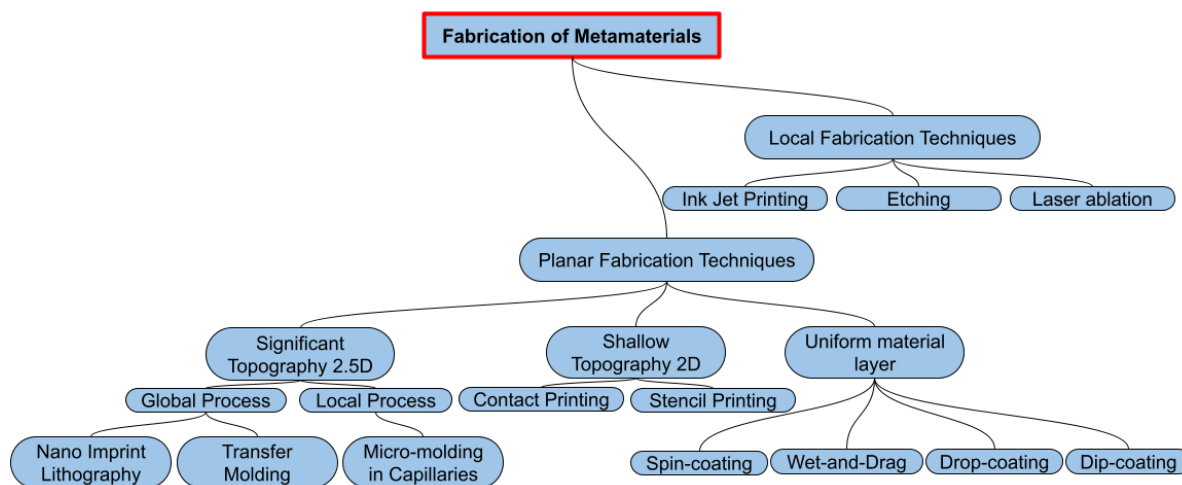


Figure 1.3: Planar Fabrication techniques

Fabrication techniques can be divided into two major groups. Firstly, there is a group of techniques that work with a generic tool that is controlled in a predetermined manner to create the desired structure, like spin-coating and laser ablation or milling at the macro scale. Secondly, there is a group of techniques that work with a design-specific tool. Good examples of this are Nano Imprint Lithography (NIL) and Micro-Transfer Molding (μ TM). In general, this second group of techniques is more accustomed to micrometre-sized structures and therefore this is the area of interest for this thesis research. An overview of the to-be-discussed fabrication techniques can be seen in Figure 1.3. The main focus fabrication techniques are the planar fabrication techniques. These techniques are NIL, μ TM, Micro Moulding In Capillaries (MIMIC) and Micro-Contact Printing (μ CP). The two techniques that show the most potential for high-throughput fabrication of micromechanical metamaterials are NIL and μ TM. In a NIL process, a liquid resist is formed in the desired shape by a stamp after which the resist is cured and polymerised by either ultraviolet (UV) light or elevated temperatures. μ TM applies the liquid resist directly on the mould and performs the polymerisation step there. After polymerisation, the cured structure will be transferred to the desired substrate. MIMIC uses a resist that is pulled into the mould from the side by capillary forces between resist and mould. μ CP inks a stamp with resist which is then transferred to the substrate. More detailed explanations of these four techniques can be found in the literature survey preceding this thesis report [16].

Whether a NIL or μ TM process is a more appropriate technique for a design, is based on the advantages and disadvantages of both techniques. A NIL process works with an uncured liquid resist that is applied to the substrate, after which it is cured and solidified [12, 28]. Hence, building on an already existing structure requires filling all voids with sacrificial material and making sure that the interface between built and sacrificial material is flat enough if NIL is the technique of choice. μ TM however, lets the resist cure in the mould, after which the cured solid structure is transferred to its final destination on the substrate. [29–31]. Such a method makes the sacrificial substrate obsolete but introduces more alignment problems. A second disadvantage of a NIL process is the fact that the working principle of the technique is a squeeze flow of the resist by the mould which necessitates an application of pressure on the mould. This could pose problems with the already built structure as this might be a bit fragile and cannot support a lot of pressure. μ TM has the drawback that the built structure has to be pulled -in this case a specific layer- out of the mould with some kind of adhesive on the substrate, which might pose a challenge if the substrate has rather thin walls. Furthermore, μ TM necessitates alignment after curing which calls for mechanical alignment and creates an interface.

Now that all fabrication techniques are known, the attributes that were formulated in subsection 1.2.1 should be rephrased to be coherent concerning fabrication, as they have originally been formulated in a metamaterial-centred way.

1. Minimum feature size of the fabrication technique;
small ($<10\mu\text{m}$), medium ($10\mu\text{m}$ to $100\mu\text{m}$) or large ($>100\mu\text{m}$)
2. Ability to fabricate a big range of feature sizes
3. Multiple identical layers
4. 2D or 2½D fabrication technique
5. Multiple material fabrication
6. Spatial arrangement of the second material; global or local
7. Subtractive or additive fabrication technique
8. Process or tool fabrication

A couple of these attributes need some further explanation. Attribute four describes whether the fabrication technique can make any significant topography. In other words, is the resulting structure 2D extruded or truly 3D? Attribute five deals with the fact if the technique can work with different materials within a single layer and thus will not look if between layers the material can be switched. The sixth attribute describes how this second material is applied within the layer. Another interesting feature of the fabrication technique is how the resin is transformed into the final structure, which most closely resembles metamaterial design attribute seven. Therefore, attribute seven describes if the material is removed from the substrate or added to the substrate. This is linked to the cost-effectiveness of the fabrication technique. For a beam element, an additive method is a more sensible choice, because it saves material that is in the voids between beam

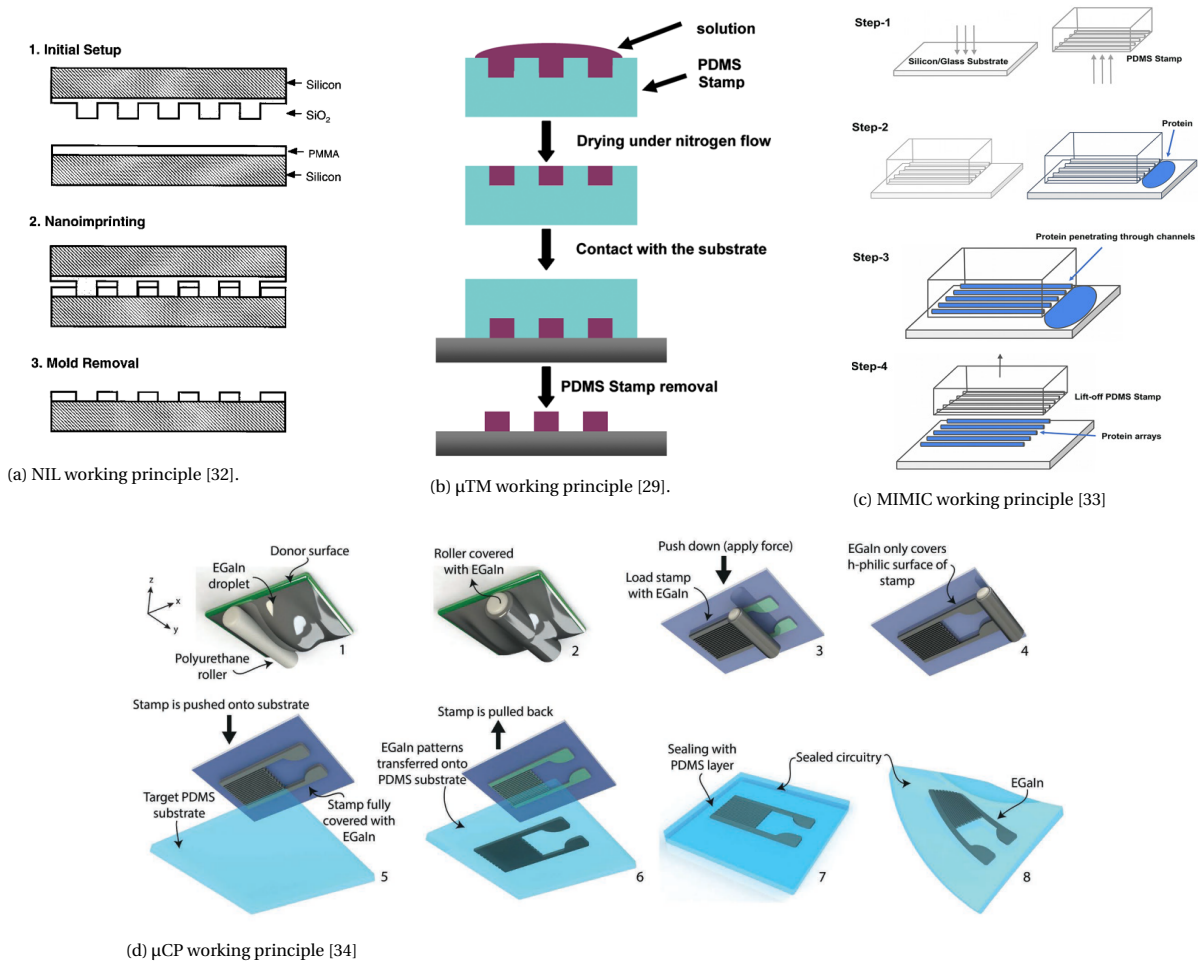


Figure 1.4: Working principles of discussed planar fabrication techniques

elements. The contrary is true if the desired structure consists mostly of plates. The final and eighth attribute details the working principle of the fabrication technique. Does a design-specific tool need to be made or can a more standard tool be used to fabricate different designs? If these attributes are scored against the five main fabrication techniques, the results are as in Table A.2.

This table shows us that the differences between the fabrication techniques seem rather small. These small differences might be enough to place a specific metamaterial design with a preferred fabrication technique. Material choice is not covered by the attributes, even though certain designs could benefit from a particular material that cannot be fabricated with the presented techniques. Bigger differences between techniques can be found in the process as a whole. What kind of pressure and temperature window is needed and what is the process time? These characteristics are difficult to link directly to attributes of a metamaterial design. Finally, as the metamaterials cannot be fabricated in one single step, combinations of techniques should be made. It is thus interesting to research fabrication process flows and see what fabrication techniques can be nicely combined to create an entire metamaterial.

Next to these four main fabrication techniques, other fabrication techniques are evaluated too, because they have supplementary benefits that could create better fabrication process flows for micromechanical metamaterials. Considering that these have not been dealt with yet, a description of these techniques, namely laser ablation, stencil printing, ink jet printing, spin-, drop-, dip-coating, wet-and-drag and etching, will be given here. Laser ablation is mainly performed by a femtosecond pulsed laser that is aimed at a small area, which is subsequently disintegrated. Material choice is important with laser ablation because the heat transmission of the substrate should be as low as possible to make the process accurate [35]. Stencil printing originated with PCB manufacturing. In a stencil print process, the stencil is patterned with the desired design by laser-cutting, electro-forming or chemically etching. Solder paste or another material will be pulled over the stencil and squeezed through the stencil with a squeegee to deposit the designed pattern on the substrate [6, 36, 37]. Due to the usage of a stencil to pattern material, this is more of a 2½D technique. Ink jet printing (IJP) involves direct jetting of ‘ink’ droplets on a substrate that solidify after being dropped in the desired location on the substrate [18, 38]. IJP can be performed in continuous or in drop-on-demand mode. The latter method is more suited for micromechanical metamaterial fabrication due to its smaller drop size and higher placement accuracy [39]. Inks can consist of a range of components such as ceramics and polymers which are predominantly mixed in a watery solvent before fabrication to form a printable suspension. Etching is a subtractive process where material is removed by another externally applied substance that can be a chemical or ions formed in plasma, for isotropic or anisotropic etching respectively. Etching according to a precise design can best be done with anisotropic etching, due to its straight-down removal of material. In the fields of polymers and silicon on the microscale, such as the semiconductor industry, O₂ reactive ion etching is the standard [12, 30, 40–42]. Dip-coating entails the immersing of a substrate into a tank containing the coating material of choice and then slowly removing the substrate from the tank and allowing the coating material to drain off the substrate to form a small layer of coating material [43, 44]. Drop-coating applies a thin layer of a solution drop-wise to the surface of the sample and allows the solvent to evaporate [45]. “Wet-And-Drag” (WAD) is the third novel fabrication technique. In a WAD process, a drop of printing material is placed just outside of the to-be-printed area and dragged at a constant speed with a metal blade. After dragging through the desired area, the prepolymer-A only fills in the channels without any residue. WAD is distinct from other coating methods because the blade in WAD is only to control the macro movement of the prepolymer, filling properties are determined by the properties (e.g. contact angle) of the polymers and substrate, and not by the gap or the speed of the blade [31, 46]. Laminating can be described as transferring the desired structure to a substrate by utilising an adhesive film. Adhesion should be tweaked in such a way that it is strong enough to pick something up but will release when desired mostly under shear forces [47]. Finally, spin-coating needs little introduction, as it is one of the most common fabrication techniques in the micro- and nano-environment. Spin-coating generally works by pouring the coating material on a substrate that is then spun at high rotational speeds to spread the material evenly on the substrate and create thin layers [48].

1.3. Research Questions

As mentioned before, the main goal of this research is to find high-throughput fabrication techniques for micromechanical metamaterials. After the results of the literature survey part of this thesis, as has been summarised in section 1.2, it has become clear that the opportunities to achieve this high-throughput fabrication are certainly there, but have not been explored yet. Knowledge has been gained on what micromechanical metamaterials generally look like and which fabrication techniques have certain possibilities and limitations. A detailed research question can now be formulated for the project part of this thesis. Key to this thesis research is finding the missing link between high-throughput fabrication and micromechanical metamaterials. Boundaries to this goal can already be set to limit the scope and make sure the performed research has a certain coherence with each other and serves the same goal. Important additions to the research question are: The focus on global fabrication techniques, i.e. techniques that can fabricate an entire plane at once, and on the potential for a consecutive process, while the fabrication of these metamaterials with planar fabrication techniques is impossible to achieve in one step. This brings the following detailed research question forward:

“How can repetitive and micromechanical metamaterials be manufactured with a global fabrication process?”

To aid in answering this overarching question, several sub-questions can be defined that will help with identifying the core problems and solving these separately to create a better overview. The first core problem lies within the fabrication techniques. A clear idea is established what the capabilities of each technique are, but it is not straightforward what parts should be fabricated with what technique. This leads to the first sub-question:

1. How can metamaterial designs be broken down into fundamental elements for the global fabrication of planar and repetitive structures?

While seeking answers to this first sub-question, stencil printing stood out as a technique with great potential for fast fabrication of 2½D features, but it is an unknown fabrication technique in the field of polymeric structures on the micrometre level and thereby leading to the second sub-question:

2. What are the most important parameters to get successful replication with stencil printing and how do these parameters influence a successful stencil print replication?

In the following chapters, answers to these questions will be sought.

2

Global Fabrication Process for Micromechanical Metamaterials

In this chapter, a metamaterial design is introduced in section 2.1 as a test vehicle, which will be analysed in detail regarding its fabrication to define a repetitive, precise, and global fabrication process for micromechanical metamaterials. Next, in section 2.2, the design of the test vehicle will be broken down into the basic material transformation steps. Fabrication techniques that match these material transformations will be sought and linked to the respective transformations. This will be followed by an analysis of possible combinations of the introduced fabrication techniques in section 2.3. Finally, in section 2.4 an important missing piece in the high-throughput metamaterial fabrication technique library, stencil printing, will be addressed.

2.1. Test Vehicle

The missing piece in research is the link between metamaterial designs on one side and high-throughput fabrication techniques on the other side. To research this missing piece, a test vehicle should be chosen that acts as a good example for a metamaterial design. The selected design is the so-called acoustic metafoam that is introduced by Lewińska et al. [2, 49] and can be seen in the Computer Aided Design (CAD) drawing of Figure 2.1. The unit cell design consists of a polyurethane cube with small membrane holes on four sides and is strengthened by extra ribs in all of its corners. Suspended halfway on one of the walls is a resonator with an optional added mass on the tip. The purpose of this metamaterial is to attenuate certain noise of specific frequencies in a broadened frequency band. In particular, the low-frequency performance is improved by incorporating the resonator [2]. This metafoam is a good general test vehicle as it has lots of features in its unit cell design that are commonplace for micromechanical metamaterials. The design includes a large amount of empty space, free-hanging features and finally thin slender walls and beams. All three of these features can be found in the example design in Figure 2.1. All material in this design is orientated in one of the three principal directions of the unit cell, meaning that no slanted features have to be created. As this is the first research into the field, the omission of slanted features eliminates one level of complexity, while most planar fabrication techniques are not suited for slanted features, because demolding becomes harder or even impossible depending on orientation, and additional post-processing steps such as thermal reflow or the thermally activated selective topography equilibration process are needed to create slanted features [50, 51].

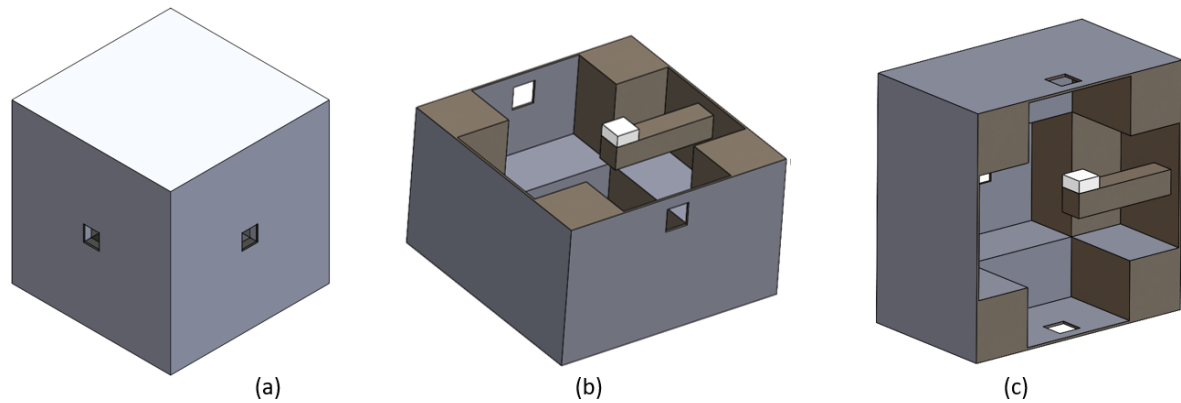


Figure 2.1: (a) unit cell design of the selected acoustic metamaterial, which consists of a cube (grey) with a big void inside, (b) cut in half top view, (c) cut in half side view. *Solidworks* CAD drawing based on [2].

2.2. Breakdown of the Metamaterial Test Vehicle Design

The goal of this section is to break down the test vehicle design in general geometric elements that can be coupled to fabrication techniques and to discover which material transformations with their respective potential fabrication techniques can be identified. These geometric elements should be general enough that they can be used for other metamaterial designs as well. Due to the necessity for physical contact with mechanical fabrication techniques, it is necessary to break up the 3D structures into $2\frac{1}{2}$ D layers that afterwards have to be merged to complete the 3D structure.

First, in subsection 2.2.1 the features that make up this design are addressed. This is followed by an analysis of the material transformations that have to be performed to achieve these discussed features in subsection 2.2.2. At last, these two steps are coupled to unite design and fabrication in subsection 2.2.3.

2.2.1. Generic Metamaterial Features

The unit cell can be built up in several ways by combining different features. Six different feature types are distinguished on basis of the test vehicle and have been described in Table 2.1. The different feature types are: Uniform layer, layer with $2\frac{1}{2}$ D geometry, hole through entire layer, layer filled with (sacrificial substrate) material and layers with global or local thin patches of material. In the first and second columns, an illustration and description of the features can be seen, respectively. The three features on the left side of the table have in common that they are stand-alone features and are established on basis of their geometry. Firstly, “Uniform Layer” consists of a homogeneous layer of material that only has a definable parameter in the thickness dimension. The difference between the features “Hole through entire layer” and “ $2\frac{1}{2}$ D geometry” lies within the fact whether the material can be present at the lowest part of the feature layer. This distinction is rather important and has a big effect on the suitable fabrication techniques, which will be addressed later in this chapter. The third and fourth columns give rise to another three features, but these features are more about interaction with the preceding features and not solely about their geometry. “Sacrificial substrate” entails that a fabricated $2\frac{1}{2}$ D pattern has to be filled and levelled with the most protruding elements of that fabricated pattern. Challenging for this feature is the transition to and cleanliness of preceding features after fabrication. The last two features of this column have in common that they are both thin layers (in comparison with the feature of the left column of Table 2.1), but the third feature is locally applied material, which has its separate challenges.

From a fabrication standpoint, however, these features are still not helpful, because, with the techniques presented in subsection 1.2.2 in mind, they still have to be fabricated in one or more steps depending on the fabrication technique of choice. Hence, a further breakdown is necessary to reach a design level that can be directly related to single fabrication steps. These single fabrication steps will be called material transformation from here on and will be discussed in the next section.

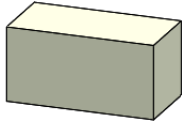
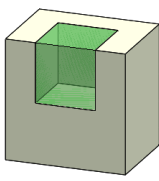
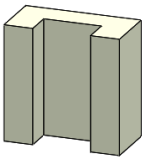
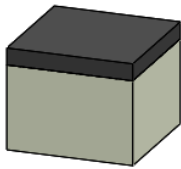
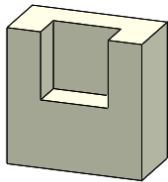
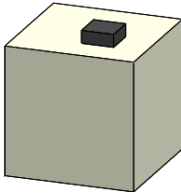
Feature	Name	Feature	Name
	Uniform layer		Sacrificial substrate
	Hole through entire structure		Global second material
	2½D geometry		Local second material

Table 2.1: Generic metamaterial features

2.2.2. Basic Material Transformations

To understand the fabrication of metamaterials, it is important to grasp the smallest elementary material transformation steps that are needed to create a metamaterial. Each of the previously introduced features can be created by one or various combined so-called material transformations. Each material transformation falls into one of the following two, self-explanatory, categories: forming, or removing transformations. The list of material transformations, with the associated technique and category, can be seen in Table 2.2. The first material transformation “Uniform layer” is identical to the feature with the same name that was mentioned in the previous section. “Local addition” entails the deposition of material on defined areas with significant height. “Local removal” is the act of removing material from a specific accurately defined area in a material layer. The fourth transformation “Laminate” contains the act of placing ‘ex situ’ fabricated thin layers on a substrate. “Filling with material” is placing material in an already built rigid layer, meaning that no rigidity of the material is necessary and the main concerns are flatness, transition to the surrounding feature and cleanliness. The final material transformation “Complete removal” means that nothing has to be salvaged and thus can be omnidirectional. The two fabrication techniques for this transformation cannot be used without some material research, because both techniques work with an additional medium that removes the desired material completely. This additional medium should be chosen in such a way that the other materials that are present in the metamaterial are not affected. For etching, wet etching techniques should be used, as these can be selective [52].

All basic transformations can be made with a single fabrication step and thus are the smallest increments in the fabrication process, but each of these transformations can be performed with several fabrication techniques. The choice of a ‘perfect’ fabrication technique for a specific material transformation cannot be made. Which fabrication technique is optimal for a certain material transformation depends on the overall design and the specific feature that the material transformation is part of.

Interesting to note is the clear division between local and global material transformations that is also visible with the associated fabrication techniques, both for forming as well as for removing techniques. Global forming fabrication techniques (i.e. spin-, drop- and dip-coating) add material to the substrate in a non-selective manner, which is great for low complexity and high-throughput. The local fabrication techniques (i.e. NIL, μ TM, μ CP, etc.) deposit material in a specific location, but they introduce a lot of complexity and resulting challenges to the fabrication process. It might therefore be easier to form a uniform layer and pattern local features with a removing fabrication technique. Another remark should be made about laser ablation

Transformation	Fabrication techniques	Category
Uniform layer	<ul style="list-style-type: none"> • Spin-coating • Drop-coating • Dip-coating • Wet-And-Drag 	<ul style="list-style-type: none"> • Forming • Forming • Forming • Forming
Local (2½D) addition	<ul style="list-style-type: none"> • Nano Imprint Lithography • Micro-Transfer Molding • Micro-Contact Printing • Micro-Molding in Capillaries • Stencil Printing 	<ul style="list-style-type: none"> • Forming • Forming • Forming • Forming • Forming
Local removal	<ul style="list-style-type: none"> • Laser Ablation • Reactive Ion Etching 	<ul style="list-style-type: none"> • Removing • Removing
Laminate	<ul style="list-style-type: none"> • Micro-Contact Printing 	<ul style="list-style-type: none"> • Forming
Filling with material	<ul style="list-style-type: none"> • Ink Jet Printing • Spin-coating • Wet-And-Drag 	<ul style="list-style-type: none"> • Forming • Forming • Forming
Complete removal	<ul style="list-style-type: none"> • Isotropic Etching • Dissolve 	<ul style="list-style-type: none"> • Removing • Removing

Table 2.2: Basic material transformations and their fabrication techniques

and IJP specifically, because these two techniques have intrinsic shortcomings concerning high-throughput fabrication. In laser ablation, the laser should be focused on the to-be-removed location. Despite the extremely quick process time of a laser, this still is a sequential process and larger features will thus take more time. Similarly, IJP deposits ink droplets from a nozzle and although set-ups exist with more than a hundred nozzles, the print process remains a step-wise technique.

2.2.3. Coupling of Design and Fabrication

After establishing the material transformations from a fabrication perspective and the generic metamaterial features from a design standpoint, these elements should be coupled together to facilitate metamaterial fabrication and eventually, establish potential process flows. This coupling can be seen in Figure 2.2. Here, each generic metamaterial feature is coupled to the basic material transformations that could make up the feature. The first takeaway from Figure 2.2 is a division in the demand for one or two material transformations for a certain feature. The path with a single material transformation is not by definition preferred over a two-transformation path, as the path option could be faster or more accurate. Figure 2.2 also shows that the preferred fabrication technique is not solely related to what material transformation has to be performed, but has a high dependency on what feature the material transformation is aiming to establish. For a local addition, this is the case, as some of the fabrication techniques are not able to create the “Hole through entire structure” feature in one material transformation because they, for example, leave behind a residual layer like NIL or are more intrinsically height limited than others like μ CP and stencil printing. After all the work in this section, it must be concluded that the fabrication of a geometric element is too much related to surrounding geometric elements to be directly linked to one single fabrication technique for an optimal fabrication of this geometric element.

2.3. Fabrication Process Flow of an Entire Metamaterial

After the breakdown and the coupling of design and fabrication in section 2.2, now it will be studied how to combine these features and material transformations into a complete layer of a metamaterial, in particular the test vehicle design. In Figure 2.3 five of the most promising sequences of features are shown. For each feature, a corresponding material transformation and fabrication technique is presented as well with the surrounding features in mind. Flow one is designed by considering the simplicity of individual steps, as each feature can be done with one material transformation. The second flow focuses on simpler features and less different techniques. For flow three the capabilities of IJP are utilised. For flow four the goal was to use the least amount of fabrication steps and circumvent sacrificial material. Finally, in flow five μ TM is eliminated from the equation to see what kind of flow that creates. These possibilities will be further analysed hereafter.

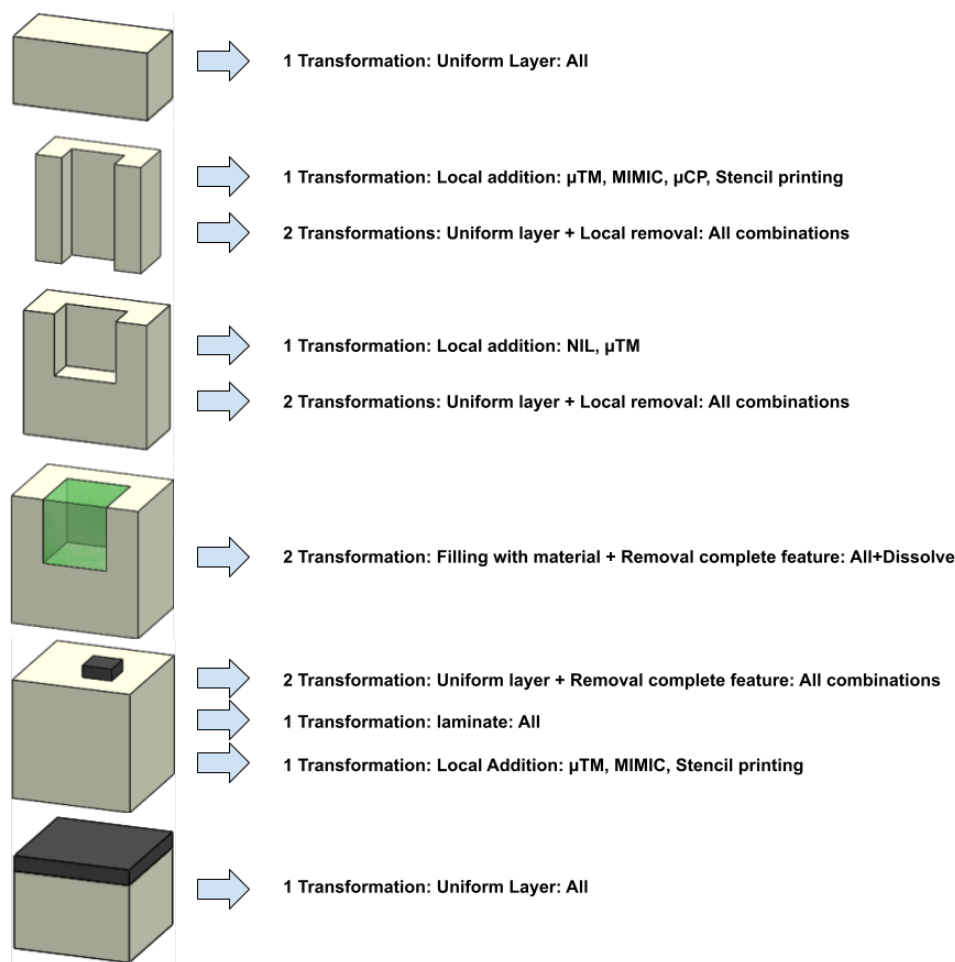


Figure 2.2: Coupling of metamaterial features and material transformations.

The choice for the ‘best’ process flow is not that straightforward and depends on multiple factors. It is desirable to use the least amount of different fabrication techniques possible. With this in mind, the fourth fabrication process flow of Figure 2.3 uses the least amount of features to make up the entire structure. However, the fabrication of overhanging features with μ TM, although possible as seen in literature [53], is rather complex and delicate to fabricate. This is true for every structure but for this design especially because the overhang is halfway down the pockets and spans half the inside distance. This leads to one of the weak points of this process flow analysis, which is the fact that it does not portray the complexity of each fabrication step that is taken. If a step is rather complex or delicate, it might take a long time to produce because great care has to be taken and it might be faster to breakdown the feature into two features with lower complexity. Additionally, a further intricacy is the level of completeness in the fabrication of a feature that has been reached when it is connected to the preceding feature. In other words: is the material transformation done in situ or ex situ? Ex situ fabrication (e.g. μ TM) demands a glueing process between features, while with in situ fabrication the polymerisation takes (sometimes only partly) care of the coupling step between the consecutive material transformations.

Another line of thought could be to use the minimum amount of different fabrication techniques. This means less equipment is used and that the overall complexity of the process is lower. Less equipment is conjointly a cost-saving measure, as manufacturing technologies can be rather expensive, and cuts out cumbersome inter-machine alignment procedures. The complexity reduction is partly due to the fact that the material choice motivation for each fabrication technique can be different because each technique has its demands for the printing material. The minimum amount of techniques possible in Figure 2.3 is two, namely in flow four.

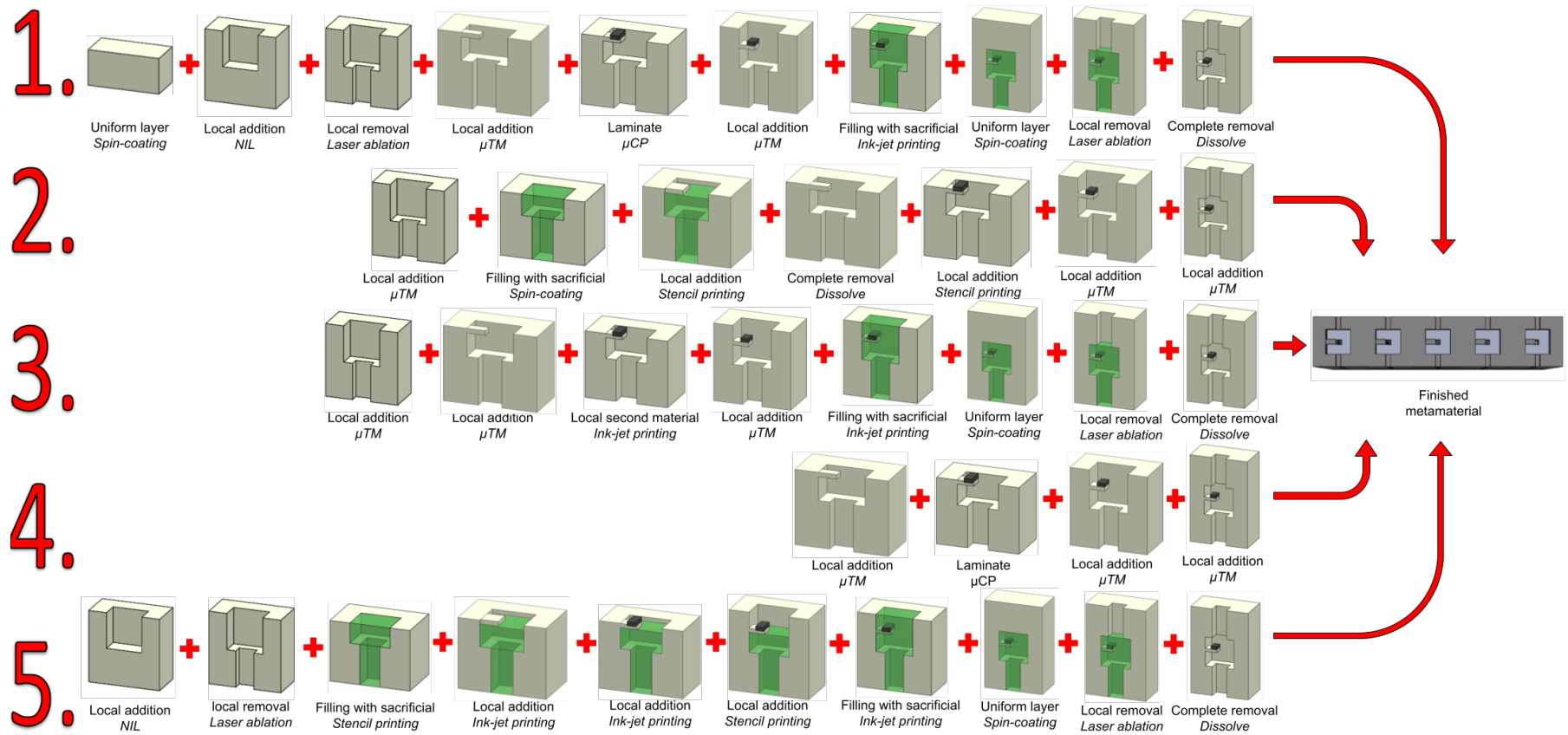


Figure 2.3: Potential generic feature combinations in fabrication process flows.

The introduction of sacrificial material means that three different materials are at least needed for the entire fabrication process. The use of different materials is likely to complicate matters as there is more interaction between different materials. However, using sacrificial material allows the use of more fabrication techniques. Related to this is the desire to fabricate the entire box with the same fabrication technique as this will improve the consistency of the performance because the material is the same everywhere. With two different techniques, the same material may behave differently from feature to feature. Even though the specific material is the same, a different fabrication technique might alter the material, and its behaviour, in a different manner.

Simplicity of each of the individual steps of a fabrication process flow is desirable because defects during fabrication can be minimised and the separate steps will be quicker. A quicker overall process in this way will however be somewhat compensated by the increased number of steps that is needed and the increase in process time that come along with more switching between steps.

A concluding choice for the perfect process is hence too difficult to make, by only listing the pros and cons of each combination of techniques. There is too much interaction between the different steps to make a decision solely based on the characteristics of each fabrication technique.

2.4. Stencil Printing: Fabrication Technique with Untapped Potential

For features that are more of the 2½D and local kind, IJP and stencil printing are the most useful techniques, as has been shown in Figure 2.3. Although they are not capable of creating features with high aspect ratios, they can accurately deposit thin patches of material. Of these two methods, IJP has more history for polymer fabrication. Lots of research has been performed on the IJP of polymeric structures, but has severe limitations with regards to high-throughput fabrication feasibility due to the drop-wise nature of the technique, establishing IJP as a sequential process and making it inadequate to produce an entire material layer at once. Stencil printing, fortunately, does not have this problem, as entire layers can be patterned at once and the limitation lies with the stencil rather than with the material deposition. Stencil printing has its origins in PCB manufacturing and a substantial amount of research has been done to optimise this critical step in the fabrication of integrated circuits [6]. This is unfortunately much less the case for stencil printing of polymers. Therefore, in the next chapter, the possibilities of polymer stencil printing will be studied.

3

Stencil Printing of Polymeric Structures

The presented process flows from section 2.3 predominantly exist of proven fabrication techniques for polymers. However, the stencil printing process has its origins in the PCB fabrication with the patterning of solder paste [6] and is not yet proven for the fabrication of polymeric structures with any significant height. It does however have great high-throughput potential and could even be performed as a continuous process [54]. Therefore, research should be carried out to evaluate the feasibility of fabricating 2½D structures with a stencil printing process.

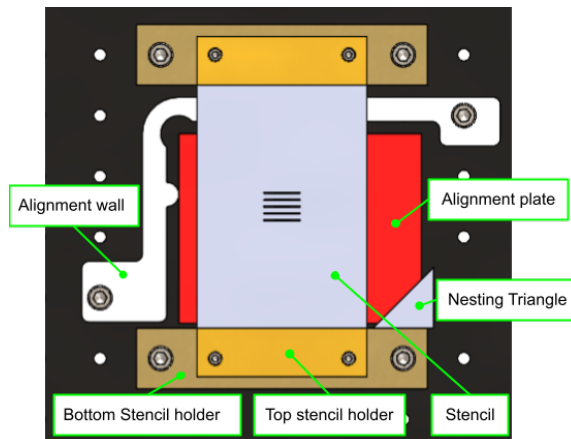
In section 3.1 the working principle of stencil printing is explained. Then, in section 3.2 the set-up which was designed to check the feasibility of stencil printing of polymers is introduced. Next, in section 3.3 influential parameters for a successful polymer stencil print process are first researched in literature, then tested with help of several experiments and finally the corresponding results will be presented and discussed. To conclude this chapter a recap will be given about the achieved result and how it was realised in section 3.4.

3.1. Basics of Stencil Printing

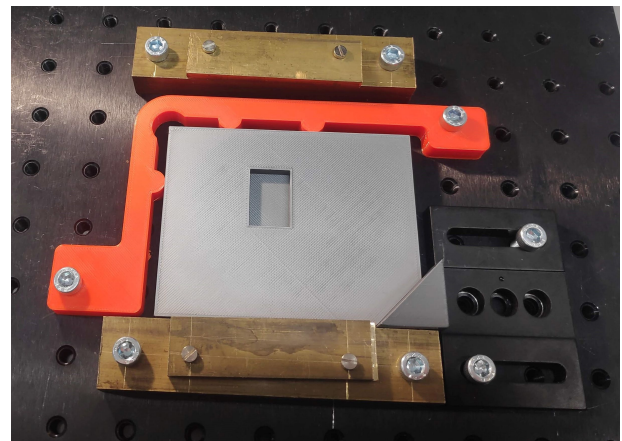
Stencil printing is widely used in the chip industry as the technique of choice to deposit solder paste on a PCB and to connect the electronic circuit to the individual components. A stencil with the desired pattern is positioned directly on (in-contact) or close to the substrate (snap-off). The thickness of the stencil determines the feature height of the printed material. The stencil print process works as follows: A squeegee is moved along the stencil surface, it forces the viscous printing material to roll in front of the squeegee which creates a high-pressure area. This high pressure pushes the printing material through the stencil apertures. The stencil is lifted off after the print stroke is finished and the printing material is left on the substrate [6, 55]. The snap-off height, also called the print gap, the angle of the squeegee blade with respect to the stencil, the pressure exerted by the blade, the speed of the printing and the rheological properties of the printing material are critical parameters to ensure optimal deposition of the printing material onto the bond pads of the integrated circuits. Widely used solder pastes are non-Newtonian materials, showing a decrease in viscosity with increasing shear rates, so-called shear-thinning [55–58]. Shear-thinning is a desirable property for stencil printing because the solder paste will become less viscous due to the applied squeegee pressure and hence allows the paste to flow through the stencil better. After printing it will be at rest on the substrate and viscosity will be restored and therefore enhancing the shape retainment of the deposited paste.

3.2. Experimental Set-up

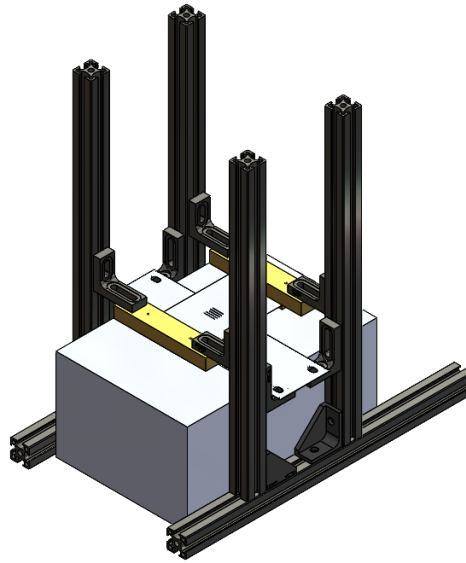
To get a grip on the stencil printing process, experiments were performed to test influential parameters. This was achieved by designing and building a straight-forward stencil printing set-up that can be seen in Figure 3.1. Detailed technical drawings can be found in Appendix G. Alignment of the substrate is fixed in this set-up with respect to the stencil printer to simplify the process. The substrate is placed in or on the alignment plate (red in Figure 3.1a, grey in Figure 3.1b), depending on the chosen substrate. This plate is 3D-printed using an FDM 3D-printer (*Prusa MK3s*) in PLA. The height of the stencil alignment plate is 10 mm, while the stencil is fixed at a height of 15 mm, thereby creating a snap-off height of 5 mm. Planar alignment of the substrate is fixed with the alignment wall (white in Figure 3.1a, orange in Figure 3.1b), which consists of 3



(a) Solidworks design, room temperature substrate.



(b) built design without stencil, room temperature substrate.



(c) Solidworks design, heated substrate

Figure 3.1: Stencil print set-up

contact points. Along with the nesting triangle and bottom stencil holder, this ensures a precisely determined alignment, as per the FACT-method [59]. All parts that make up the stencil printer are labelled in Figure 3.1a.

The stencil is clamped on two sides and is compliant enough to allow the stencil to reach the substrate. Printing with a snap-off height is, therefore, possible as well. The stencil is made of 0.1 mm thick spring steel and is patterned with five apertures that measure 0.5 mm by 15 mm with a spacing of 2.3 mm between them, based on the test vehicle design (Figure 2.1) and fabrication equipment limitations. These dimensions are outside the critical zone for good replication, as will be explained in subsection 3.3.4. The alignment of the stencil to the substrate is done by hand.

As the polymer printing material, PDMS is chosen. PDMS is a versatile and widely used polymeric material in the field of micrometre-level polymeric structures, particularly with microfluidic devices [48, 60] and conformal layers within the moulds for the planar fabrication techniques that are introduced in chapter 1 [61]. The specific PDMS formulation that has been chosen for this research is *Sylgard 184* (The Dow Chemical Company, purchased via *Sigma Aldrich*), due to its good availability in the PME lab and the fact that most of the research found in literature is done with this PDMS variant. *Sylgard 184* is delivered in two separate components, a base elastomer and a curing agent, with an advised mixing ratio of 10:1 by weight. When they are mixed, cross-linking commences immediately [62].

Next to the set-up for printing at room temperature, a second set-up is designed (Figure 3.1c) to print with a heated substrate because the chosen material, *Sylgard 184* PDMS, is a heat-curing polymer. The decision

was made to heat the substrate by incorporating a hot plate (*Stuart US150*) in the set-up instead of designing a separate substrate holder with embedded heating elements. Aside from the parts that were already fabricated for the set-up in Figure 3.1, prefabricated parts from *Thorlabs* are used to heighten the print set-up to allow the hot plate to sit underneath the stencil assembly. Only the substrate holder should be redesigned as the 3D-printed version will not survive the heating. A revised design in metal is seen in Appendix G. This set-up is presented in Figure 3.1c. It was decided that due to time constraints this set-up will not be built in real life, however, the effect of a heated substrate is tested separately in subsection 3.3.1 and proven successful there.

The two designed stencil print set-ups are based on the usage of a heat-curing PDMS polymer, but other polymer curing mechanisms exist as well. UV light can also be employed for polymer curing. As was already discovered during the literature survey [16], UV photopolymers are used extensively with NIL and μ TM. These UV-fabrication techniques are presented as fast-curing alternatives to the heat-curing fabrication techniques [63, 64]. The most obvious challenge that has to be tackled with a UV stencil print set-up is the uniform exposure of the printed material to UV light. Illumination from the top is not possible, due to the print assembly being located there and the presence of uncured print material that has to stay unpolymerised on that side of the stencil. The next possible orientation would be illumination from the sides, but this does not create a satisfactory result as well, because the polymerisation reaction is dependent on film thickness and thus a side illumination would create an uneven cured polymer [65]. Therefore, the only realistic direction for UV illumination is the bottom side. If the polymerisation process is initiated from the bottom, this has multiple limiting implications on the print set-up: The substrate as well as the printing material have to be transparent to enable the UV light to polymerise the entirety of the material. Although the UV-curing is much faster than thermal curing, it still takes at least 1.5 s [66] which might already be too long to prevent spreading enough. All in all, the disadvantages outweigh the advantages and this concept thus was not further developed.

Balancing the curing time is a precarious endeavour that is intrinsic to stencil printing with polymers. To achieve a high throughput, it should be as small as possible, but not that short that polymerisation is already carried too far and curing is completed on top of the stencil before it has been pushed through the stencil and patterned on the desired substrate. If a heated substrate assembly is further developed, this is a big challenge as well. Similarly, while using a heated substrate, the top side should remain cold enough to not speed up the cross-linking process too much in the printing material preprint. Especially with in-contact printing this is a challenge.

3.3. Influential Parameters

With the basic stencil print set-up, as presented in section 3.2, the first prints could be made and are visible in Appendix B. What can be deduced from these first prints is, although parts of the intended design can somewhat be recognised, the need for lots of improvement to the fabrication process before it can accurately replicate polymeric structures and can be used as a good solution for high-throughput fabrication. Potential improvements to obtain accurate replication will be discussed in the next sections of this report. To get a better grasp of the stencil printing process and understand how it can be improved, a literature study has been performed on what parameters are influential in a regular stencil printing process with solder paste for PCB fabrication. These parameters are presented in Figure 3.3 and the most important ones will be described hereafter with the effect they might have on the stencil print process, how their effect can be tested for use in the specific case of stencil printing of polymeric structures and what the result of these experiments is.

3.3.1. Viscosity

Even before the first print was made, it became clear that native uncured PDMS is not viscous enough for use as a printing material for stencil printing of shape-retaining structures. Therefore, literature was investigated for typical PCB solder paste viscosity values. Typical viscosities vary a bit but are on average around 1.5×10^4 Pa·s [6, 55, 56, 58, 68–70]. For the specific PDMS that was used (*Sylgard 184*) the (uncured) viscosity is 3.5 Pa·s [71] at the advised mixing ratio. Even with changing this mixing ratio, the target viscosity will not be reached as the most viscous of the two parts only has a viscosity of 5.1 Pa·s [71]. This is not remotely close enough and a solution should be found to try and get a polymeric printing material with a viscosity that is closer to that of PCB solder paste.

Multiple potential solutions exist to this problem. The first solution could be to increase the viscosity of the PDMS by partial cross-linking [72]. In the papers by Schneider et al. [62] and Helmer et al. [73] it is shown that the viscosity starts to increase instantaneously during the curing process. This curing process can be sped up if it is performed at elevated temperatures [71]. Schneider et al. also showed that the viscosity will

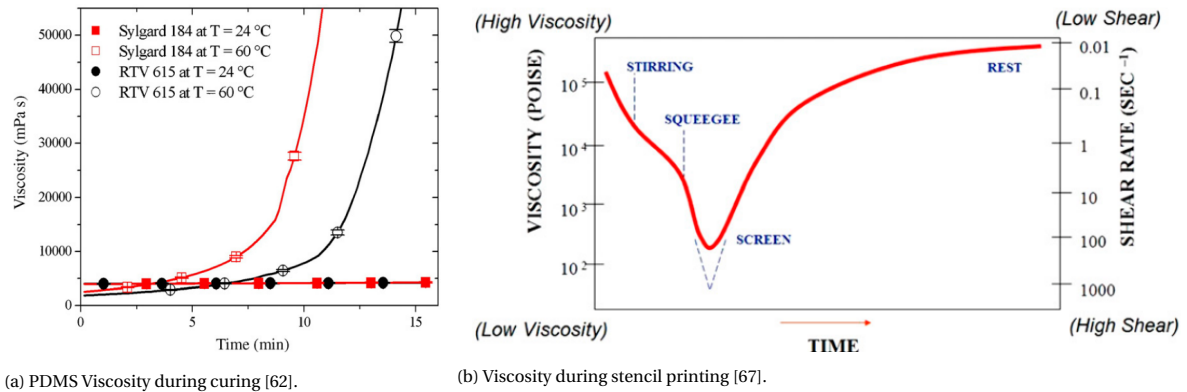


Figure 3.2: viscosity characteristics.

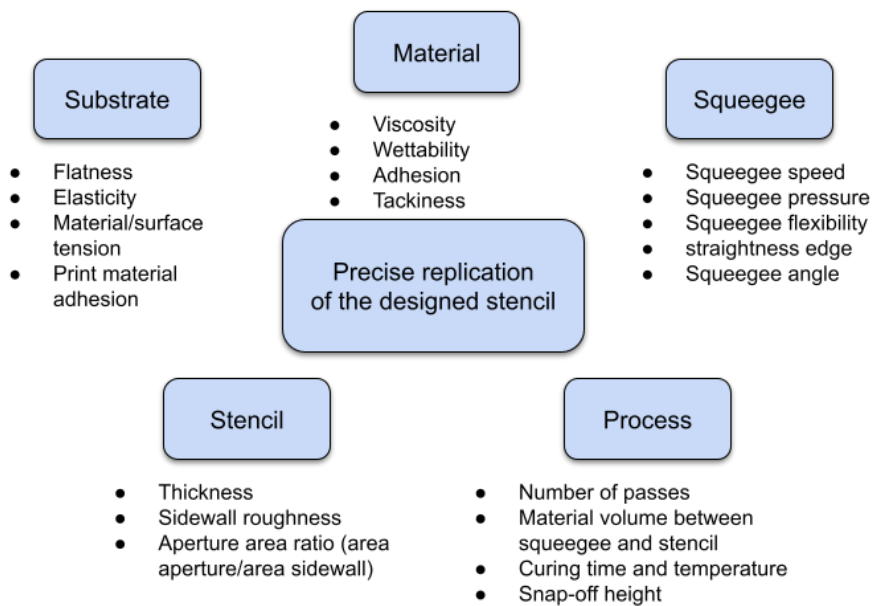


Figure 3.3: Parameters of importance to achieve a high-precision stencil printing process

increase faster with curing at high temperatures, as shown in Figure 3.2a. At room temperature (± 25 °C) fully curing the mixed PDMS will take 48 h, while at a temperature of 150 °C curing for just 10 min is sufficient for complete polymerisation [71]. One could use the fact that this process is gradual to tweak the viscosity of the PDMS by pre-curing it [62, 72]. To check if this is a feasible technique to get shape-retaining PDMS structures, an experiment is performed. By placing the PDMS in the oven at 70 °C with pre-curing times of 2 min to 8 min, it was attempted to increase the viscosity enough to create faithful replications of the stencil. Below 6 min no replication could be made, as the PDMS would just spread to a uniform layer. Above 8 min the cross-linking process has been carried too far to be printable, as the polymer chains want to stick together. The pre-curing time frame of interest lies between 6 min to 8 min. Microscopic pictures were made of these stencil prints with a digital microscope (*Keyence VHX-6000*) and are presented in Figure B.1d-B.1f. As can be seen, the viscosity transition happens in an extremely short time frame. One might be able to stretch this time frame by pre-curing at a lower temperature than the 70 °C that was used. However, this still is not a solution as the PDMS becomes tacky before reaching a viscosity that is high enough to be shape-retaining, as can be seen in Figure B.1f. Therefore, pre-curing is not a satisfactory approach to increase the viscosity of PDMS enough.

The gradually heat-curing property of PDMS polymers could be used in another capacity as well. One of the potential solutions to ensure more shape-retaining stencil printing is to print on a heated substrate. The motivation for this idea is, once again, the fact that the curing time of PDMS is highly dependent on the curing time. It is hypothesised that with a substrate that is at 150 °C the cross-linking reaction will start

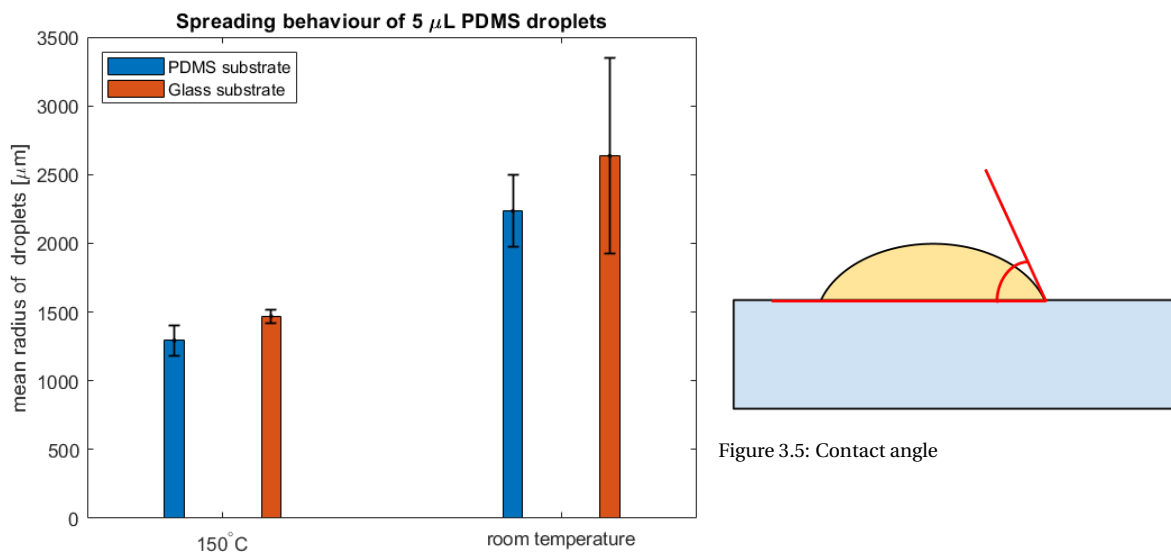


Figure 3.4: Spreading behaviour of 5 µL droplets.

immediately at the interface between substrate and deposited PDMS, thereby hindering the spreading of PDMS by “pinning” the PDMS to the substrate. To test this hypothesis a proof-of-concept experiment was established and performed. In this experiment, small droplets of 5 µL are deposited with a mechanical pipette (*Eppendorf Research plus*) on a glass microscope slide that acts as a flat substrate. This is done with two substrates of which one is heated to 150 °C on a hot plate (*Stuart US150*) while the other substrate is kept at room temperature (25 °C). The PDMS is mixed in a 10:1 ratio of base and curing agent, respectively, and degassed in a desiccator for 3×5 min. With the pipette, the droplets are deposited on the two substrates. The room temperature substrate is then placed in the oven for 1 h to finish the curing. For the droplet on the hot plate, 10 min on the plate is enough to finish the curing process. Now the two different specimens can be analysed with a microscope (*Keyence VHX-6000*) to see the difference in spreading behaviour and whether a “pinning” effect of the PDMS can be seen. This pinning is expected to result in a smaller radius for droplets on a heated substrate. Radii are digitally measured on the microscope and subsequently analysed with a *MATLAB* script (section H.2) to get values for the mean radius and standard deviations

This experiment led to the results as can be seen in Figure 3.4. The microscopic pictures that these measurements are based on can be found in Figure C.1 in Appendix C. The predicted pinning effect can indeed be seen in this graph as the droplet radii at 150 °C are almost half of the radii at room temperature. This means that stencil printing on a heated substrate will indeed lead to better shape retainment.

A third way of increasing PDMS viscosity would be to make a PDMS composite where fillers act as an extra coupling agent between the polymer chains [74]. These fillers could be fumed silica [75], carbon nanotubes [76, 77], polytetrafluoroethylene (PTFE) [3], poly ether ether ketone [78] or even PDMS microbeads [79]. While the exact composition of the used PDMS (*Sylgard 184*) compound is not disclosed by the manufacturer, it is reported in literature that silica is added in the PDMS formulation to act as filler [61]. Therefore, the most logical step to increase the viscosity of the PDMS with fillers would be to simply increase the weight percentage of silica present in the PDMS base elastomer. In literature, this is a quite common technique to increase the viscosity of PDMS [74, 75, 77, 80]. However, this introduces new complexities as PDMS is hydrophobic and silica is hydrophilic [77]. A silanisation procedure should be performed to make silica hydrophobic as well and establish a good PDMS-silica composite. This could take up to 12 hours to 48 hours [81–84].

Based on research by Zheng et al. [3] PTFE was chosen as a more suitable viscosity enhancer for the uncured PDMS because PTFE is already hydrophobic and will better mix into the PDMS matrix. With a PTFE to PDMS mixing ratio of 1:1 by weight, the viscosity should be about 1×10^4 Pa·s [3], which is close to the desired value of 1.5×10^4 Pa·s. The size of the particles that will be used is 1 µm instead of the 5 µm of Zheng et al. The smaller the particles, the more effective they will be as viscosity enhancers [85]. However, the minimum particle size allowed in the PME laboratory is 100 nm. PTFE particles of 1 µm thus are the best fit both in availability and compatibility. For this research, the PTFE particles were acquired from *Sigma Aldrich* (1 µm free-flowing particles, art.-nr. 430935). As can be seen in Figure 3.6 the printability of the PTFE-

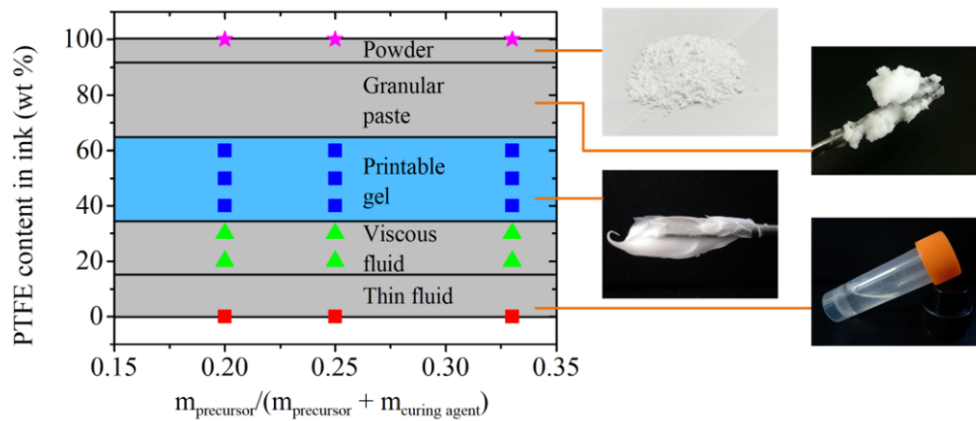


Figure 3.6: Effect of different PTFE-PDMS mixing ratios [3].

PDMS composite is independent of PDMS base to curing agent mixing ratio and only depends on the PTFE content. The area of interest for stencil print application lies between 40 and 60 wt% PTFE in the composite as can be seen in Figure 3.6. PTFE-PDMS composites are prepared by first hand-mixing the PDMS base elastomer with the PTFE powder at specific weight percentages. Next, the PDMS curing agent is added to the mixture in a 10:1 ratio to the base elastomer. Four different mixtures (0, 40, 50, 60 wt% PTFE to PDMS) are measured on a Rheometer (*Anton Paar MCR302*) with a parallel plate set-up. A flat plate of 25 mm in diameter is used with a measuring gap of 1 mm at a constant temperature of 25 °C. The measurements are performed with increasing and decreasing shear rates ranging from 10^{-2} Hz to 10^2 Hz, as shear thinning and thixotropic effects are expected (which will be explained further in subsection 3.3.3). *MATLAB* (section H.1) is used to evaluate these measurements and create a logarithmic plot of the viscosity values. The mix ratio choice is justified by the expected viscosity values of the mixture based on literature as the 50/50wt% mix is at the desired viscosity level.

The result of the viscosity measurements on the rheometer can be seen in Figure 3.7. Native *Sylgard 184* PDMS indeed shows a Newtonian viscosity of $3.5 \text{ Pa} \cdot \text{s}$ and with an increase of PTFE content the viscosity rises, as expected, to $1 \times 10^4 \text{ Pa} \cdot \text{s}$ at low shear rates. If a stencil print is performed with the PTFE-PDMS composite in this mixing ratio, the printing result is excellent as is visible in Figure 3.8. Lines are properly straight and are on average $683 \mu\text{m}$ wide with a standard deviation of $20.8 \mu\text{m}$ only. It should be noted that the laser-cut stencil apertures are bigger than intended in the design, at $500 \mu\text{m}$, with an aperture width of $585 \mu\text{m}$ (see Figure F.1c).

Finally, two techniques to increase PDMS viscosity that looked promising have been researched but were later discarded because of separate reasons. Firstly, the viscosity could be increased by choosing a PDMS variant with higher viscosity, such as *Sylgard 186*. However, with a viscosity of the base part of $123.8 \text{ Pa} \cdot \text{s}$ [86], this still is nowhere in the neighbourhood of the desired viscosity of $1.5 \times 10^4 \text{ Pa} \cdot \text{s}$ and thus this path was not further investigated. Secondly, infrared heating is a possible solution to speed up the curing process [87]. However, this would involve significant work to incorporate into the print set-up and face the same drawbacks as a UV-printing set-up mentioned in section 3.2.

All in all, two good solutions exist to increase the viscosity of *Sylgard 184* PDMS enough to establish a polymeric material which has sufficient shape-retaining ability and is, therefore, suitable for stencil printing.

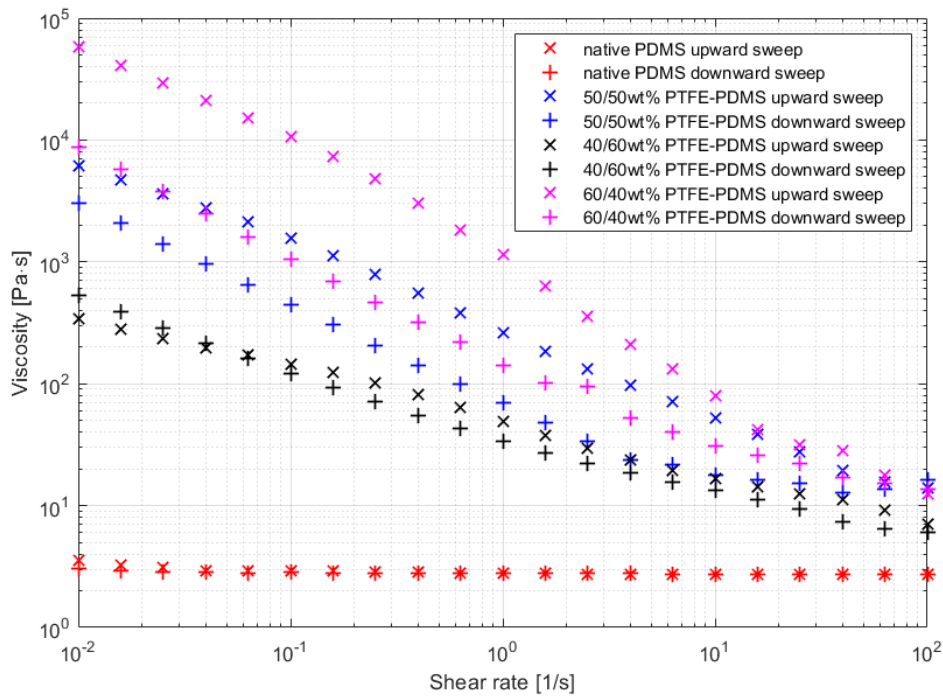


Figure 3.7: Viscosity measurements of different PDMS-PTFE composites

3.3.2. Wettability

Spreading of liquid on a substrate is also affected by the surface energy between the two materials. This so-called wettability is commonly measured with help of the contact angle that is defined, as can be seen in Figure 3.5. The contact angle is an equilibrium between three different surface tensions at the solid-liquid, solid-gas, and gas-liquid interfaces [88]. For a droplet of PDMS on an untreated fully cured PDMS substrate, the contact angle is 109°, while on a glass substrate the same PDMS droplet has a contact angle of 20° [4]. With an equal droplet volume, a higher contact angle means that there is less spreading because the liquid material wants to stay together more. This will result in more height in the printed layer and thus more shape-retaining capability in the stencil print process. Hence, it is expected that a droplet on a PDMS substrate has a smaller radius than on glass with the same material volume.

In an experiment that is analogous to the ‘heated substrate’ experiment from above, 5 μ L droplets of PDMS are deposited on two different substrates, namely a flat layer of fully cured PDMS and again a glass micro-

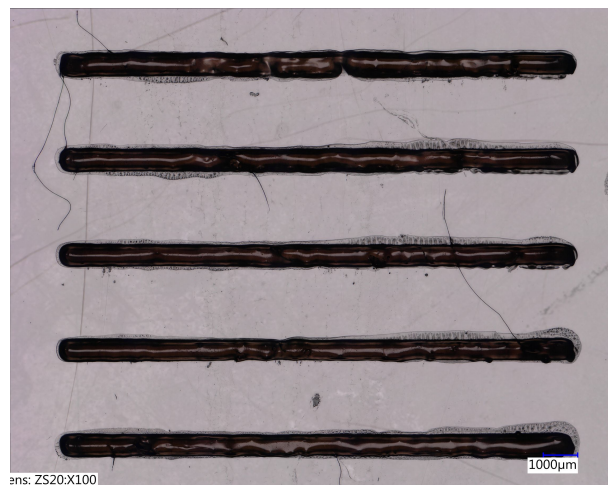
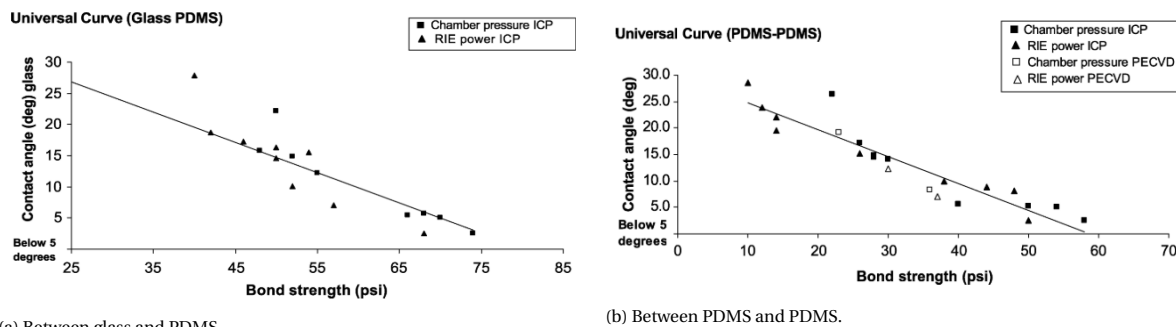


Figure 3.8: PTFE-PDMS (50/50wt%) stencil prints with zero snap-off height



(a) Between glass and PDMS.

(b) Between PDMS and PDMS.

Figure 3.9: Relation between contact angle and bond strength [4].

scope slide. Next, the radii of the droplets are measured with the digital microscope and analysed with help of the *MATLAB* script of section H.2. Results of this experiment can once more be found in Figure 3.4. The hypothesis that was just stated is indeed proven to be correct. The mean radius of a droplet on a PDMS substrate is smaller than on a glass substrate. The main takeaway from this experiment is that substrate choice should be done carefully. For stencil printing PDMS on PDMS, this is a promising result as it means that stencil printed structures will not spread a great deal and have good shape-retainment. However, extra care should be given to the inter-layer bonding, as a supplementary effect that a higher contact angle has, concerns the bonding strength between substrate and liquid printing material. With a higher contact angle, spreading can be limited and feature height will be more in line with stencil thickness as is intended. However, increasing the contact angle hurts the layer-to-layer bonding strength, which can be clearly seen in Figure 3.9 for the PDMS-PDMS and PDMS-glass deposition cases. Higher contact angles can also be gained with the help of surface modification such as coatings and plasma treatments, but the increased contact angle will fade again with time [89].

3.3.3. Shear-Thinning & Thixotropy

Shear-thinning is a phenomenon which occurs in some non-Newtonian fluids. Non-Newtonian fluids have a non-constant viscosity under applied shear and exist in two variants; shear-thickening and shear-thinning. For regular PCB fabrication shear thinning is an exceptionally useful material property, but native PDMS is just a Newtonian fluid [58, 70, 80], as was already shown in Figure 3.7. Shear-thinning entails that with increasing shear applied to a material the viscosity will reduce. This effect is especially interesting for stencil printing because there is the need to combine high and low viscosity effects in different stages of the printing process as can be seen in Figure 3.2b. During printing itself, hence when shear is applied to the material, a low viscosity is favourable, because the printing material will have to be pushed through the stencil. However, after this printing step, a high viscous material is preferable to assure that the material remains in the as-designed pattern and does not spread, which would create a loss of feature height [55, 67, 69, 90]. Thixotropy is an additional rheologic property on top of shear thinning and entails that the viscosity of your fluid is not only dependent on the applied shear but also on the previously applied shear. If, for example, a constant shear is applied, the viscosity will still drop over time. Hysteresis is hence present in the printing material during a printing operation. Therefore, extra care should be taken when using such a material in a printing process. Standard PDMS is a Newtonian fluid, meaning that the viscosity is independent of the applied shear, but if particles are introduced into the PDMS matrix shear-thinning and thixotropic effects can be expected [76–78, 80, 91]. The PTFE-PDMS composite that was introduced in subsection 3.3.1 has this added benefit and shear thinning behaviour should be expected during stencil printing [3]. Predicted viscosity behaviour can be seen in Figure 3.10.

To check if the chosen PTFE particles are behaving as promised and show the predicted viscosity behaviour, the rheometer measurements of subsection 3.3.1 should be inspected more closely. Shear-thinning behaviour should be tested over a range of shear rates. The chosen range is 10^{-2} s^{-1} to 10^2 s^{-1} because Zheng et al. [3] take this range in their work that motivated the choice of PTFE particles as a viscosity enhancer and such a shear rate range is also typical for PCB stencil print processes [55]. Once again looking at the generated graph of Figure 3.7, the downward sloping lines with an increased shear rate of all mixtures indicate that the PTFE-PDMS composites are indeed shear thinning. In addition to shear thinning, thixotropic effects can be seen as well. As expected for a thixotropic fluid with a first upward and then downward shear rate sweep, the

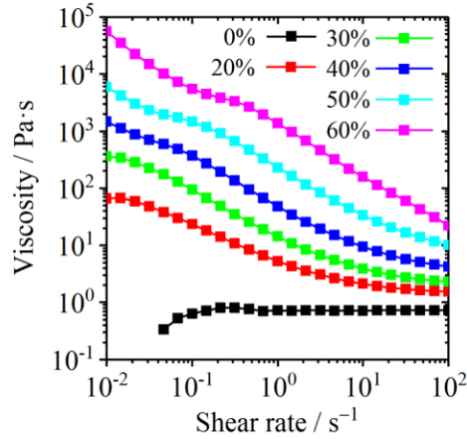


Figure 3.10: Viscosity behaviour of PTFE-PDMS mixtures [3]

viscosity is lower when the shear rate descends from 10^2 s^{-1} to 10^{-2} s^{-1} . This can be explained by the fact that thixotropy means that the shear rate history affects the viscosity values and thus the values will be lower if the material is exposed to shear longer. Hysteresis will increase with rising PTFE content in the composite. Even to such a degree that the downward sweep of the 60/40wt% mix has lower viscosity values than the upward sweep of the 50/50wt% mix.

3.3.4. Stencil Design

Naturally, one of the most important aspects for accurate stencil print replication is the design of the stencil itself. The amount of material that is deposited is a balance between on one hand the pulling forces of the printing material and substrate due to material tackiness and on the other hand the drag forces between stencil aperture walls and printing material caused by adhesion [5], as can be seen in Figure 3.11. Two ratios can be formulated to quantify this equilibrium, namely the aspect ratio (AR) and area aspect ratio (AAR), with the equations as in Equation 3.1 and Equation 3.2 [5] and important parameters as defined in Table 3.1. The first ratio is defined as the correlation between the width of the apertures divided by the thickness of the stencil and is only defined for rectangular apertures. The latter is the relationship between the size of the aperture and the inside wall area of the aperture. Experiments in literature have shown that in PCB fabrication optimal values for these ratios are at least 0.6 for the AAR and 1.5 for the AR [5, 6, 57, 92]. These two ratios can also be combined into one final ratio: The R-Ratio. This ratio is presented in Equation 3.3 and gives a balance between the average drag force and the average pulling force of a certain stencil aperture. A lower R-value will yield better printing results [5].

Quantity	Name	Unit
W	width	m
L	length	m
t	stencil thickness	m
r	radius circular aperture	m
η	velocity liquid component solder paste	m/s
v	particle velocity parallel to stencil wall	m/s
a	particle radius	m
h	gap between particle and wall	m
A_{PAD}	surface area of aperture	m^2
A_{WALL}	surface area of inside aperture wall	m^2
F_D	drag force of aperture wall on printing material	N
F_P	pulling force between substrate and printing material	N

Table 3.1: Important parameters for material deposition in stencil printing.

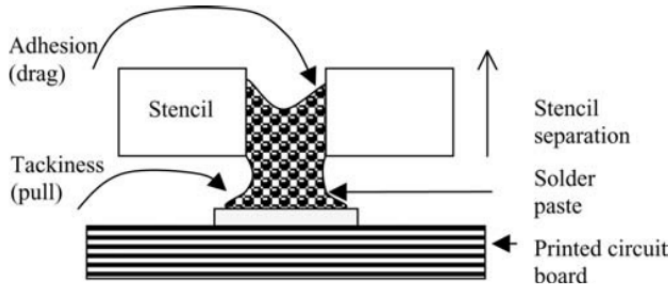


Figure 3.11: stencil print deposition characteristics [5]

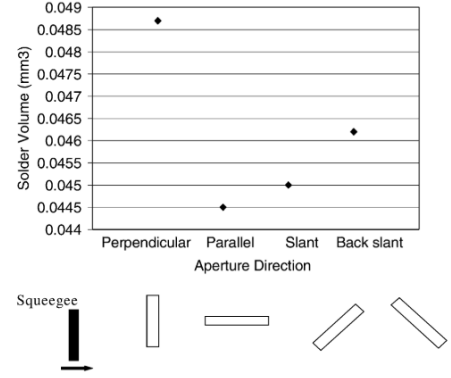


Figure 3.12: Amount of solder transfer with respect to aperture orientation [6]

$$A_1 = \text{Aspect ratio} = \frac{\text{Aperture Width}}{\text{Stencil Thickness}} = \frac{W}{t} \quad (3.1)$$

$$A_2 = \text{Area Aspect Ratio} = \frac{A_{\text{PAD}}}{A_{\text{WALL}}} \quad (3.2a)$$

$$\text{For a rectangular aperture: } A_2 = \frac{L \times W}{2 \times t \times (L + W)} \quad (3.2b)$$

$$\text{For a circular aperture: } A_2 = \frac{\pi \times r^2}{2 \times t \times \pi \times r} = \frac{r}{2 \times t} \quad (3.2c)$$

$$R = \frac{A_{\text{WALL}} \times F_D}{A_{\text{PAD}} \times F_P} = \frac{A_{\text{WALL}} \times 6\pi\eta v a \frac{1}{2} \ln\left(\frac{a}{h}\right)}{A_{\text{PAD}} \times 6\pi\eta v a \frac{a}{h}} \approx \frac{A_{\text{WALL}} \times 0.67}{A_{\text{PAD}} \times 3.92} \quad (3.3)$$

In MATLAB (section H.4) these ratios are applied to the test case of this thesis research. If, for example, an aperture length of 5 mm and a stencil thickness of 0.1 mm are chosen, the minimal widths to reach the minimum levels of AR and AAR as specified are calculated to be 0.32 mm and 0.06 mm respectively. To get a better idea of the workable area for a polymer printing process, all four ratios are parameterised with a constant stencil thickness of 0.1 mm in MATLAB with an input range of 0.05 mm to 1 mm for both length and width of the apertures, which results in the four graphs of Figure 3.13. The red planes symbolise the minimal optimal values of the AR and AAR that were introduced before. Everything above these planes should be perfectly printable. Figure 3.13d shows that printability has asymptotic behaviour. Above 0.2 mm for both W and L good printability should be assured, based on the R ratio. As far as the AR is concerned, the length of an aperture does not influence the print performance. This is seen clearly in Figure 3.13a and logical if Equation 3.1 is studied, as the aperture length does not appear in this formula. The AAR does have a two-parameter dependence on L and W . Thanks to the fact that A_{PAD} and A_{WALL} do not scale in the same manner with regard to L and W this leads to a more interesting relation as shown in Figure 3.13b. However, above widths and lengths of ~ 0.15 mm to 0.2 mm, all should be well. For circular apertures Equation 3.2c does define an AAR as well, which can be seen in Figure 3.13c.

Two other stencil geometry factors also influence the printing performance. The first factor of influence is the orientation of slots with respect to the direction of travel of the squeegee. Pan et al. [6] (Figure 3.12) did research into this orientation and found that aligning the aperture perpendicular to the squeegee direction of travel yields the highest material deposition volume. Perpendicular in this case means that the smallest dimension of the aperture is aligned with the printing direction. This is a well-known experimental phenomenon, but a theoretical explanation is lacking. The second factor of influence is the pitch which describes the distance between two successive apertures. If the pitch is chosen too small "bridging" will occur and the depositions of the two apertures will be connected after printing. The minimal allowed pitch is dependent on the printing material of choice [93].

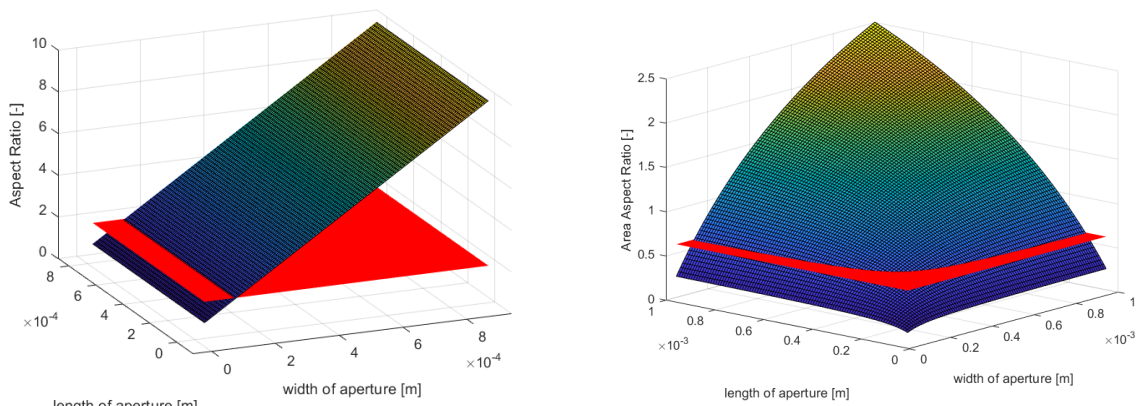
To test all these literature findings about stencil geometry and to see whether the effect of these parameters is the same with polymer stencil printing, two stencils are specifically designed and fabricated to test this. The designs can be seen in Figure 3.14 and the dimensions are given in the technical drawings in Appendix G. The stencils are cut on the *Lasea* laser-cutter in the PME lab and microscopic pictures can be seen

in Appendix F. The smallest holes have not been cut through entirely, and therefore should not be expected in the stencil print. Printing is done without snap-off height and with one squeegee pull.

Figure 3.15 shows the resulting prints with these stencils. Interestingly, the minimum optimal ratio does not hold for rectangular slots, as with a slot length of 5 mm, the 0.1 mm, 0.2 mm and 0.3 mm wide slots should not be transferred correctly, but Figure 3.16a shows that these lines have been printed perfectly fine. However, if the prints of stencil 2 are investigated closely, it becomes clear that square apertures become circular (e.g. Figure 3.16b, when the dimensions become smaller. Hence, no good transfer is achieved. This is a gradual process, but it becomes significant between 0.2 mm and 0.3 mm. This latter tipping point is in line with the AAR as visualised in Figure 3.13b. For a circular aperture, the tipping point should be between 0.1 mm and 0.2 mm, yet the 0.2 mm aperture has already failed in contrast to what Figure 3.13c suggests. Pan et al. [6] have mentioned a circular variant of the AAR, although no mention of the AR is present. This might be the cause of the failure.

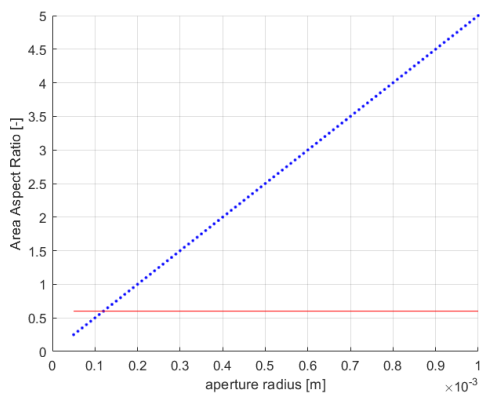
As was suggested by Pan et al. [6], it is hypothesised that perpendicular slots yield better printing results than parallel printing. In the case of this thesis, the prints as seen in Figure 3.15a do not show a significant difference in comparison to the printed dimensions. It does look like the perpendicular slots create a bit cleaner print, while the parallel slots have more of the thin film bordering the printed lines.

All in all, it can be concluded that the ratios of Equations 3.1-3.3 do give a bit of a clue about the performance of polymer stencil printing, but are less effective than when they are used in their regular PCB solder paste stencil printing application. Partially, this might be due to a different particle size in the PTFE-PDMS suspension in comparison to standard solder paste and the different task of the particles in the suspension. In solder pastes the particles act as the main binding material between components and the integrated circuit. The flux medium only acts as a transportation medium that facilitates the printing and no chemical interaction is present [69]. Within the PTFE-PDMS composite, the PTFE particles interact with the liquid PDMS and

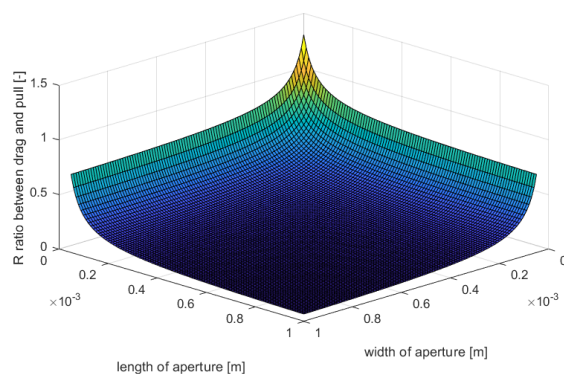


(a) Aspect Ratio, in red the optimal minimum value

(b) Area Aspect Ratio, in red the optimal minimum value



(c) Area Aspect Ratio for circular aperture, in red the optimal minimum value



(d) R ratio

Figure 3.13: Aperture dimension defined ratios by MATLAB

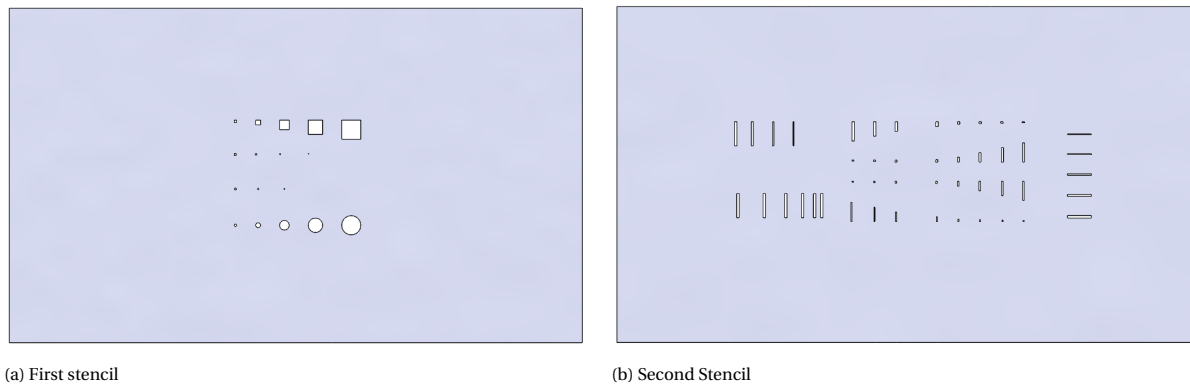


Figure 3.14: Test stencils for stencil geometry experiments

act as the connecting elements between individual polymer chains. Besides this particle interaction difference, the solidification of the print material is based on two different working principles for solder pastes and heat-curing polymers like PDMS. The former becomes solid by evaporation of the liquid flux medium that carries the desired metallic particles at elevated temperatures in a reflow oven [57, 68, 92]. The latter solidifies by polymer cross-linking, which is a gradual process that starts as soon as the PDMS base elastomer and the curing agent are mixed [62]. This solidification difference could partially be the reason for the dissimilar printing performance of polymer stencil printing.

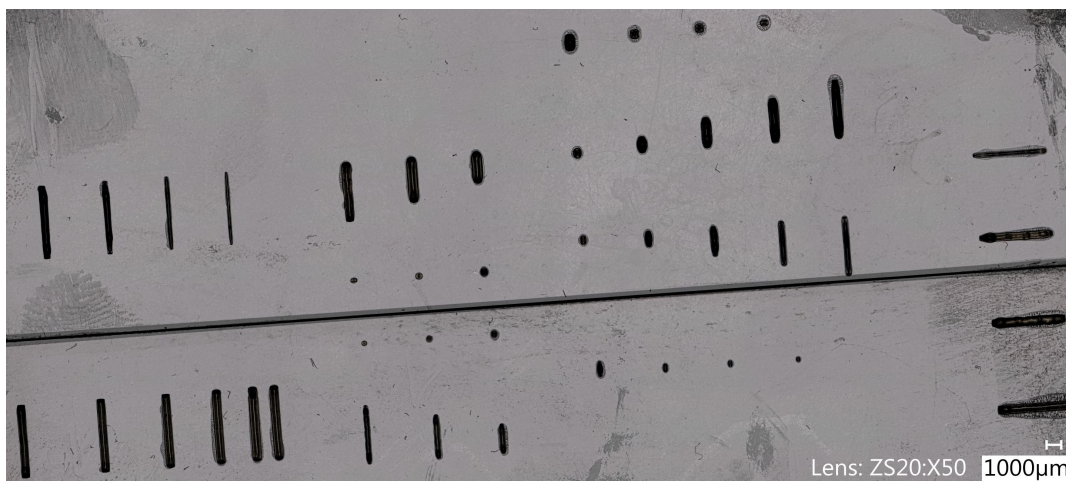
Figure 3.16c is an attempt to test the limits of the pitch in polymer stencil printing. However, as can be seen, no bridging is occurring. In literature, no quantifiable ratio or limit, that depends on the other relevant dimensions, has been found to express a minimum pitch. This might be because this is more of a material than a stencil-specific property. To test pitch limits, this distance should have been made smaller, although at some point the limits of the stencil itself and its fabrication will become non-negligible. Compliance of thin (i.e. in-plane) stencil sections or unwanted local laser-infused stencil material modification could negatively influence printing performance when nearing these pitch limits.

Interesting to note is the thin film capillary spreading that can be seen in Figure 3.16d, which seems to be omnidirectional and hence independent of the squeegee pull direction for this square aperture. For the rectangular apertures of Figure 3.15a, it seems to be much more directional. This raises the suspicion that the capillary spreading is related to the dimensions of the aperture. More detailed microscopic pictures can be found in Appendix D.

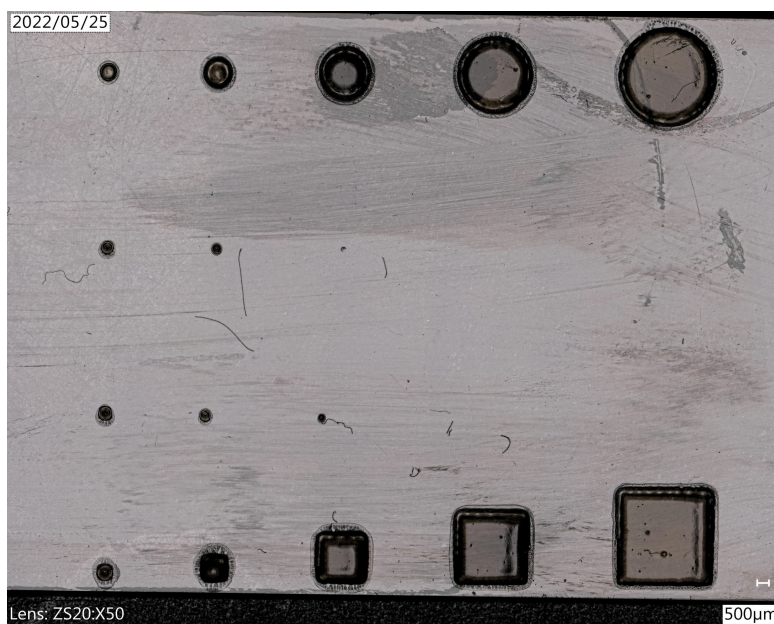
3.3.5. Snap-off Printing

Snap-off height is defined as the distance between stencil and substrate at rest. Snap-off printing is a necessary part of the standard PCB stencil print process to eliminate flux bleeding (i.e. capillary forces pulling the liquid part of the solder paste suspension between stencil and substrate), which typically happens with in-contact stencil printing without snap-off height [57, 92]. To check the effect of snap-off height in this specific stencil print process, an experiment is set up to test the effect of this parameter. The standard stencil, as introduced in section 3.2, is first used in the print set-up with a 5 mm gap between stencil and glass substrate, followed by a print where the stencil is directly placed on the glass substrate with zero snap-off height. Both prints are made with one squeegee pull over the stencil.

In Figure 3.8 and Figure 3.17a, the difference between these two print situations is visible. In-contact printing results in much better defined lines, that are straight and all of equal length, for polymer stencil printing with the 50/50 wt% PTFE-PDMS composite that was introduced before. The snap-off printing also clearly shows the desired straight lines but has a thin layer bordering the lines, which is most probably caused by the squeeze flow that the rolling contact line of the stencil and substrate in snap-off printing creates. If material is deposited in front of the contact line, the pressure of the stencil will generate a lot of shear in the material and the printing material will thus experience shear thinning. This shear thinning will make the PDMS composite less viscous and the PDMS will in consequence spread more. The liquid component of the PTFE-PDMS suspension will thus flow. Interestingly, the printing direction for Figure 3.17a was from top to bottom, meaning that the spreading effect that creates the thin film gets worse further along the stencil. Additionally, the thin films have an intricate network of thin lines, these might be the PDMS polymer chains. To check how true to design these prints are, they are again measured with the digital microscope (see Appendix D) and analysed



(a) Stencil 1



(b) Stencil 2

Figure 3.15: Stencil prints with 50/50 wt% PTFE-PDMS composite and in-contact printing

with help of the *MATLAB* script of section H.3. Figure 3.18 shows that snap-off printing, despite its messier print, results in line widths that are closer to the stencil design. A trade-off should therefore be made here.

3.3.6. Number of Squeegee Pulls

Alongside the results of the previous section, another parameter is tested as well with the same experiment: The number of passes to get a good printing result. Figure 3.17a uses one squeegee pull, while Figure 3.17b uses multiple pulls. It is visible that for the multiple squeegee pull print the thin film, caused by squeeze flow, is even worse than with one squeegee pull and completely covers the entire printing area. The printing material even accumulates between the desired lines to form additional features. Thixotropy is once again suspected to be the cause for this poor print performance with more squeegee pulls, as multiple squeegee pulls mean that shear is applied to the printing material for a longer time. Therefore the viscosity will drop more with multiple pulls as shear rate history dependence is present. Figure 3.18 shows that the print with multiple squeegee pulls also produces wider lines, thus it also performs worse in that regard. The standard deviation of the multiple pull print is also significantly higher than the single pull print. If precise printing is to be achieved, the standard deviation should be as low as possible.

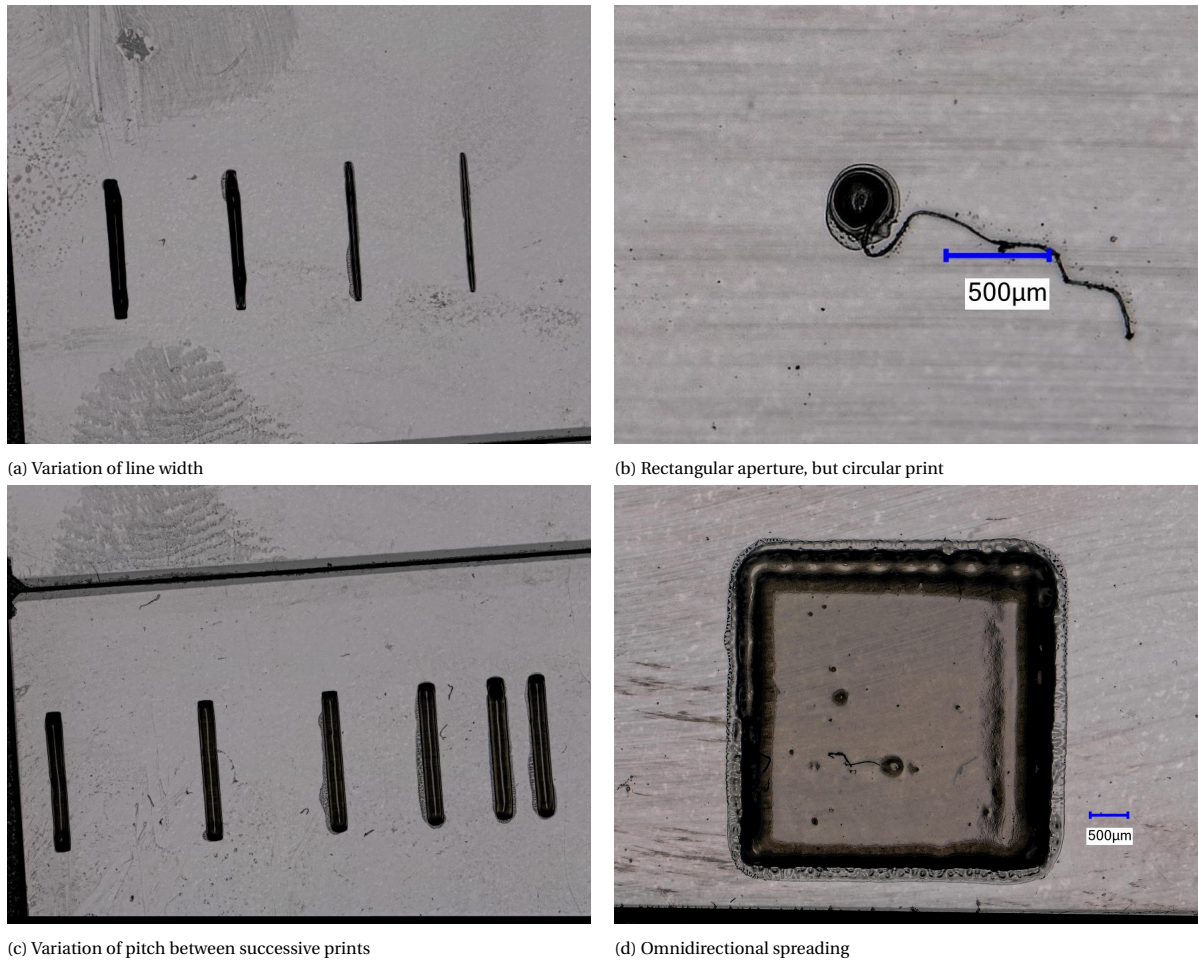


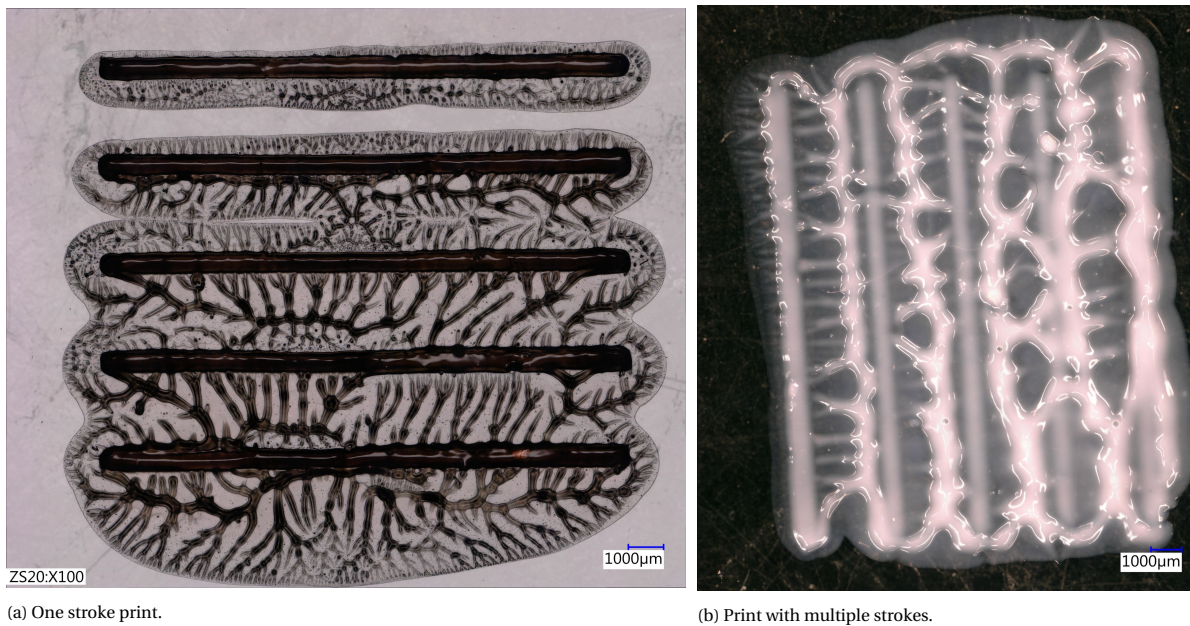
Figure 3.16: Details of PTFE-PDMS prints with test stencils

3.3.7. Elasticity of the Substrate

Elasticity of the substrate could result in a better printing result because elasticity that is present between stencil and substrate can better ensure conformal contact. As nothing is perfectly flat, a small gap will exist between a rigid stencil and substrate where capillary forces will pull liquid printing material into. The elasticity of PDMS is dependent on the mixing ratio of base and curing agent, as shown in Figure 3.19 [7]. In a metamaterial that consists of multiple layers of the same material, this might be a property that can be tweaked to ensure a more shape-retaining stencil print process, because printing occurs on top of another polymeric layer. However, it should be kept in mind that tweaking the elasticity will also affect the overall behaviour of the structure. This might be a disadvantage if the resulting metamaterial has to have certain properties or behaviour and the material has to perform identically throughout the entire metamaterial.

3.3.8. Functionalising the Substrate Surface

Finally, the last solution to get a more shape-retaining print process is at the substrate. With local chemical treatment of the substrate surface, printing material can be better contained. If the PDMS-to-PDMS bond strength versus contact angle graph of Figure 3.9b is studied, it becomes clear that the bonding between substrate and printing material will be better if the surface wettability of the substrate is increased (i.e. lower contact angle) [4]. Multiple solutions exist to improve the surface wettability, among which oxygen plasma and corona treatment are the most popular techniques [4, 72, 94]. Corona treatment has the big advantage that it can be performed outside of a cleanroom environment, which makes incorporating this in a fabrication process much easier [72, 94] than an O_2 plasma treatment that needs specialised cleanroom equipment. The stencil that is already used for the stencil printing itself, can also serve as a mask to localise this surface modification to the areas that are patterned only. The PDMS base to curing agent mixing ratio does not influence the surface wettability of PDMS [95].



(a) One stroke print. (b) Print with multiple strokes.

Figure 3.17: PTFE-PDMS composite stencil print with snap-off height

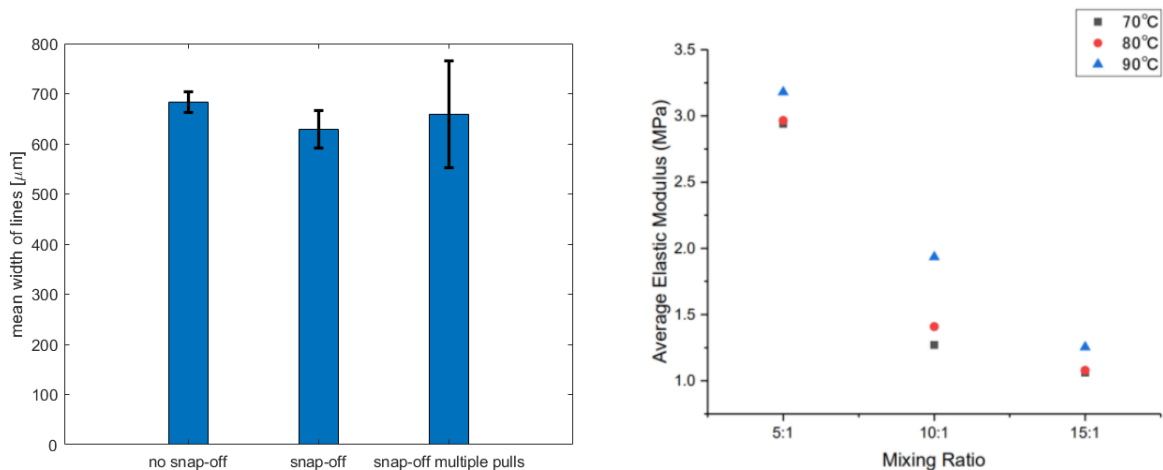


Figure 3.18: Line width of PTFE-PDMS composite (50/50 wt%)

Figure 3.19: elasticity of PDMS for different mixing ratios and curing temperatures [7].

3.4. Successful Polymer Stencil Printing

The journey that was undertaken in the previous section to achieve a better stencil print process has proven to be quite successful. Starting from the initial prints that can be seen in Figure B.1, it was clear that a lot of improvement was necessary before polymer stencil printing could be considered a feasible high-throughput fabrication technique for micromechanical metamaterials. By adding PTFE particles to PDMS the viscosity was increased enough to be similar to PCB solder paste. A supplementary benefit of the particles was the creation of shear-thinning behaviour, which aids in successful stencil printing. Further improvements to the process are using a substrate that has a high contact angle with respect to PDMS, heating the substrate to speed up the curing process, printing without snap-off height between stencil and substrate and only using one squeegee pull. These improvements have led to the accurate stencil print that can be seen in Figure 3.8 and the promising experimental results of Figure 3.4 and Figure 3.18. Other parameters that are suspected to further improve polymer stencil printing are: Elasticity of the substrate and local chemical treatment to add specific surface wettability to specific areas on the substrate.

4

Conclusion & Future work

In this final chapter, the results of chapters 2 and 3 will be reviewed once more. The acquired knowledge is used in section 4.1 to find the answers to the research question along with its sub-questions that were introduced in section 1.3. Accompanying these answers is a small analysis of the relevance of the achieved results and how they contribute toward the high-throughput fabrication of micromechanical metamaterials. In section 4.2 this chapter will be closed off with the future work that could be performed to further improve the high-throughput fabrication of metamaterials.

4.1. Conclusion

This section will give answers to the research questions. To refresh the mind, a reiteration of the overarching research question is given below.

“How can repetitive and micromechanical metamaterials be manufactured with a global fabrication process?”

To aid in answering this overarching question two sub-questions have been defined of which the first was stated as follows:

1. How can metamaterial designs be broken down into fundamental elements for the global fabrication of planar and repetitive structures?

This first sub-question was dealt with in chapter 2 and was addressed in two parts, of which the first part was successfully answered by breaking down the test vehicle design into six general geometric elements called basic features (Table 2.1), which can also be used to construct other metamaterial designs. However, these features cannot be built in one single fabrication step or one unique combination of fabrication steps. Therefore, no comments could yet be made on a fabrication process flow based on this breakdown. From a fabrication standpoint, the most elementary steps were found to be the so-called material transformations (Table 2.2). These material transformations consist of the smallest steps that are made in a fabrication process. If these material transformations are coupled to the basic features, a successful breakdown of a metamaterial design to its most fundamental elements for fabrication can be performed. The second part of this sub-question, combining the fabrication of single material transformations to a complete process flow, has proven to be more difficult, because there is no single perfect combination of material transformations and consequent fabrication techniques to create a chosen test vehicle. As a sole material transformation can be made with multiple fabrication techniques, the ‘best’ choice depends on the surrounding material transformations. More research on the specific characteristics of each fabrication technique for polymeric materials is necessary, especially on their interaction with already built feature layers and the specific influence they have on the material itself, i.e. are the properties or behaviour altered.

Answering this sub-question has resulted in gained knowledge on the way that micromechanical metamaterials could be constructed with potential high-throughput fabrication techniques. With help of the design breakdown of a metamaterial design into geometric features and eventually material transformations that can be directly related to high-throughput mechanical contact-based fabrication techniques, a clear understanding of the consecutive high-throughput fabrication possibilities for micromechanical metamaterials has been gained.

After this dive into a complete fabrication process for micromechanical metamaterials, a closer look was taken at polymer stencil printing. This technique, originating from PCB manufacturing, has characteristics that look promising with the fabrication attributes of subsection 1.2.2 in mind. This led to the second sub-question:

2. What are the most important parameters to get successful replication with stencil printing and how do these parameters influence a successful stencil print replication?

Chapter 3 answers this sub-question. Initial prints (shown in Appendix B) were quite poor and showed significant spreading of the printing material, but the desired pattern could already be somewhat recognised. A literature study on PCB stencil printing acknowledged the most probable influential parameters for precise stencil printing in section 3.3. These parameters are summarised in Figure 3.3 and include, among others, viscosity, wettability, squeegee operation and stencil design. To test the real-world influence of these parameters on polymer stencil printing, a rudimentary stencil print set-up is designed and built in section 3.2. Shape-retainment of the PDMS printing material has proven to be a big challenge. Two different paths were considered to achieve this, namely viscosity enhancement and substrate pinning. Viscosity enhancement can be realised in multiple manners. First, it was attempted to partially cross-link the PDMS before stencil printing by pre-curing it. However, the transition between too much and too little cross-linking has proven to be too narrow to use because the tackiness, caused by cross-linked polymer chains, occurs before shape-retainment. The second and more successful viscosity enhancement technique has proven to be mixing 1 μm sized PTFE particles into the PDMS matrix. The viscosity reached by adding 50 wt% is similar to the viscosity of PCB solder paste (Figure 3.7 and Figure 3.10) and the achieved stencil print (Figure 3.8) shows good replication with a mean line width of 638 μm alongside a standard deviation of 20.8 μm (Figure 3.18) against a 585 μm line width of the laser-cut stencil. An additional benefit of mixing PTFE particles into the PDMS matrix is the introduction of shear-thinning, which is also found in the traditional PCB solder paste. Shear-thinning helps the printing material to be fluid enough to pass through the stencil during printing while remaining viscous enough at rest to obtain shape-retainment afterwards.

Next, shape-retainment by temperature pinning was proven by comparing equal volume droplet spreading on room-temperature and heated (150 $^{\circ}\text{C}$) glass substrates. The curing characteristics of PDMS, especially the used *Sylgard 184* variant, indicate that higher temperatures speed up the curing time significantly. Pinning of the PDMS to the substrate occurs because the cross-linking starts immediately at the interface. This behaviour can indeed be seen and leads to a significant drop in the radius of the spread droplets, as seen in Figure 3.4. A second experiment with the same procedure shows the effect of wettability on shape-retainment. As was hypothesised based on the PDMS contact angle difference in relation to a glass (20 $^{\circ}$) or PDMS (109 $^{\circ}$) substrate, PDMS on a PDMS substrate spreads significantly less than on glass, as shown in Figure 3.4.

Literature for PCB stencil printing suggests that snap-off height leads to better printing results, however, the opposite has been the case. The effect of squeeze flow caused by the rolling contact of the stencil in snap-off printing leads to more spreading than capillary bleeding does with in-contact printing. In the same literature, several parameters regarding limitations of the stencil design itself were brought forward that led to three ratios that can be tested. First, Matlab was used to gain insight into the dimensional limitations of apertures (Figure 3.13). Afterwards, experiments on these ratios showed that they could not be straightforwardly applied to polymer stencil printing in the more extreme cases. As long as the width and length of apertures stay below ≈ 0.5 mm for a 0.1 mm thick stencil, they do carry significance and give a useful insight into the boundaries of a print process. Finally, the number of pulls that is used for stencil printing was varied. It was suspected that one squeegee pull might not be enough to achieve good replication and that multiple pulls would be necessary, but Figures 3.18 and 3.17b show poor print performance caused by the squeeze flow of multiple squeegee pulls. It can therefore be said that the influential parameters for a successful polymer stencil print process have been researched and exploited to get a well-performing stencil print process.

All in all, it can be concluded that answers have been found for the overarching research question, although not completely in the anticipated form. The research question was answered by contributing to the thought process for high-throughput fabrication of micromechanical metamaterials in general by establishing generalised building blocks that link design and fabrication together and more specifically by establishing the basis for a successful polymer stencil print process as a potential high-throughput fabrication technique for micromechanical metamaterials.

4.2. Future Work

As is expected when embarking on a scientific research journey, not everything that was planned to be investigated in the beginning could eventually be done. During the experiments freshly gained insights sparked further research paths. Therefore, this section will briefly discuss the potential future work that could be performed in the field of this thesis.

To take the high-throughput fabrication process to the next step, more research should be performed on the effect that fabrication techniques have on each other in a consecutive process. Achieving this should be done by applying the different fabrication techniques that were introduced in subsection 1.2.2 on an already patterned substrate to see how the fabrication techniques perform in a consecutive process. This will also show how the substrate reacts to certain fabrication techniques and their necessary process parameters such as temperature and pressure among others. Similarly, it is not known yet how high the throughput genuinely is for each fabrication technique separately and in a complete process.

One critical step in the complete fabrication process flows of section 2.3 is the sacrificial material filling of a built layer. Challenging here is whether the sacrificial material can be deposited flat enough that it has a smooth transition to the most protruding features of the preceding layer and whether there is no material deposited on these protruding features such that the succeeding layer can be fabricated correctly.

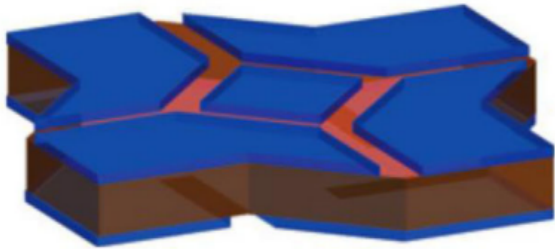
A further challenge is the joining of the individually fabricated layers. For now, this is still a considerable unknown. If the material transformation is performed 'ex situ' (e.g. μ TM) adhesion promotion is certainly necessary and in literature several methods have already been found, as was briefly mentioned in subsection 3.3.2. Techniques such as using uncured PDMS as an adhesive, varying PDMS mixing ratio, partial curing of the substrate, corona discharge or O_2 plasma treatment could be utilised [72]. For 'in situ' fabrication it is not known yet to what degree the uncured PDMS adheres to the already fully cured PDMS layer after fabrication. This could be tested with the help of a dynamic mechanical analyser or nano indenter. Related to this challenge is the alignment of fabricated layers. For this research, alignment during the fabrication of the layers was completely ignored. However, this is a nontrivial part of a complete fabrication process flow and hence deserves thorough research. Some ideas for this are incorporating optical alignment marks in each layer or an interlocking mechanism for mechanical alignment.

The interaction between stencil, substrate and printing material deserves more attention. In this thesis, an exploratory study was done in subsection 3.3.4 with help of three ratios defined by Durairaj et al. [5] for PCB stencil printing with standard solder paste. The results for the relating experiments were not completely in line with the expected outcome based on an analytical study in *MATLAB* of these ratios. A more thorough analysis of the polymer material behaviour and its interaction with stencil and substrate is useful to better predict the physical limits of polymer stencil printing.

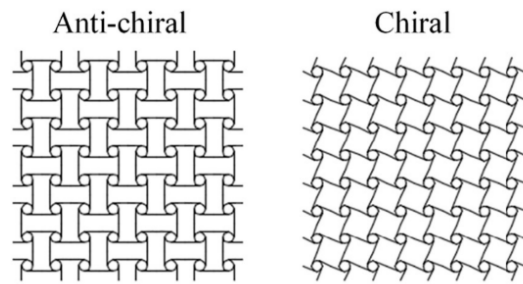
Interesting to investigate as well, would be the effect of stencil thickness on print height. In theory, these parameters should be directly related to each other, but the spreading of printed material might have a bad influence. This could not be tested with the digital microscope directly, due to the transparency and reflectivity of PDMS and the PTFE-PDMS composite, respectively. However, sputter coating a thin gold layer can negate this problem. This technique was once done on a stencil print and delivered a specimen that could be measured for height, but the extra process step, required (clean room) training and added time did outweigh the added benefits of getting extra dimensional data. However, it would still be a good thing to do if time is no constraint. If the printed height is known together with the area that can already be determined, calculations on deposited volume can be performed and a transfer efficiency can be determined.

A

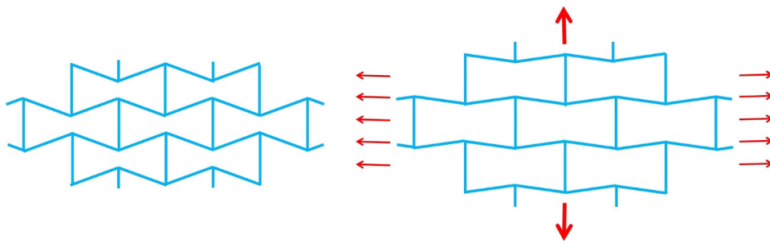
Micromechanical Metamaterial Designs



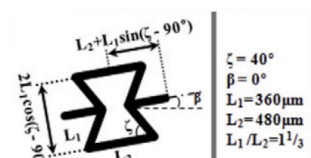
(a) Trilayer origami metamaterial [18].



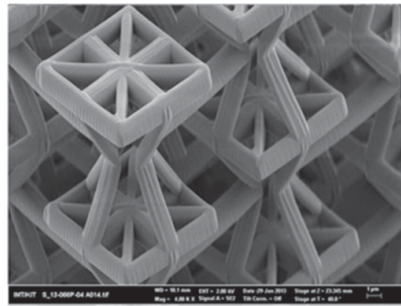
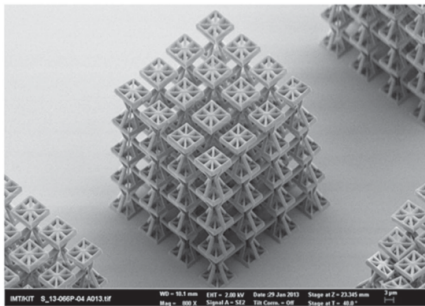
(b) Anti-chiral and chiral honeycomb structures [20].



(c) 2D re-entrant structure [11].



(d) Geometry of 2D re-entrant structure [96].



(e) 3D re-entrant structure [11].

Figure A.1: Multiple auxetic metamaterials

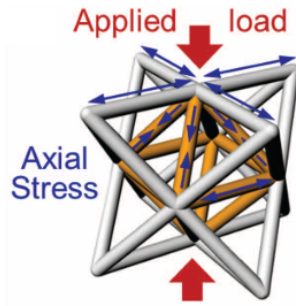
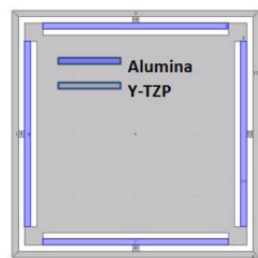
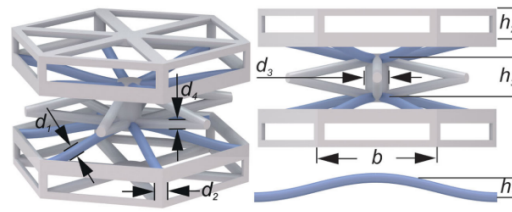


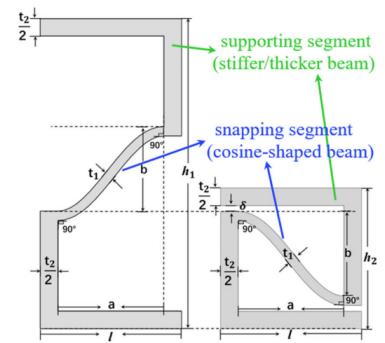
Figure A.2: Octet truss unit cell [8].



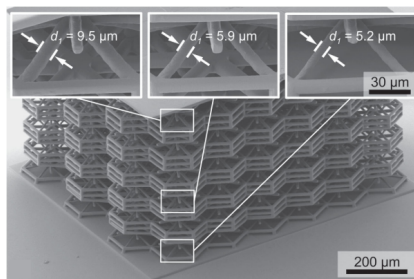
(a) Unit cell design for negative stiffness metamaterial [97].



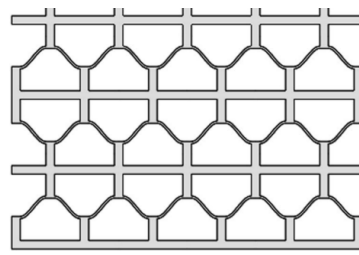
(b) Unit cell buckling metamaterial [24].



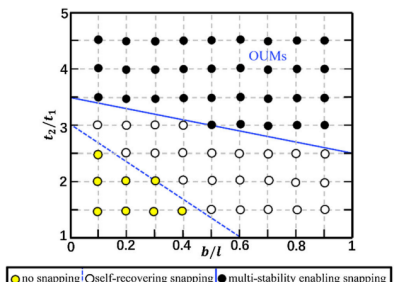
(c) quarter unit cell 2D buckling metamaterial [98]



(d) Complete buckling metamaterial structure with insert showing the gradient [24].

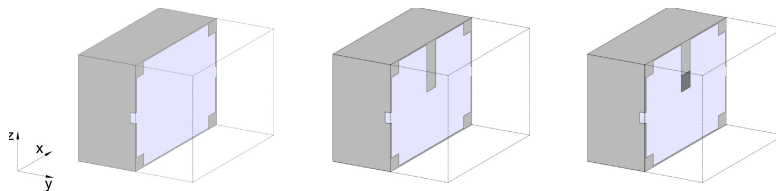


(e) structure 2D buckling metamaterial [98]

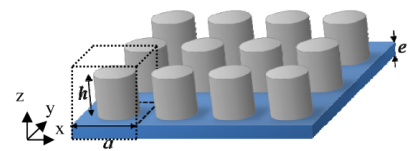


(f) Buckling behaviour of the metamaterial of Figure A.3e[98].

Figure A.3: metamaterials with bistability.

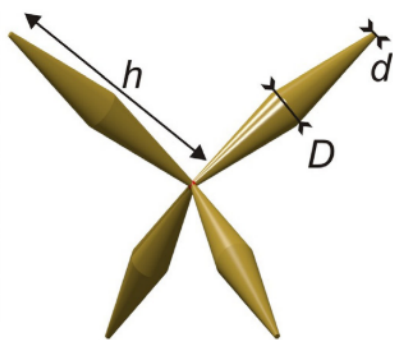


(a) Unit cell designs (cut in half) of an acoustic metamaterial with in dark grey PU, and light grey air. From left to right; without and with resonators and resonator plus added mass [2].

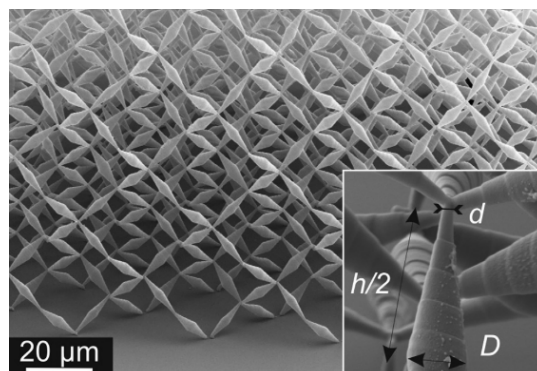


(b) Acoustic metamaterial with steel nanopillars on silicon plate [99].

Figure A.4: Acoustic metamaterials.

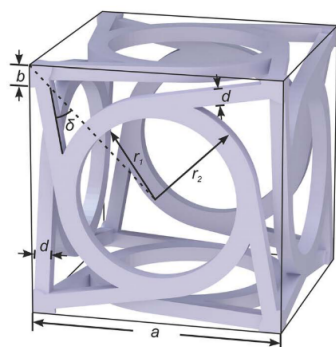


(a) Unit cell design of pentamode metamaterial [27].

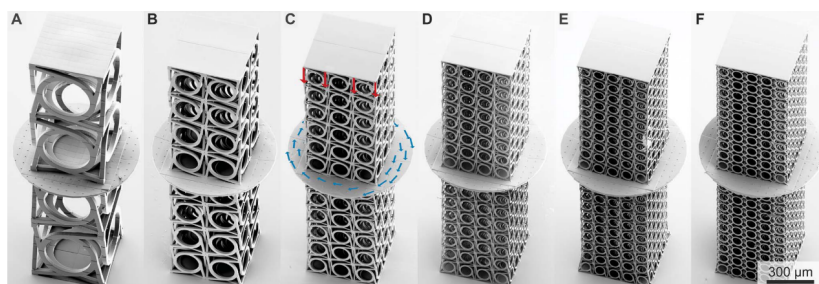


(b) Fabricated Pentamode material with definition of geometry parameters. [27].

Figure A.5: Pentamode metamaterial



(a) Unit cell design



(b) Overall structure with different sizes of the unit cell

Figure A.6: Metamaterial that twists under a compressive load [9].

		Metamaterial Designs											
		Trilayer origami	2D Re-entrant	3D Re-entrant	Twist under compression	High load low density	Pentamode	Acoustic metafoam	Acoustic nanopillar	Negative stiffness	3D bistable	2D bistable	
Attributes	minimum feature size	medium	medium	small	small/medium	medium/large	small	small	small	N/A	small	large	
	Range of feature sizes	small	small	small	big	big	small	big	small	big	small	small	
	Multiple identical layers	no	no	yes	yes	yes	yes	yes	no	no	yes	yes	
	2D or 3D features in a layer	2D	2D	3D	3D	3D	3D	3D	2D	3D	3D	2D	
	One or multiple materials	multiple	one	one	one	one	one	multiple	multiple	multiple	one	one	
	Spatial arrangement of second material	globally	N/A	N/A	N/A	N/A	N/A	N/A	locally	locally	globally	N/A	N/A
	Typical geometry variety of the unit cell	plate	truss	truss	truss	truss	truss	plate	plate	plate	truss	truss	
	no	yes	yes	yes	yes	yes	yes	yes	no	yes	yes		

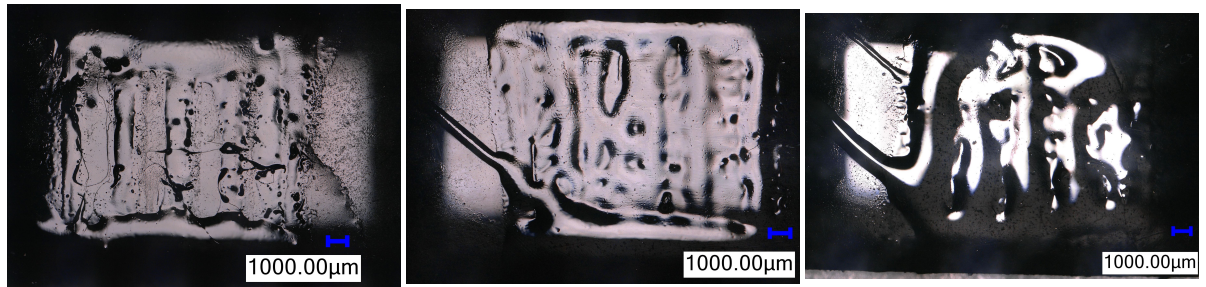
Table A.1: Attributes of the presented metamaterial designs

		Fabrication Technique				
		T-NIL	UV-NIL	μTM	MIMIC	μCP
Attributes	minimum feature size	small	small	small	small	small or medium
	Able to fabricate a big range of feature sizes	yes	yes	yes	no	yes
	Multiple identical layers	no	no	yes	no	yes
	2D or 2.5D fabrication	2.5D	2.5D	2.5D	2.5D	2D
	multiple materials fabrication	no	no	yes	yes	yes
	Spatial arrangement of the second material	N/A	N/A	global	local	global
	subtractive or additive fabrication technique	subtractive	subtractive	additive	additive	additive
	Process or tool fabrication technique	process	process	process	process	process

Table A.2: Attributes of the fabrication techniques

B

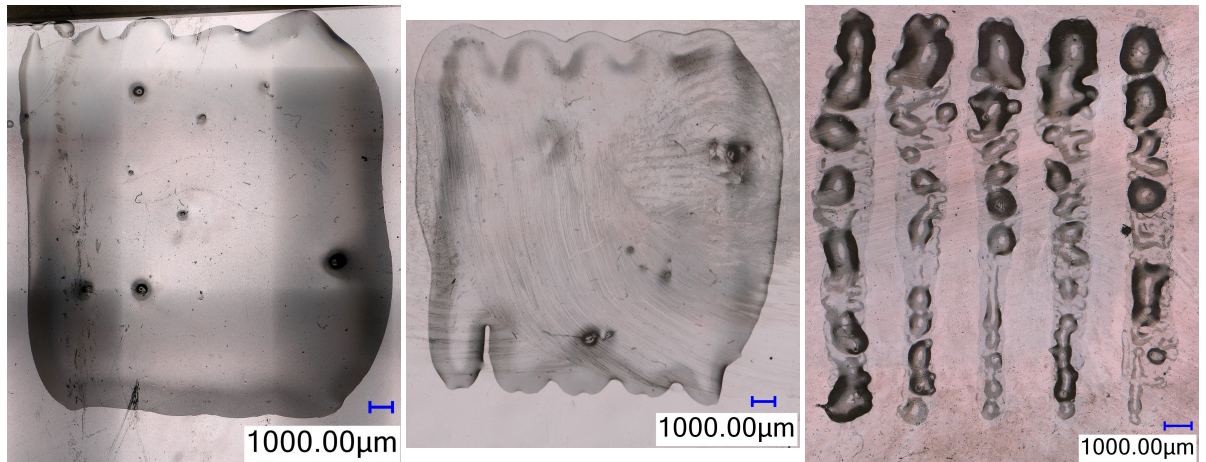
Initial Prints



(a) 7 min. precure on a cured PDMS substrate (no precure), printed with snap-off height.

(b) 7 min. precure on a cured PDMS substrate (2 min. precure), printed with snap-off height.

(c) 7 min. precure on a cured PDMS substrate (4 min. precure), printed with snap-off height.



(d) 6 min. precure, printed directly on a glass substrate.

(e) 6.5 min. precure, printed directly on a glass substrate.

(f) 7 min. precure, printed directly on a glass substrate.

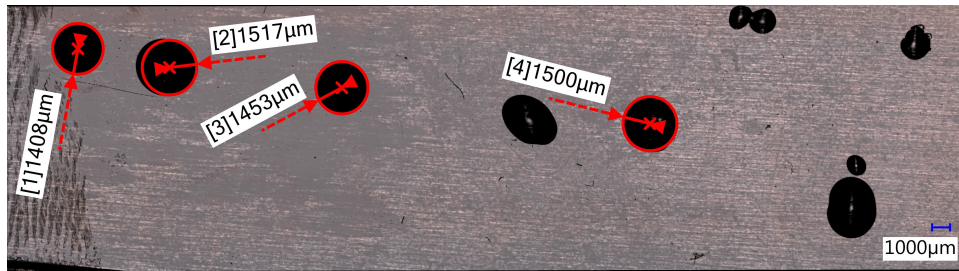


(g) 7 min. precure, printed with snap-off height.

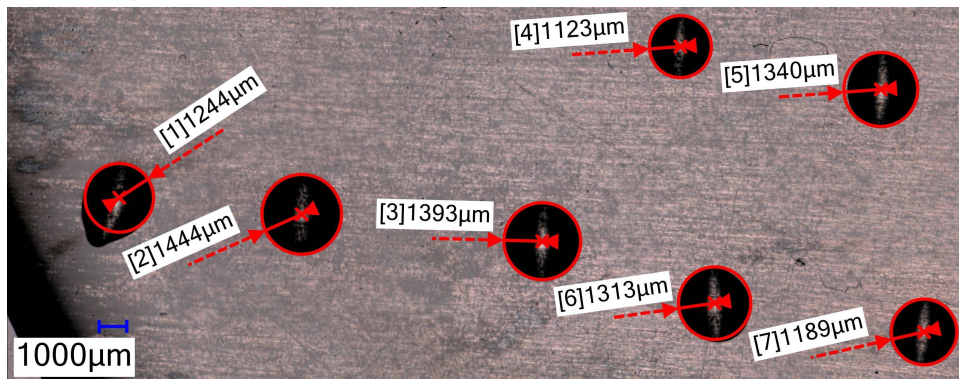
Figure B.1: Initial stencil prints, with a curing temperature of 70 °C

C

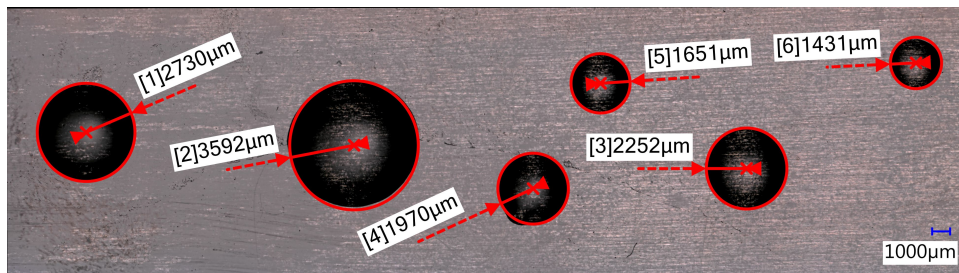
Spreading Behaviour



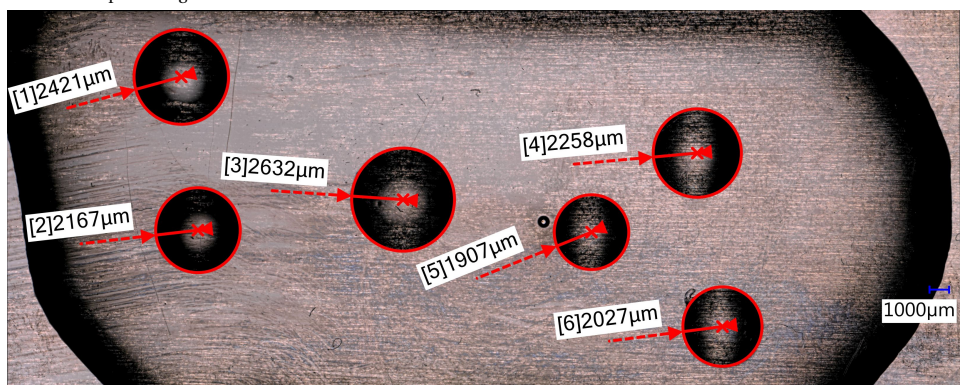
(a) On a heated glass substrate.



(b) On a heated PDMS substrate.



(c) On a room temperature glass substrate.



(d) On a room temperature PDMS substrate.

Figure C.1: Spreading behaviour of 5 μ L droplets

D

PTFE-PDMS Composite Prints

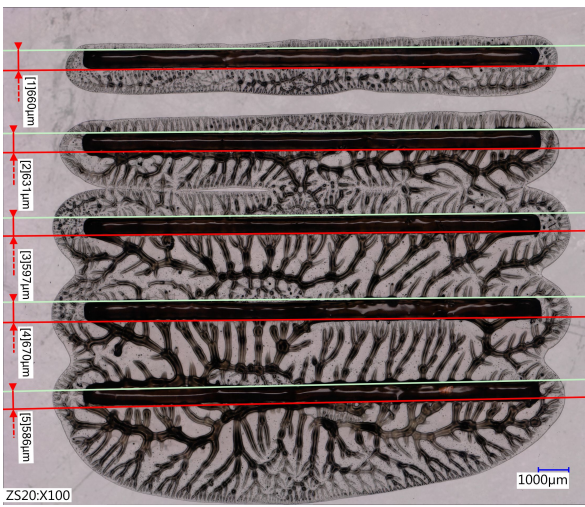


Figure D.1: PTFE-PDMS (50/50wt%) 1 stroke snap off, line width measured

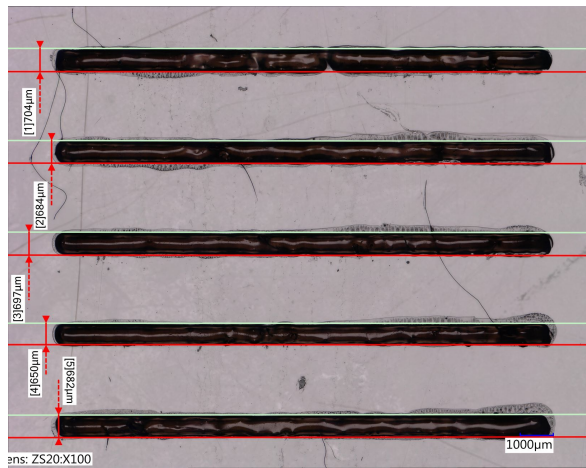


Figure D.2: PTFE-PDMS (50/50wt%) 1 stroke no snap off, line width measured

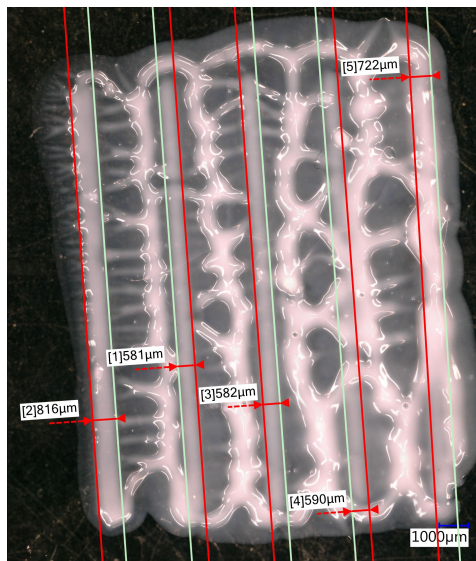
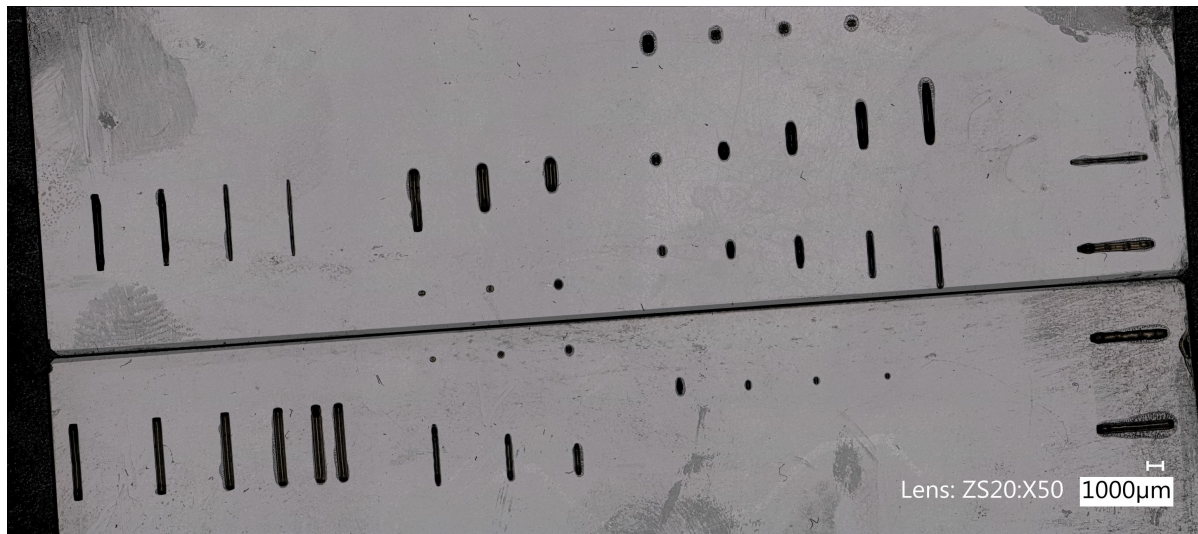
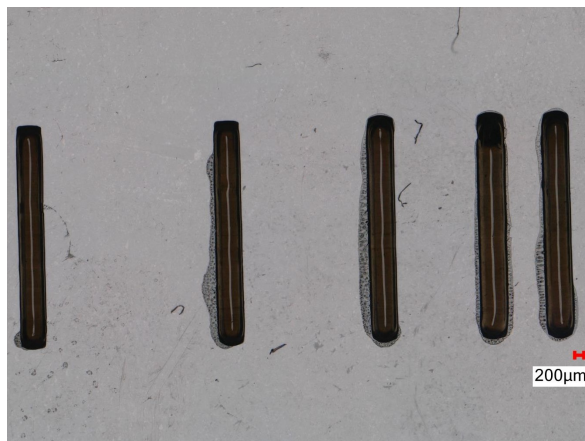


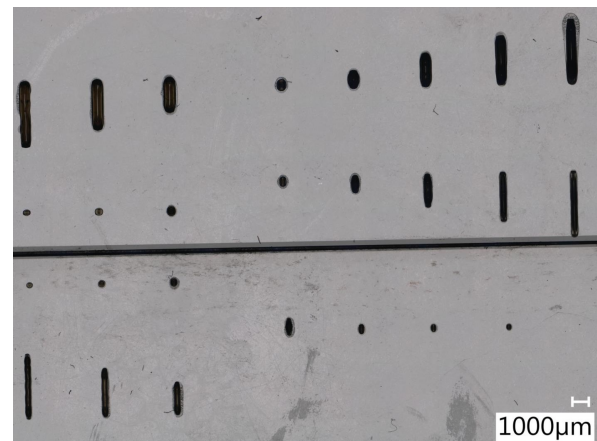
Figure D.3: PTFE-PDMS (50/50wt%) multiple strokes snap off, line width measured



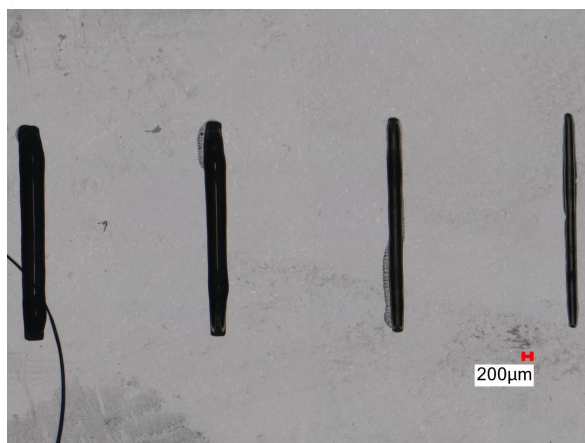
(a) Overview



(b) Detail 1



(c) Detail 2

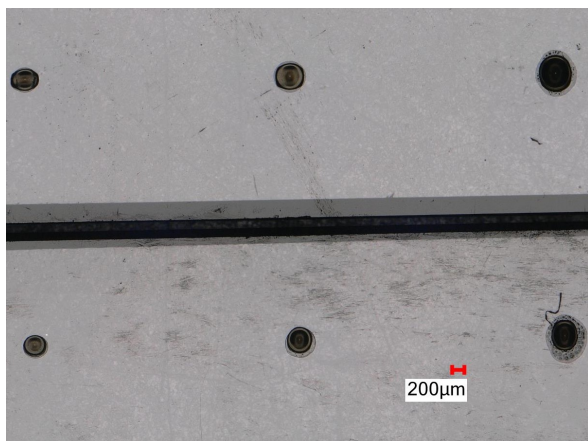


(d) Detail 3



(e) Detail 4

Figure D.4: Stencil print of test stencil 1

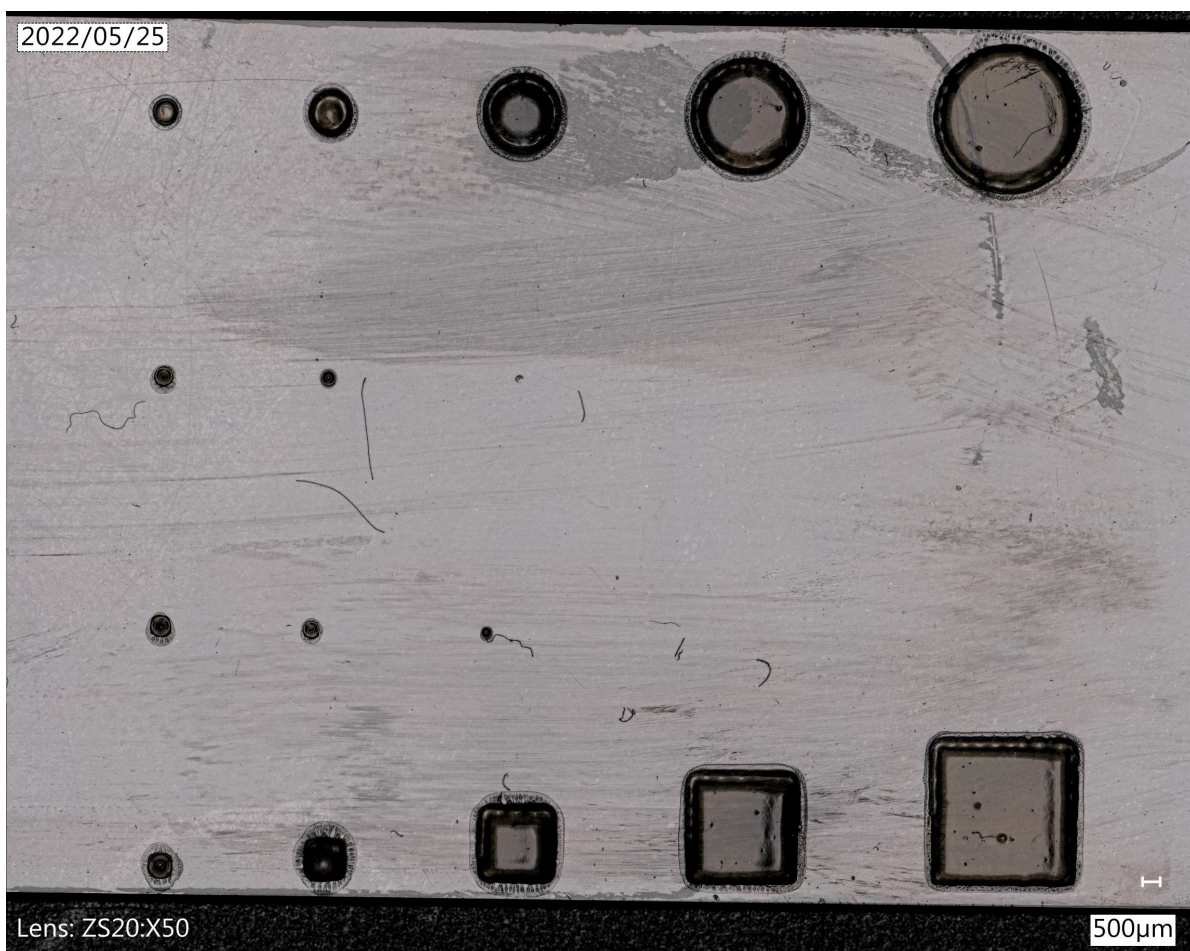


(f) Detail 5



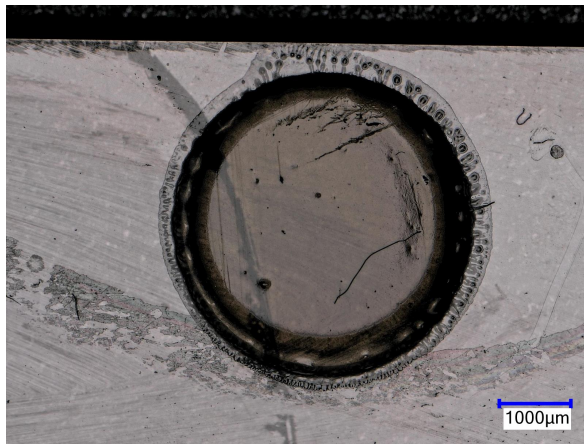
(g) Detail 5

Figure D.4: Stencil print of test stencil 1 (cont.)

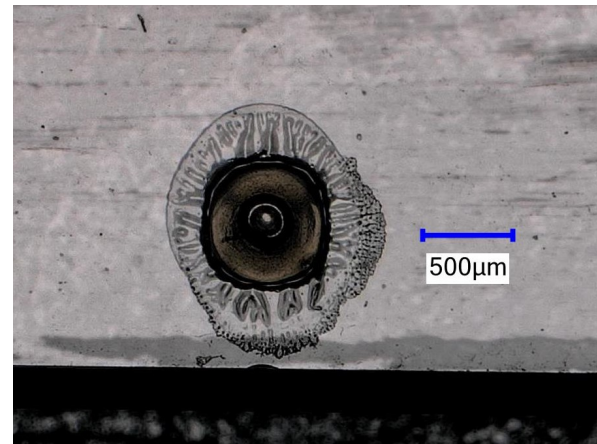


(a) Overview

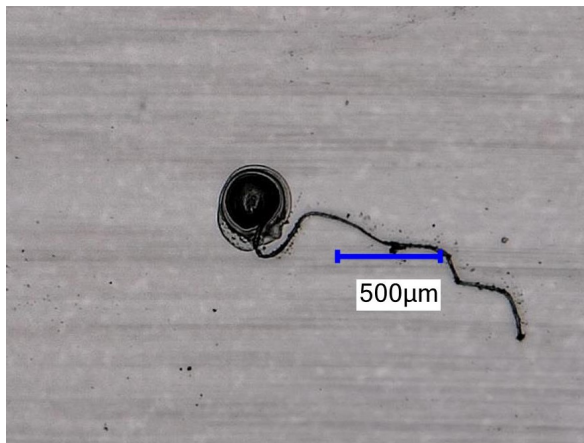
Figure D.5: Stencil print of test stencil 2



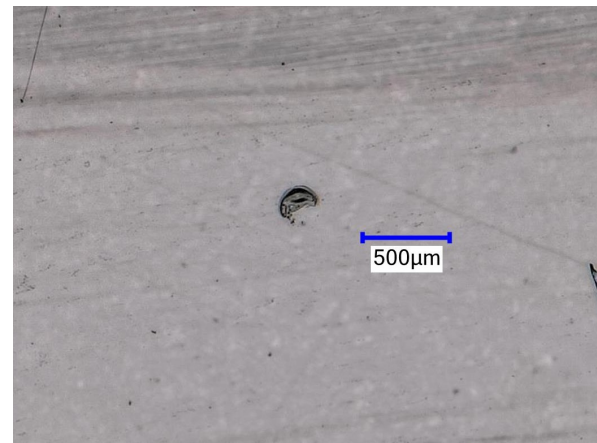
(b) Detail 1



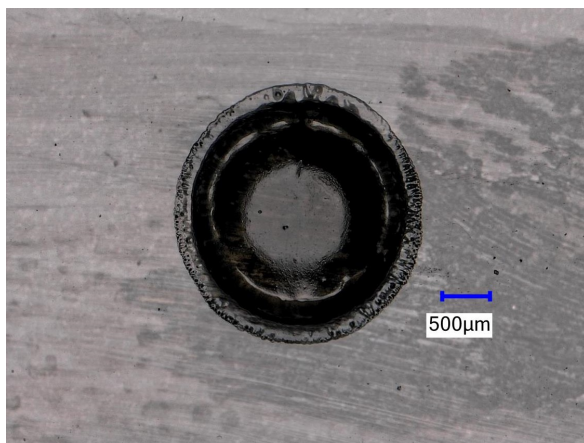
(c) Detail 2



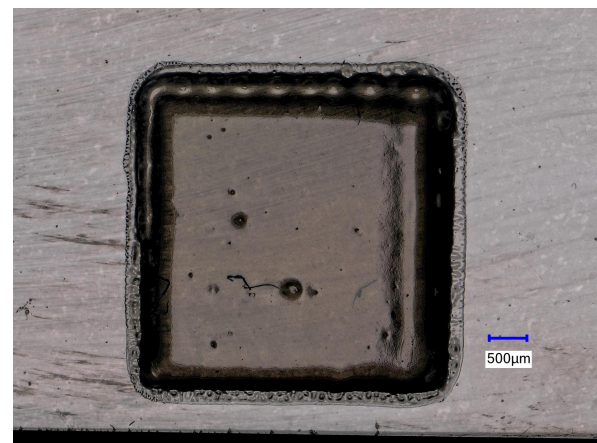
(d) Detail 3



(e) Detail 4



(f) Detail 5



(g) Detail 6

Figure D.5: Stencil print of test stencil 2 (cont.)

E

Viscosity Measurements

Point No.	Shear Rate [s ⁻¹]	Shear Stress [mPa]	Viscosity [Pa·s]	Temperature [°C]	Torque [mN·m]	Time [s]	Rotational Speed [rpm]	Gap [mm]	Normal Force [N]
1	0.01	35.521	3.5529	25	0.000164	25	0.011455	1	-0.01
2	0.0158	51.736	3.2648	25	0.000238	30	0.018156	1	-0.01
3	0.0251	77.656	3.0923	25	0.000358	35	0.028774	1	-0.01
4	0.0398	115.39	2.8989	25	0.000531	40	0.045607	1	-0.01
5	0.0631	184.63	2.9266	25	0.00085	45	0.072283	1	-0.01
6	0.1	292.51	2.9256	25	0.001347	50	0.11456	1	-0.01
7	0.158	460.49	2.9057	25	0.00212	55	0.18158	1	-0.01
8	0.251	7.20E+02	2.8652	25	0.003313	60	0.28778	1	-0.01
9	0.398	1.12E+03	2.8253	25	0.005178	65	0.45613	1	-0.01
10	0.631	1.77E+03	2.798	25	0.008127	70	0.7229	1	-0.01
11	1	2.78E+03	2.7784	25	0.012791	75	1.1457	1	-0.01
12	1.58	4.38E+03	2.7648	25	0.020172	80	1.8159	1	-0.01
13	2.51	6.92E+03	2.7561	25	0.031871	85	2.878	1	-0.01
14	3.98	1.09E+04	2.7481	25	0.050366	90	4.5613	1	-0.01
15	6.31E+00	1.73E+04	2.7402	25	0.079597	95	7.2292	1	-0.01
16	1.00E+01	2.73E+04	2.7339	25	0.12586	100	11.458	1	-0.01
17	1.58E+01	4.32E+04	2.7283	25	0.19907	105	18.159	1	-0.01
18	25.1	68460	2.7255	25	0.31517	110	28.78	1	-0.01
19	39.8	1.08E+05	2.7248	25	0.49939	115	45.613	1	0
20	63.1	1.72E+05	2.7267	25	0.79205	120	72.292	1	0
21	100	2.72E+05	2.7225	25	1.2534	125	114.58	1	0

(a) Upward sweep

Point No.	Shear Rate [s ⁻¹]	Shear Stress [mPa]	Viscosity [Pa·s]	Temperature [°C]	Torque [mN·m]	Time [s]	Rotational Speed [rpm]	Gap [mm]	Normal Force [N]
1	100	2.72E+05	2.7248	25	1.2542	130	114.55	1	-0.01
2	63.1	1.72E+05	2.7328	25	0.79362	135	72.277	1	-0.01
3	39.8	1.09E+05	2.7384	25	0.50178	140	45.603	1	-0.01
4	25.1	68859	2.7419	25	0.31701	145	28.774	1	-0.01
5	15.8	43524	2.7467	25	0.20037	150	18.156	1	-0.01
6	10	27524	2.7528	25	0.12671	155	11.456	1	-0.01
7	6.31	17395	2.7572	25	0.080083	160	7.2287	1	-0.01
8	3.98	11000	2.7633	25	0.050641	165	4.5611	1	-0.01
9	2.51	6939.1	2.7626	25	0.031945	170	2.8779	1	-0.01
10	1.58	4386.5	2.7678	25	0.020194	175	1.8159	1	-0.01
11	1	2771.3	2.7713	25	0.012758	180	1.1458	1	-0.01
12	0.631	1751.6	2.7761	25	0.008064	185	0.72292	1	-0.01
13	0.398	1106.6	2.7795	25	0.005094	190	0.45614	1	-0.01
14	0.251	6.99E+02	2.7819	25	0.003217	195	0.28781	1	0
15	1.58E-01	439.89	2.7756	25	0.002025	200	0.18159	1	-0.01
16	1.00E-01	282.18	2.8218	25	0.001299	205	0.11458	1	-0.01
17	6.31E-02	176.76	2.8013	25	0.000814	210	0.072295	1	0
18	0.0398	112.99	2.838	25	0.00052	215	0.045615	1	0
19	0.0251	71.981	2.8657	25	0.000331	220	0.028779	1	-0.01
20	0.0158	46.392	2.9275	25	0.000214	225	0.018157	1	0
21	0.01	30.686	3.0686	25	0.000141	230	0.011458	1	0

(b) Downward sweep

Table E.1: Viscosity measurement data for native PDMS

Point No.	Shear Rate [s ⁻¹]	Shear Stress [mPa]	Viscosity [Pa·s]	Temperature [°C]	Torque [mN·m]	Time [s]	Rotational Speed [rpm]	Gap [mm]	Normal Force [N]
1	0.01	3.40E+03	3.40E+02	25	0.015637	25	0.011457	1	0.01
2	0.0158	4.40E+03	2.77E+02	25	0.020242	30	0.018158	1	0.01
3	0.0251	5.96E+03	2.37E+02	25	0.027429	35	0.028777	1	0.01
4	0.0398	7.77E+03	1.95E+02	25	0.035754	40	0.045609	1	0.01
5	0.0631	1.08E+04	1.71E+02	25	0.049591	45	0.072285	1	0.01
6	0.1	1.46E+04	145.57	25	0.067009	50	0.11456	1	0.01
7	0.158	1.96E+04	123.43	25	0.090055	55	0.18158	1	0.01
8	0.251	2.57E+04	102.14	25	0.1181	60	0.28778	1	0.01
9	0.398	3.27E+04	82.067	25	0.1504	65	0.4561	1	0.01
10	0.631	4.04E+04	64.096	25	0.18617	70	0.7229	1	0.01
11	1	4.94E+04	49.374	25	0.22729	75	1.1457	1	0.01
12	1.58	6.03E+04	38.026	25	0.27744	80	1.8158	1	0.01
13	2.51	7.45E+04	29.679	25	0.34319	85	2.8779	1	0.01
14	3.98	9.45E+04	23.745	25	0.43516	90	4.5612	1	0.01
15	6.31E+00	1.23E+05	19.507	25	0.56659	95	7.2291	1	0.01
16	1.00E+01	1.65E+05	16.483	25	0.75878	100	11.457	1	0.02
17	1.58E+01	2.27E+05	14.311	25	1.0441	105	18.159	1	0.02
18	25.1	3.17E+05	12.626	25	1.46	110	28.78	1	0.03
19	39.8	4.42E+05	11.096	25	2.0335	115	45.613	1	0.04
20	63.1	5.73E+05	9.0765	25	2.6365	120	72.296	1	0.05
21	100	7.09E+05	7.0947	25	3.2662	125	114.58	1	0.06

(a) Upward sweep

Point No.	Shear Rate [s ⁻¹]	Shear Stress [mPa]	Viscosity [Pa·s]	Temperature [°C]	Torque [mN·m]	Time [s]	Rotational Speed [rpm]	Gap [mm]	Normal Force [N]
1	100	6.05E+05	6.0479	25	2.7839	130	114.56	1	0.05
2	63.1	4.02E+05	6.3803	25	1.853	135	72.28	1	0.03
3	39.8	2.91E+05	7.2993	25	1.3375	140	45.604	1	0.02
4	25.1	2.34E+05	9.2998	25	1.0752	145	28.774	1	0.01
5	15.8	1.78E+05	11.261	25	0.82149	150	18.156	1	0
6	10	1.32E+05	13.225	25	0.60879	155	11.456	1	-0.01
7	6.31	9.78E+04	15.497	25	0.45012	160	7.2288	1	-0.01
8	3.98	7.32E+04	18.386	25	0.33696	165	4.5612	1	-0.01
9	2.51	5.57E+04	2.22E+01	25	0.25642	170	2.878	1	-0.01
10	1.58	43106	2.72E+01	25	0.19845	175	1.8159	1	-0.02
11	1	33852	3.39E+01	25	0.15584	180	1.1458	1	-0.02
12	0.631	27036	4.28E+01	25	0.12447	185	0.72293	1	-0.02
13	0.398	21789	5.47E+01	25	0.10031	190	0.45614	1	-0.02
14	0.251	1.77E+04	7.06E+01	25	0.081698	195	0.28781	1	-0.02
15	1.58E-01	14597	9.21E+01	25	0.067201	200	0.1816	1	-0.02
16	1.00E-01	12101	1.21E+02	25	0.055712	205	0.11458	1	-0.02
17	6.31E-02	10105	1.60E+02	25	0.04652	210	0.072297	1	-0.02
18	0.0398	8492	213.29	25	0.039094	215	0.045617	1	-0.02
19	0.0251	7195.2	286.42	25	0.033124	220	0.028782	1	-0.02
20	0.0158	6159.9	388.65	25	0.028358	225	0.018159	1	-0.02
21	0.01	5331.7	533.13	25	0.024546	230	0.011458	1	-0.02

(b) Downward sweep

Table E.2: Viscosity measurement data for 40/60 wt% PTFE-PDMS composite

Point No.	Shear Rate [s ⁻¹]	Shear Stress [mPa]	Viscosity [Pa·s]	Temperature [°C]	Torque [mN·m]	Time [s]	Rotational Speed [rpm]	Gap [mm]	Normal Force [N]
1	0.01	6.16E+04	6.16E+03	25.01	0.28371	25	0.01146	1	0.21
2	0.0158	7.54E+04	4.76E+03	25	0.34721	30	0.018162	1	0.2
3	0.0251	9.16E+04	3.65E+03	25.01	0.4218	35	0.028785	1	0.19
4	0.0398	1.11E+05	2.79E+03	25	0.51143	40	0.045619	1	0.17
5	0.0631	1.33E+05	2.11E+03	25.01	0.61323	45	0.072299	1	0.15
6	0.1	1.57E+05	1566.5	25	0.72115	50	0.11458	1	0.12
7	0.158	1.79E+05	1132.1	25	0.82597	55	0.18159	1	0.1
8	0.251	2.00E+05	796.51	25	0.92102	60	0.2878	1	0.08
9	0.398	2.19E+05	549.68	25	1.0074	65	0.45613	1	0.07
10	0.631	2.39E+05	379.45	25	1.1021	70	0.72291	1	0.07
11	1	2.64E+05	264.38	25	1.217	75	1.1457	1	0.07
12	1.58	2.95E+05	186.14	25	1.358	80	1.8159	1	0.08
13	2.51	3.36E+05	133.61	25	1.5449	85	2.878	1	0.09
14	3.98	3.85E+05	96.597	25	1.7703	90	4.5613	1	0.11
15	6.31E+00	4.46E+05	70.615	25	2.051	95	7.2293	1	0.13
16	1.00E+01	5.22E+05	52.177	25	2.4019	100	11.458	1	0.16
17	1.58E+01	6.10E+05	38.49	25	2.8082	105	18.16	1	0.19
18	25.1	6.95E+05	27.689	25	3.2018	110	28.783	1	0.22
19	39.8	7.80E+05	19.6	25	3.592	115	45.618	1	0.21
20	63.1	9.87E+05	15.64	25	4.5429	120	72.301	1	0.24
21	100	1.41E+06	14.106	25	6.4936	125	114.59	1	0.26

(a) Upward sweep

Point No.	Shear Rate [s ⁻¹]	Shear Stress [mPa]	Viscosity [Pa·s]	Temperature [°C]	Torque [mN·m]	Time [s]	Rotational Speed [rpm]	Gap [mm]	Normal Force [N]
1	100	1.64E+06	16.415	25	7.5552	130	114.56	1	0.2
2	63.1	8.55E+05	13.555	25	3.9373	135	72.299	1	0.18
3	39.8	5.10E+05	12.816	25	2.3485	140	45.61	1	0.11
4	25.1	3.82E+05	15.204	25	1.7578	145	28.776	1	0.1
5	15.8	2.60E+05	16.377	25	1.1949	150	18.159	1	0.07
6	10	1.78E+05	17.818	25	0.82011	155	11.456	1	0.06
7	6.31	1.36E+05	21.597	25	0.6274	160	7.23	1	0.02
8	3.98	9.48E+04	23.804	25	0.43625	165	4.5612	1	0.01
9	2.51	8.45E+04	3.36E+01	25	0.3889	170	2.878	1	0.02
10	1.58	75890	4.79E+01	25	0.34938	175	1.8159	1	0.01
11	1	69051	6.90E+01	25	0.31789	180	1.1458	1	0.01
12	0.631	62561	9.91E+01	25	0.28801	185	0.72297	1	0
13	0.398	56769	1.43E+02	25	0.26135	190	0.45617	1	0
14	0.251	5.20E+04	2.07E+02	25	0.23944	195	0.28783	1	-0.01
15	1.59E-01	47996	3.03E+02	25	0.22096	200	0.18161	1	-0.01
16	1.00E-01	44481	4.45E+02	25	0.20478	205	0.11459	1	-0.01
17	6.31E-02	41301	6.55E+02	25	0.19014	210	0.0723	1	-0.01
18	0.0398	38350	963.2	25	0.17655	215	0.045618	1	-0.01
19	0.0251	35501	1413.2	25	0.16344	220	0.028783	1	-0.01
20	0.0159	32740	2065.6	25	0.15073	225	0.018161	1	-0.01
21	0.01	30044	3004.2	25	0.13832	230	0.011459	1	-0.01

(b) Downward sweep

Table E.3: Viscosity measurement data for 50/50 wt% PTFE-PDMS composite

Point No.	Shear Rate [s ⁻¹]	Shear Stress [mPa]	Viscosity [Pa·s]	Temperature [°C]	Torque [mN·m]	Time [s]	Rotational Speed [rpm]	Gap [mm]	Normal Force [N]
1	0.01	5.76E+05	5.76E+04	25	2.6539	25	0.011467	1.001	1.2
2	0.0158	6.55E+05	4.13E+04	25	3.0141	30	0.018172	1.001	1.14
3	0.0251	7.44E+05	2.96E+04	25	3.4266	35	0.0288	1.001	1.05
4	0.0398	8.43E+05	2.12E+04	25	3.8822	40	0.045642	1.001	0.93
5	0.0631	9.49E+05	1.50E+04	25	4.3709	45	0.072333	1	0.79
6	0.1	1.06E+06	10598	25	4.8794	50	0.11463	1	0.65
7	0.158	1.15E+06	7272.3	25	5.3064	55	0.18166	1	0.55
8	0.251	1.21E+06	4811.5	25	5.5642	60	0.28789	1	0.44
9	0.398	1.22E+06	3065.3	25	5.6183	65	0.45625	1	0.32
10	0.631	1.16E+06	1839.1	25	5.3411	70	0.72304	1	0.52
11	1	1.16E+06	1161.8	25	5.3472	75	1.1461	1.001	0.9
12	1.58	1.01E+06	638.51	25	4.6576	80	1.8168	1.001	1.23
13	2.51	8.89E+05	353.94	25	4.0913	85	2.8805	1.001	2.04
14	3.98	8.41E+05	211.17	25	3.8702	90	4.5662	1.001	1.77
15	6.31E+00	8.34E+05	132.17	25	3.8418	95	7.2372	1	0.69
16	1.00E+01	8.04E+05	80.385	25	3.7011	100	11.464	1	0.68
17	1.58E+01	6.70E+05	42.249	25	3.0828	105	18.162	1	0.17
18	25.1	7.96E+05	31.674	25	3.6623	110	28.78	1	0.24
19	39.8	1.12E+06	28.08	25	5.1464	115	45.62	1	0.24
20	63.1	1.13E+06	17.966	25	5.2187	120	72.301	1	0.16
21	100	1.24E+06	12.38	25	5.6987	125	114.58	1	0.24

(a) Upward sweep

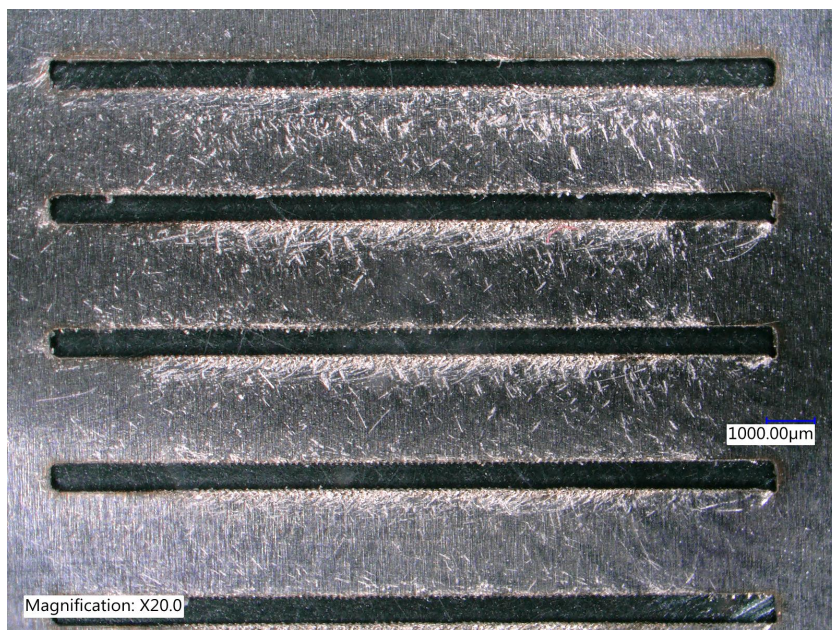
Point No.	Shear Rate [s ⁻¹]	Shear Stress [mPa]	Viscosity [Pa·s]	Temperature [°C]	Torque [mN·m]	Time [s]	Rotational Speed [rpm]	Gap [mm]	Normal Force [N]
1	100	1.37E+06	13.668	25	6.2909	130	114.57	1	0.24
2	63.1	9.55E+05	15.144	25	4.3979	135	72.283	1	0.15
3	39.8	6.74E+05	16.947	25	3.1051	140	45.606	1	0.14
4	25.1	5.52E+05	21.993	25	2.5432	145	28.782	1	0.12
5	15.8	4.07E+05	25.71	25	1.8759	150	18.16	1	0.08
6	10	3.10E+05	31.051	25	1.4294	155	11.457	1	0.06
7	6.31	2.55E+05	40.469	25	1.1756	160	7.2302	1	0.06
8	3.98	2.11E+05	52.965	25	0.9705	165	4.5605	1	0.05
9	2.51	2.37E+05	9.42E+01	25	1.0899	170	2.8786	1	0.02
10	1.59	1.62E+05	1.02E+02	25	0.7438	175	1.8161	1	0.02
11	1	1.43E+05	1.43E+02	25	0.65627	180	1.1458	1	0.04
12	0.631	1.37E+05	2.18E+02	25	0.63254	185	0.72301	1	0.02
13	0.398	1.27E+05	3.18E+02	25	0.5832	190	0.45618	1	0.01
14	0.251	1.17E+05	4.66E+02	25	0.53909	195	0.28783	1	0
15	1.59E-01	1.10E+05	6.97E+02	25	0.50826	200	0.18161	1	0
16	1.00E-01	1.05E+05	1.05E+03	25	0.48543	205	0.11459	1	0
17	6.31E-02	1.02E+05	1.61E+03	25	0.46822	210	0.0723	1	0
18	0.0398	98142	2465	25	0.45182	215	0.045617	1	0
19	0.0251	94552	3763.9	25	0.43529	220	0.028782	1	-0.01
20	0.0158	91082	5746.6	25	0.41931	225	0.01816	1	-0.01
21	0.01	87574	8757.5	25	0.40316	230	0.011457	1	-0.01

(b) Downward sweep

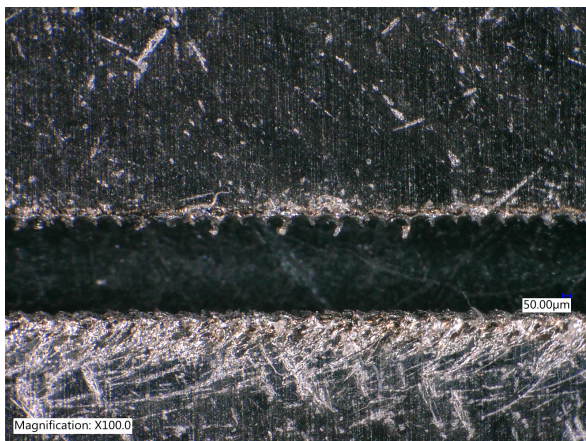
Table E.4: Viscosity measurement data for 60/40 wt% PTFE-PDMS composite

F

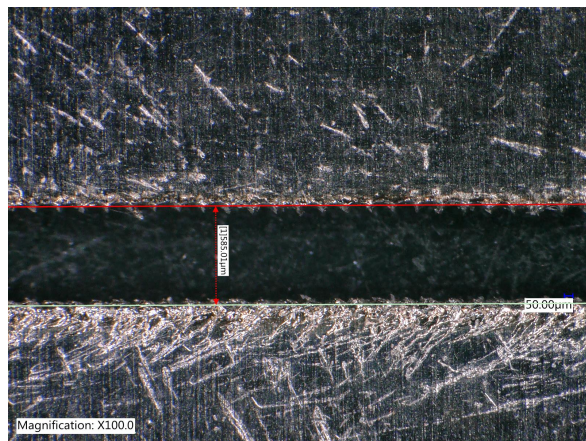
Stencil Pictures



(a) overview



(b) Detail, poor line definition

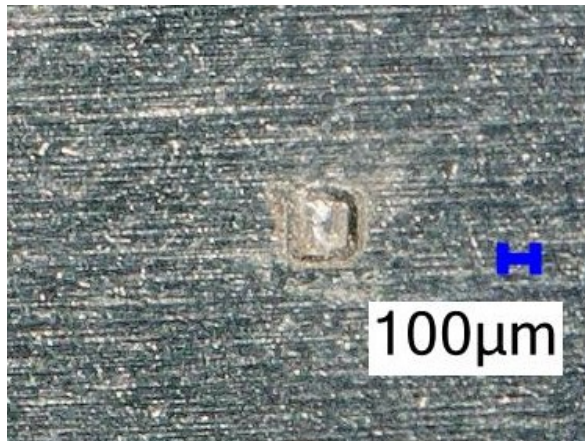


(c) Width

Figure F.1: Stencil with main design, laser-cut by IWS 3ME



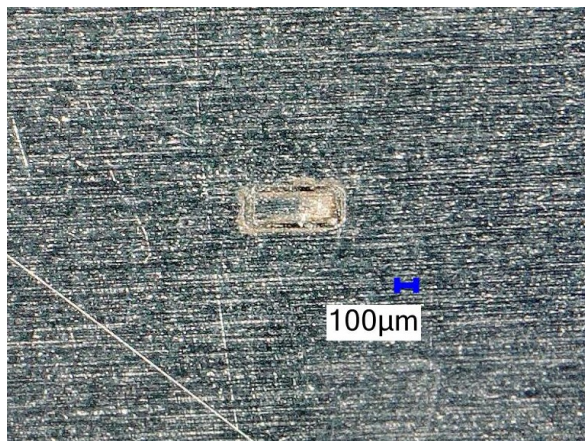
(a) Overview



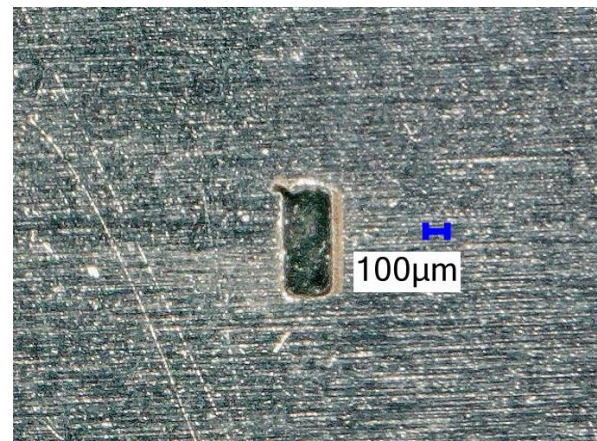
(b) Detail 1, aperture not cut



(c) Detail 2, aperture not cut

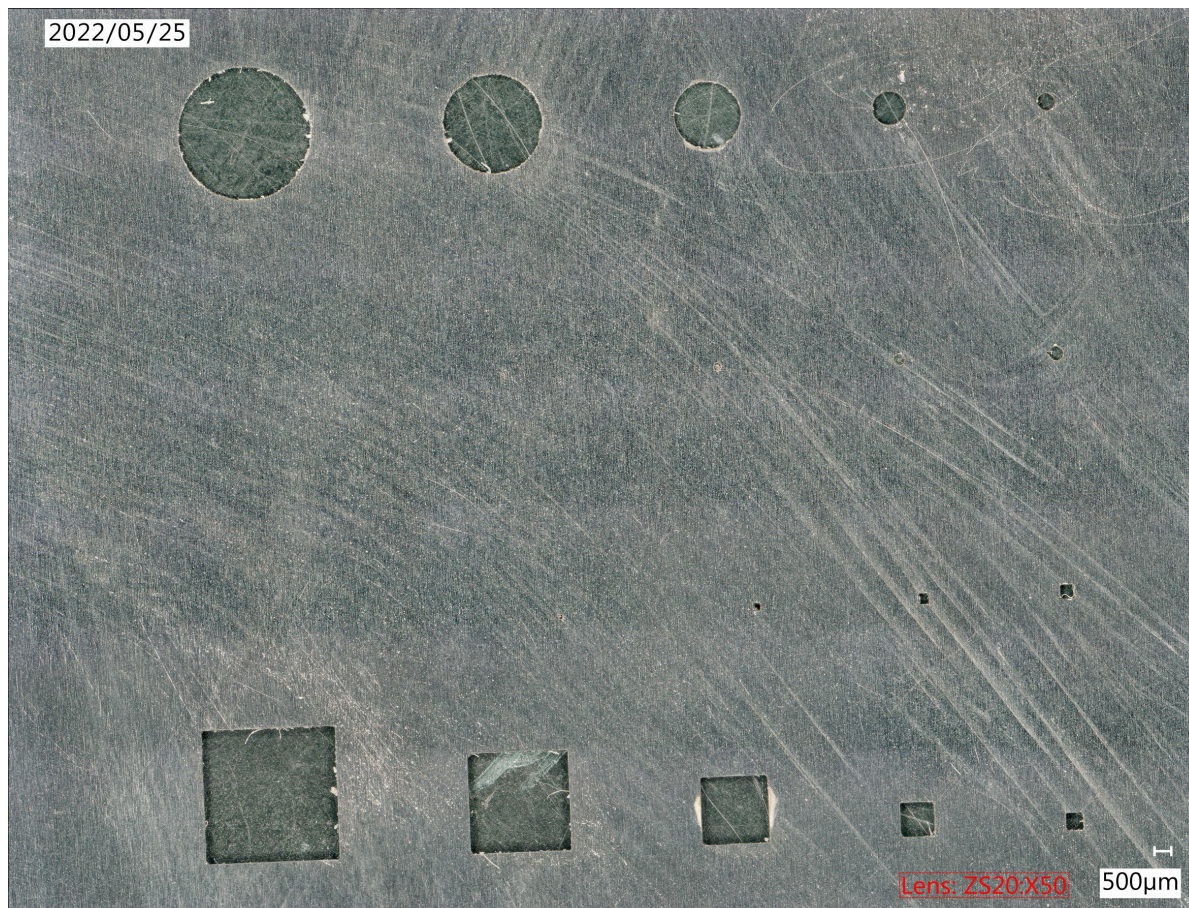


(d) Detail 3, aperture not cut

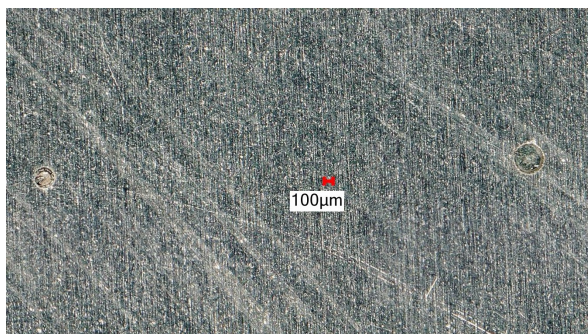


(e) Detail 4

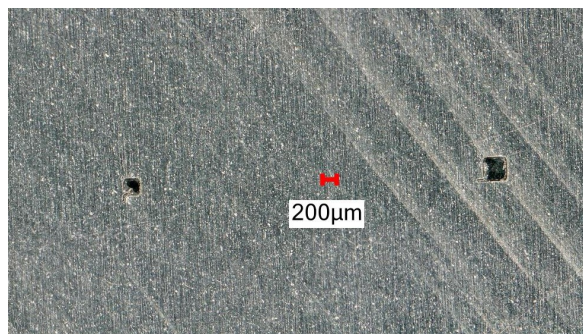
Figure E2: First test stencil, laser-cut on *Lasea* laser-cutter at the PME lab



(a) Overview



(b) Detail 1, smallest apertures not cut

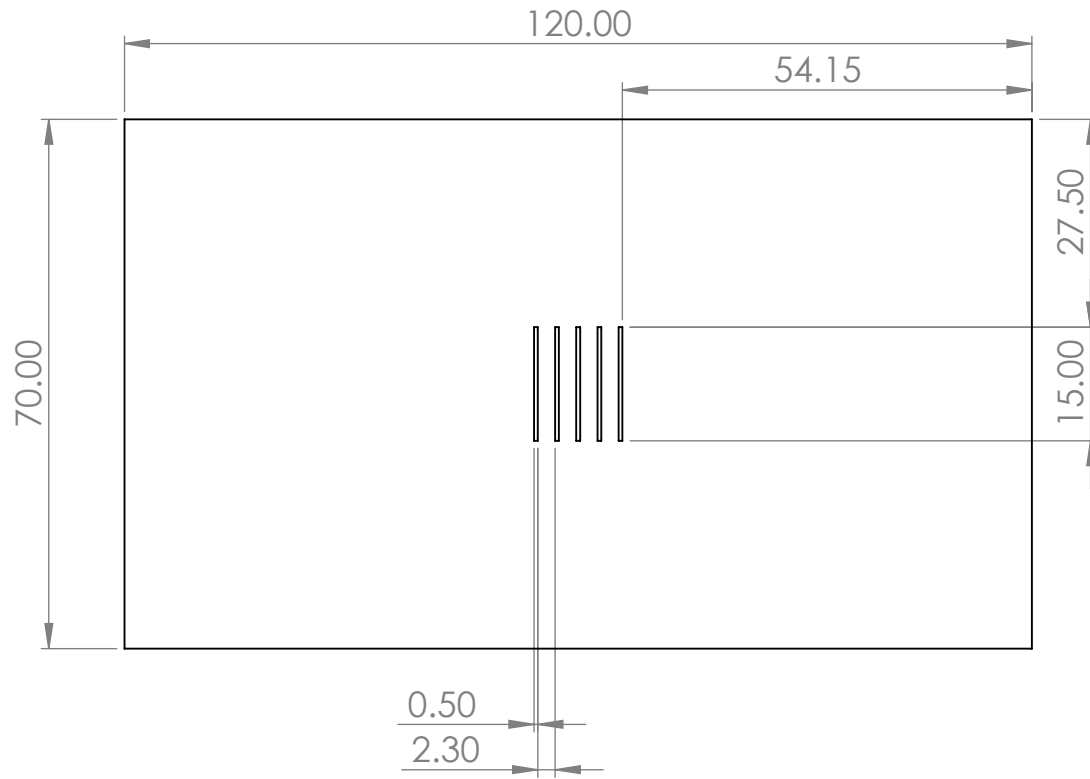


(c) Detail 2, smallest apertures cut

Figure E3: Second test stencil, laser-cut on *Lasea* laser-cutter at the PME lab

G

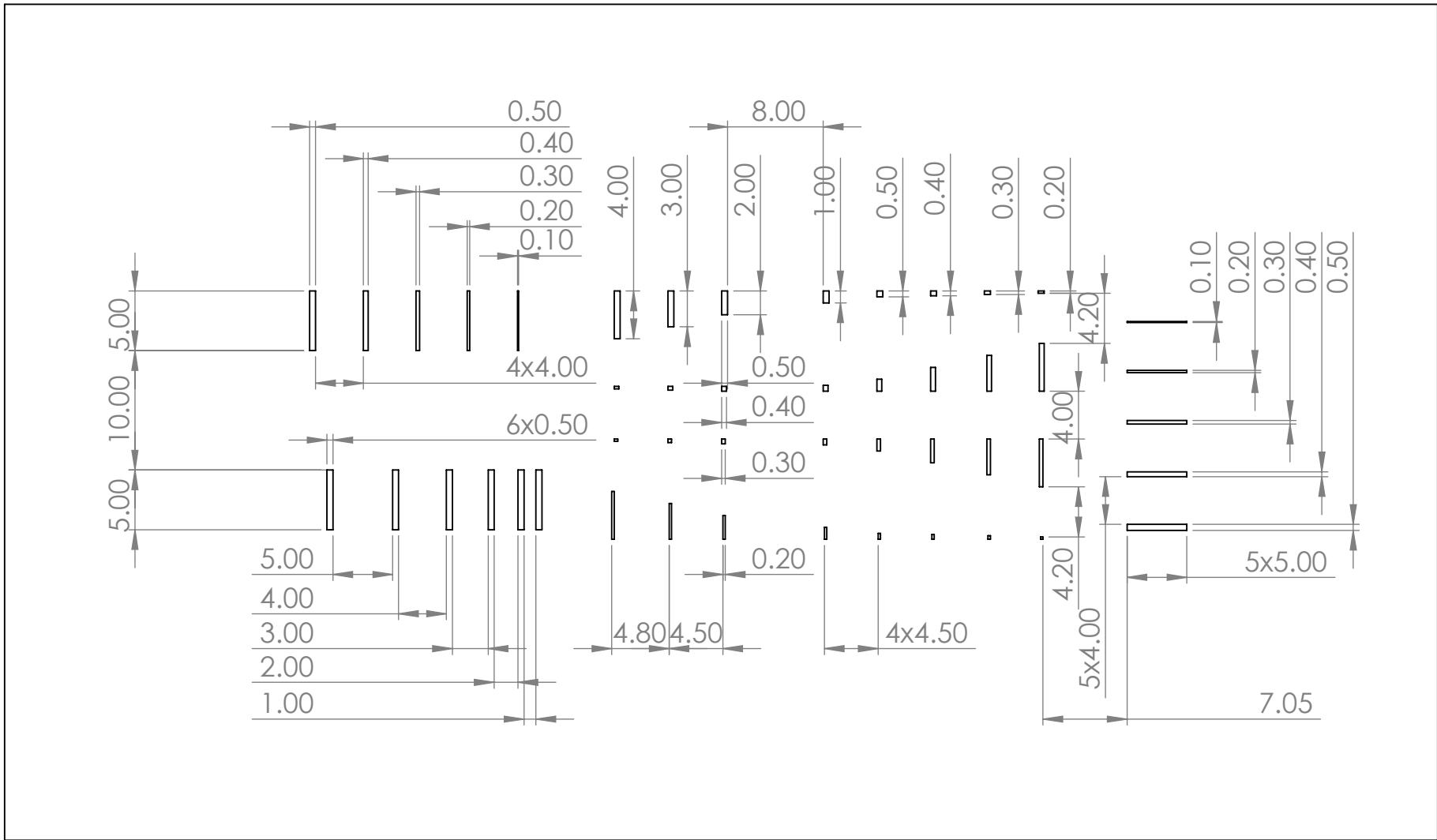
Technical Drawings



name **Stencil**

C:\Users\stan_\OneDrive\Documenten\TU Delft\Master\2020-2021\Thesis\nonliteratuur\SW Model\Stencil

	units	mm	scale	1:1	quantity	1	date	24-5-2022	remark	-
	material					mass	gr			
	author	C.C.H. Otte - 4488407			group	-	format	A4	drawing no.	1



name

Stencil

C:\Users\stan_OneDrive\Documenten\TU Delft\Master\2020-2021\Thesis\nonliteratuur\SW Model\Stencil



units mm

scale 2:1

quantity 1

date 24-5-2022

remark -

material

mass gr

author C.C.H. Otte - 4488407

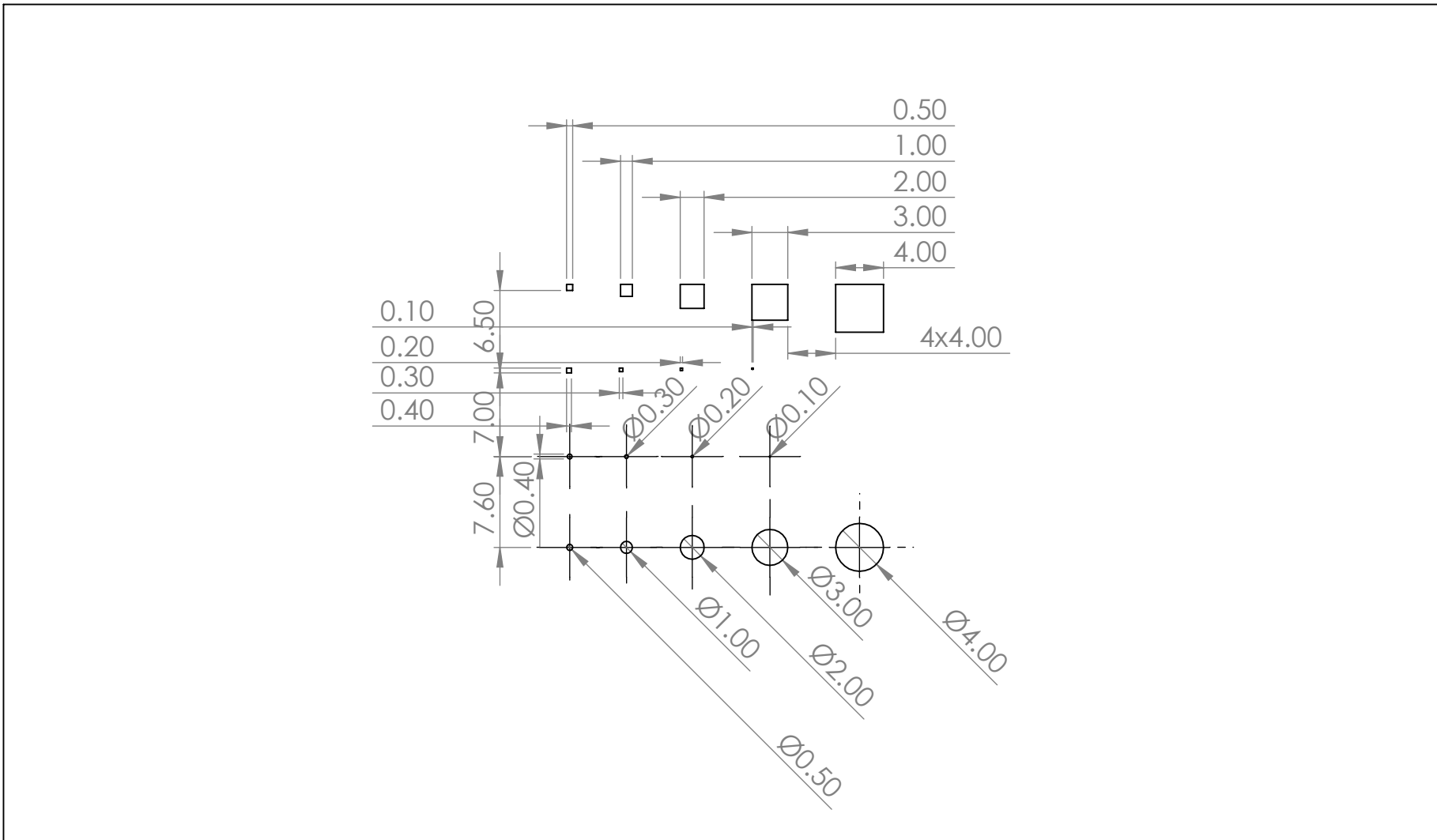
group -

format

A4

drawing no.

2



name

Stencil

C:\Users\stan_\OneDrive\Documenten\TU Delft\Master\2020-2021\Thesis\nonliteratuur\SW Model\Stencil



units mm

scale 2:1

quantity 1

date 24-5-2022

remark -

material

mass gr

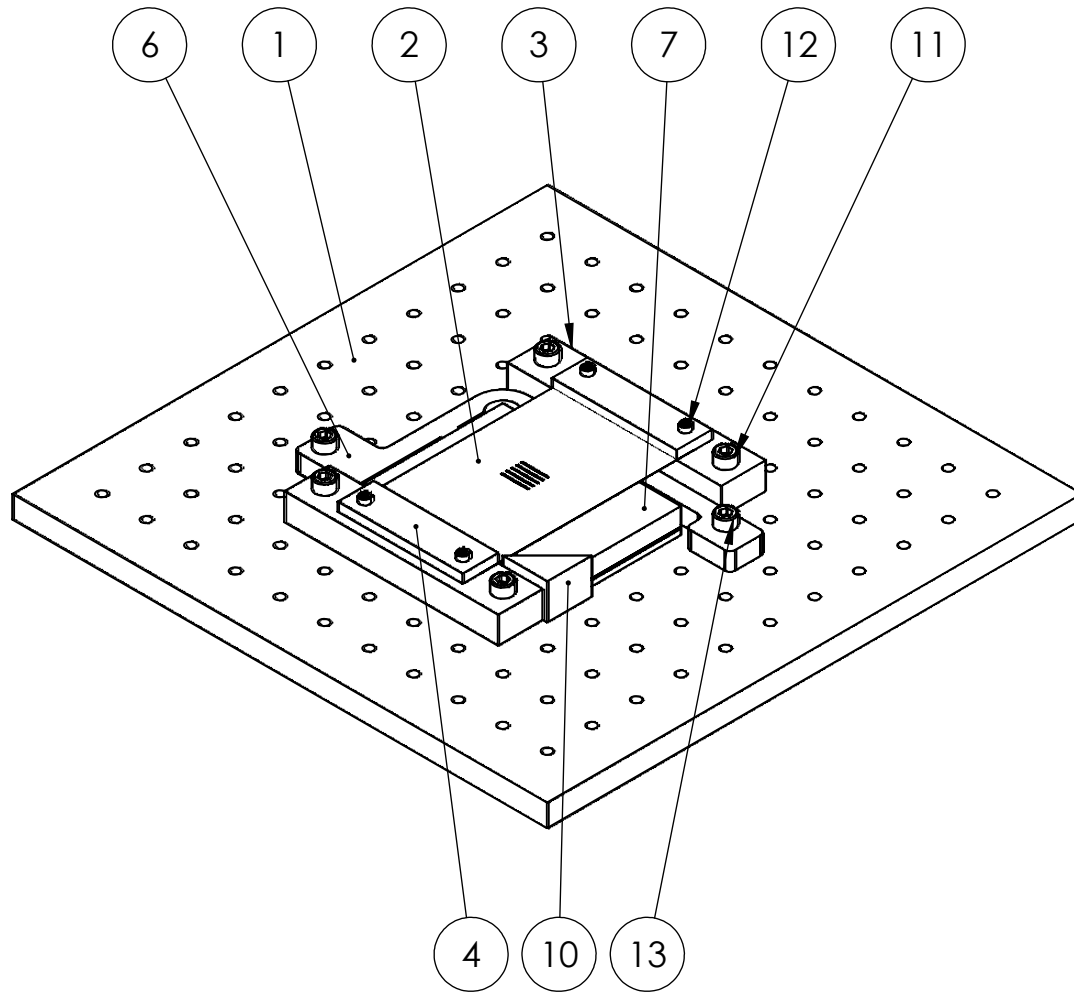
author C.C.H. Otte - 4488407

group -

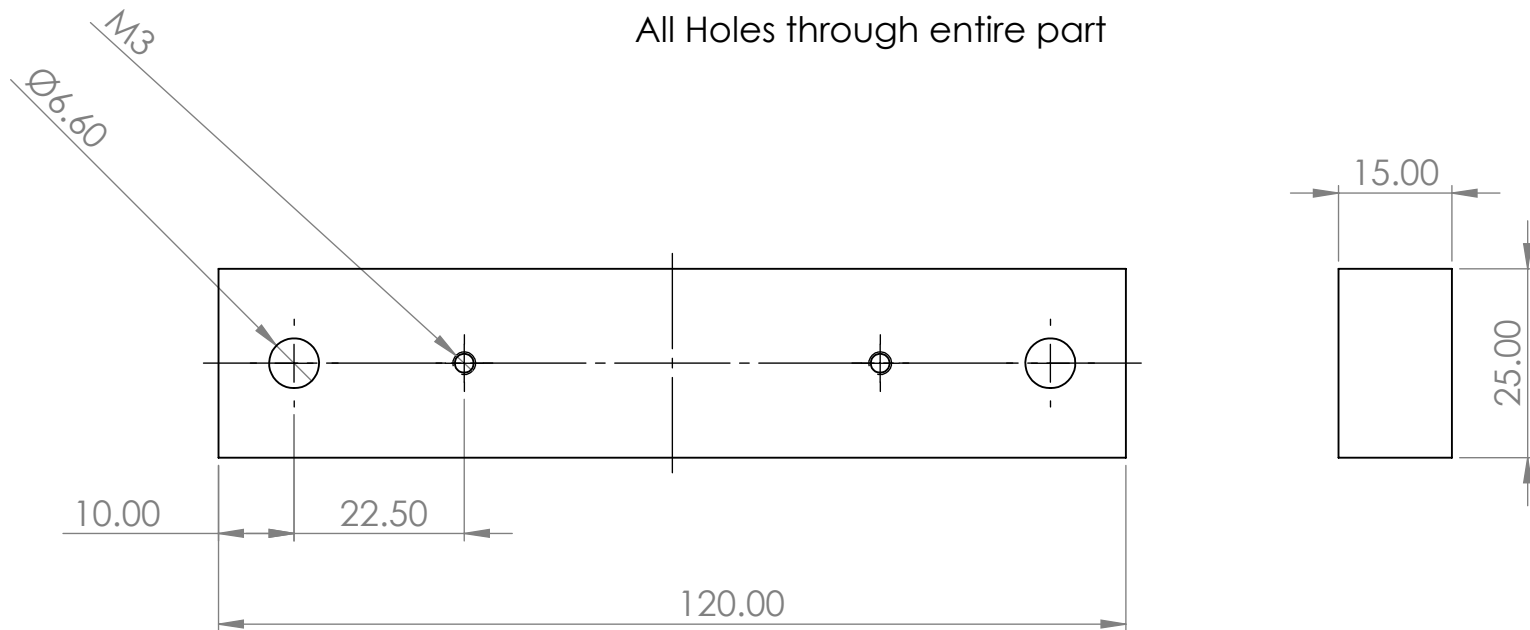
format

A4

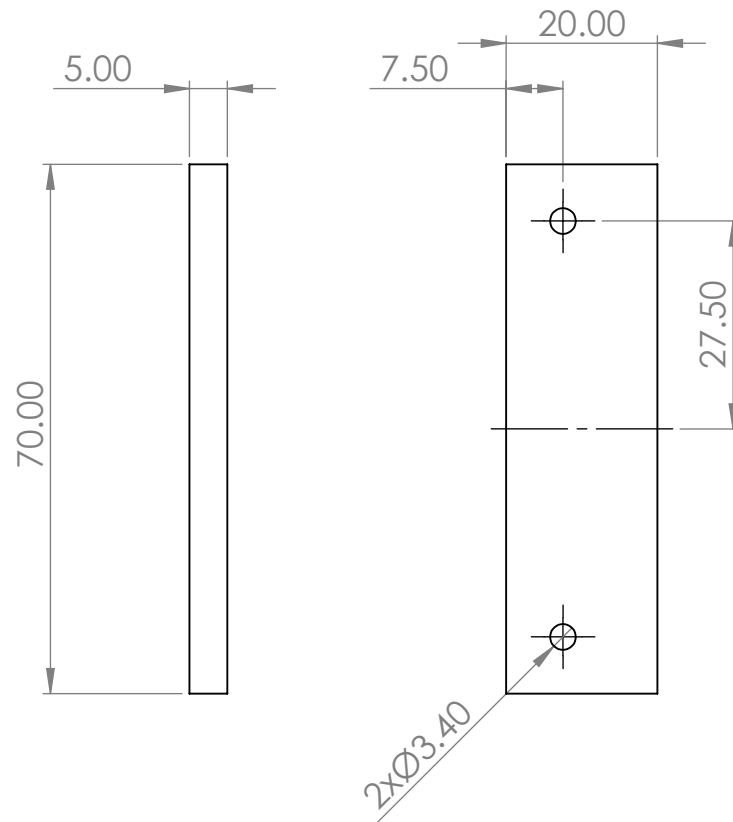
drawing no. 3



ITEM NO.	PART NUMBER	QTY.
1	StencilPrinterV4_Breadbord	1
2	StencilPrinterDraft_Stencil	1
3	StencilPrinterV4_BottomStencilHolder	2
4	StencilPrinterDraft_StencilHolder	2
6	StencilPrinter_AlignWall	1
7	StencilPrinter_AlignmentPlateV2	1
10	StencilPrinterV4_NestingTriangle	1
11	EN ISO 4762 M6 x 30 - 24N	4
12	EN ISO 4762 M3 x 6 - 6N	4
13	EN ISO 4762 M6 x 10 - 10N	2



		units mm	scale 1:1	quantity 2	date 24-5-2022	remark -
material					mass gr	
author C.C.H. Otte - 4488407				group -	format A4	drawing no. 3



All holes through entire part



name
StencilPrinter

C:\Users\stan_\OneDrive\Documenten\TU
Delft\Master\2020-
2021\Thesis\nonliteratuur\SW Model\Stencil
Printer



units mm scale 1:1

quantity 2

date 24-5-2022

remark -

material

mass gr

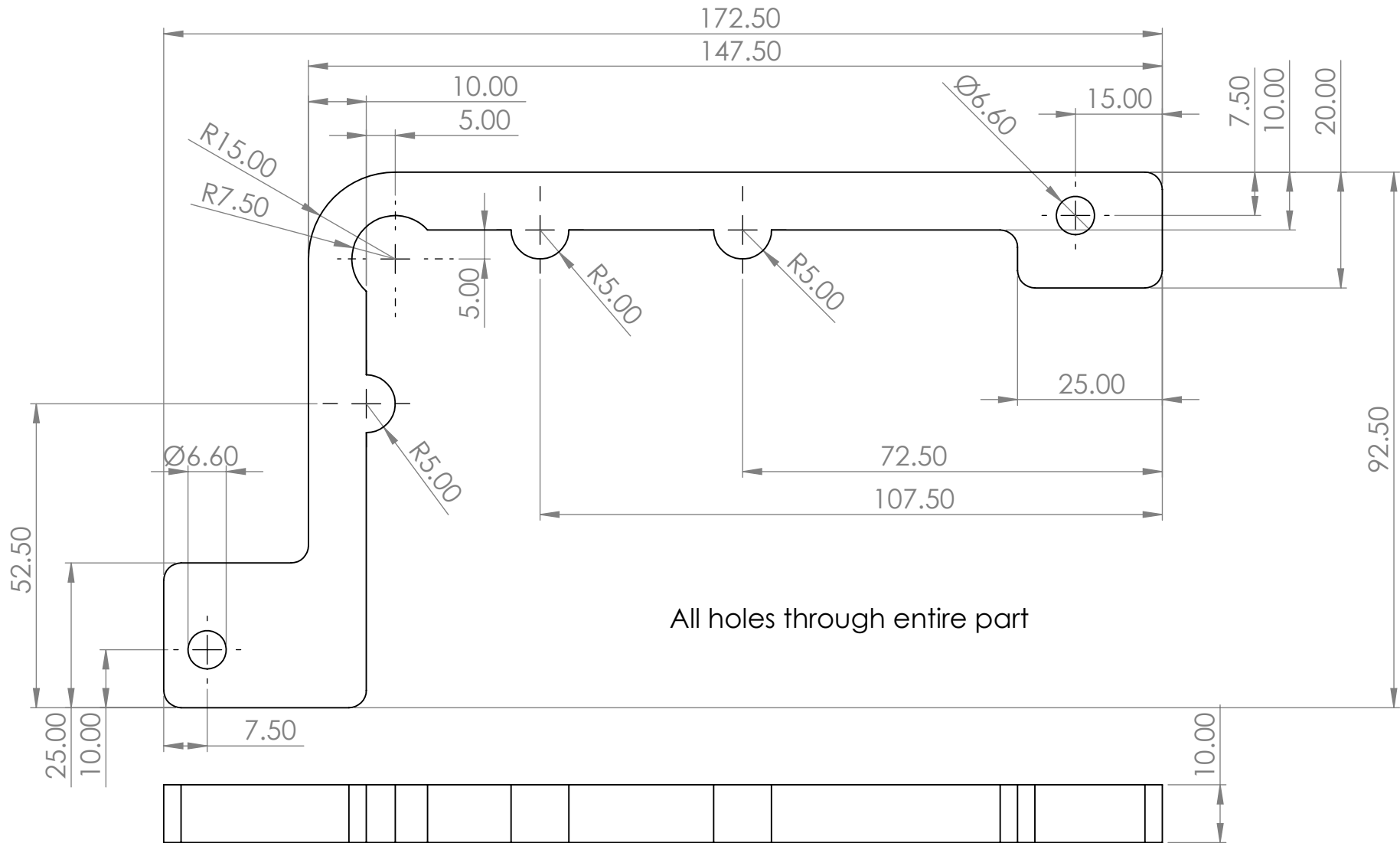
author C.C.H.Otte - 4488407

group -

format

drawing no. 4

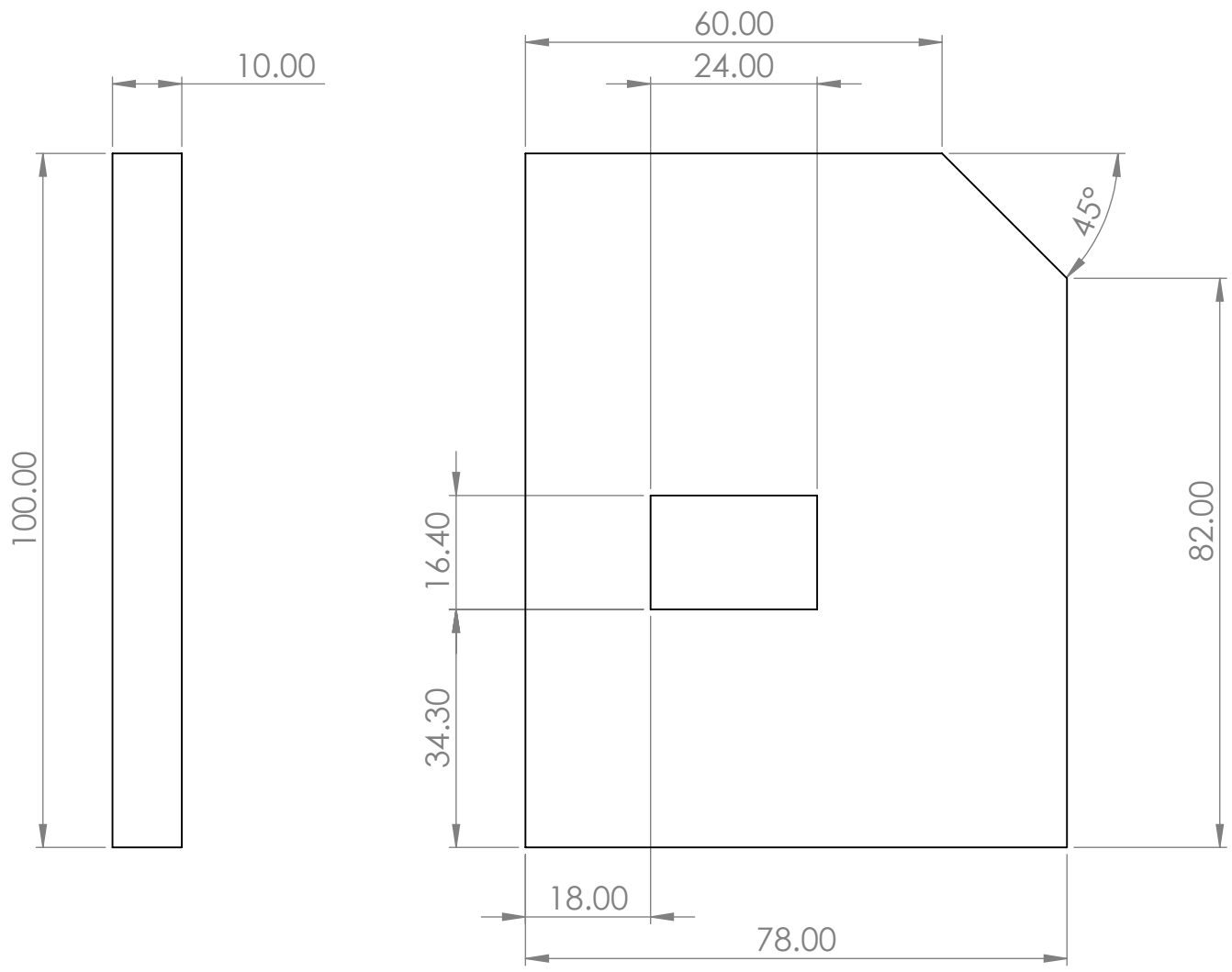
A4



name
StencilPrinter

C:\Users\stan_OneDrive\Documenten\TU Delft\Master\2020-2021\Thesis\nonliteratuur\SW Model\Stencil Printer

	units mm	scale 1:1	quantity 1	date 24-5-2022	remark -
material				mass gr	
author C.C.H. Otte - 4488407	group -	format A4		drawing no. 6	



name
StencilPrinter

C:\Users\stan_OneDrive\Documenten\TU Delft\Master\2020-2021\Thesis\nonliteratuur\SW Model\StencilPrinter



units
mm

scale
1:1

quantity
1

date
24-5-2022

remark
-

material

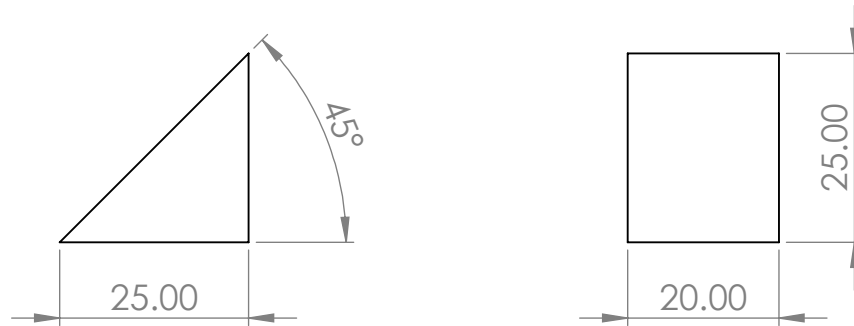
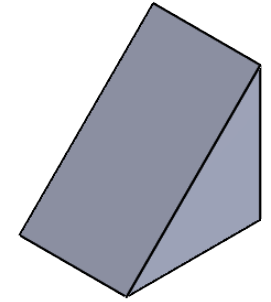
mass
gr

author C.C.H. Otte - 4488407

group
-

format
A4

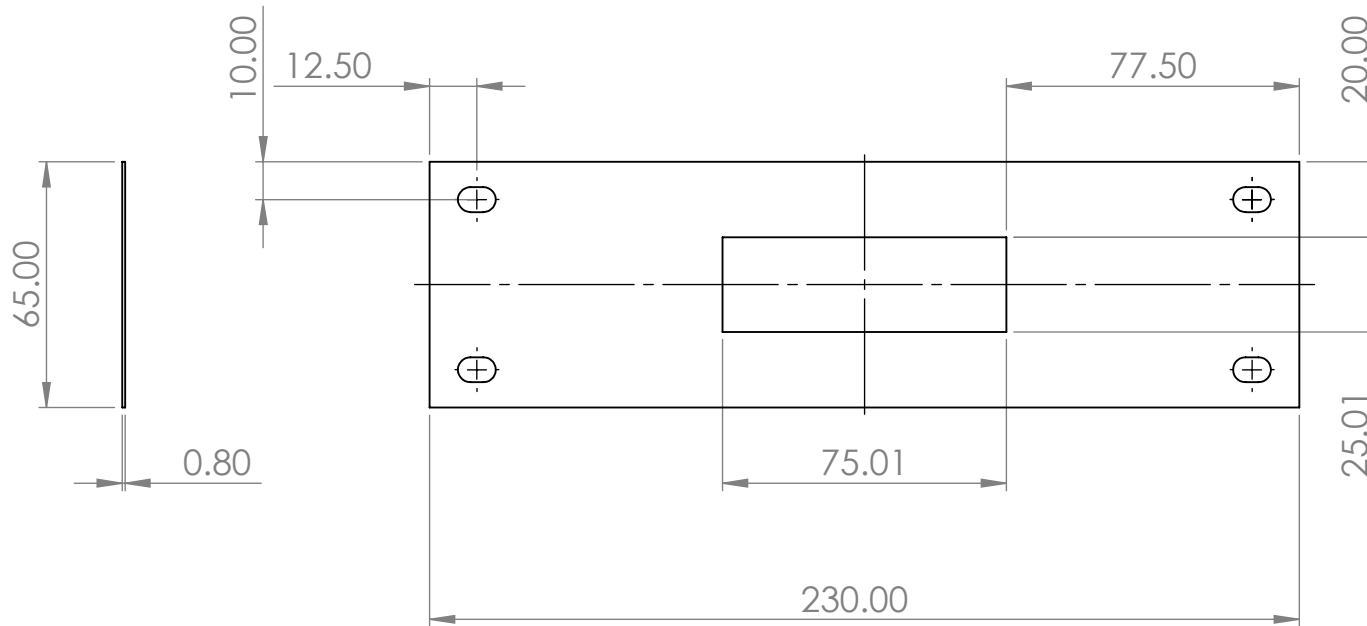
drawing no.
7

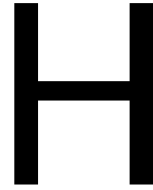


name
StencilPrinter

C:\Users\stan_\OneDrive\Documenten\TU Delft\Master\2020-2021\Thesis\nonliteratuur\SW Model\StencilPrinter

	units mm	scale 1:1	quantity 1	date 24-5-2022	remark -
material				mass gr	
author C.C.H. Otte - 4488407	group -	format A4	drawing no. 10		





Matlab Code

H.1. Viscosity of PDMS PTFE Mixtures

```
% Stan Otte 4488407
% written for the Msc. thesis at TU Delft, PME department
% goal: Determine mean and standard deviation of the width
% for PTFE-PDMS mix stencil print lines
clear all; close all; clc;

%% importing excel tables
% 100 wt%PDMS 0wt%PTFE
shear0up = readmatrix('native PDMS 2e poging.xlsx','Sheet','oplopend','
    Range','B2:B22');
vis0up = readmatrix('native PDMS 2e poging.xlsx','Sheet','oplopend','
    Range','D2:D22');
shear0down = readmatrix('native PDMS 2e poging.xlsx','Sheet','aflopend'
    , 'Range','B2:B22');
vis0down = readmatrix('native PDMS 2e poging.xlsx','Sheet','aflopend','
    Range','D2:D22');

shear50up = readmatrix('PDMSPTFE5050-poging2.xlsx','Sheet','oplopend','
    Range','B2:B22');
vis50up = readmatrix('PDMSPTFE5050-poging2.xlsx','Sheet','oplopend','
    Range','D2:D22');
shear50down = readmatrix('PDMSPTFE5050-poging2.xlsx','Sheet','aflopend'
    , 'Range','B2:B22');
vis50down = readmatrix('PDMSPTFE5050-poging2.xlsx','Sheet','aflopend','
    Range','D2:D22');

% 60wt%PDMS 40%PTFE
shear60up = readmatrix('PDMSPTFE6040.xlsx','Sheet','oplopend','Range','
    B2:B22');
vis60up = readmatrix('PDMSPTFE6040.xlsx','Sheet','oplopend','Range','D2
    :D22');
shear60down = readmatrix('PDMSPTFE6040.xlsx','Sheet','aflopend','Range'
    , 'B2:B22');
vis60down = readmatrix('PDMSPTFE6040.xlsx','Sheet','aflopend','Range','
    D2:D22');

% 40wt%PDMS 60%PTFE
```

```

shear40up = readmatrix('PDMSPTFE4060.xlsx','Sheet','oplopend','Range','
    B2:B22');
vis40up = readmatrix('PDMSPTFE4060.xlsx','Sheet','oplopend','Range','D2
    :D22');
shear40down = readmatrix('PDMSPTFE4060.xlsx','Sheet','aflopend','Range'
    ,'B2:B22');
vis40down = readmatrix('PDMSPTFE4060.xlsx','Sheet','aflopend','Range','
    D2:D22');

tau50up = readmatrix('PDMSPTFE5050-poging2.xlsx','Sheet','oplopend','
    Range','C2:C22');
tau0up = readmatrix('native PDMS 2e poging.xlsx','Sheet','oplopend','
    Range','C2:C22');

%% plot
figure(1)
% hold on
loglog(shear0up,vis0up,'rx',shear0down,vis0down,'r+',...
    shear50up,vis50up,'bx',shear50down,vis50down,'b+',...
    shear60up,vis60up,'kx',shear60down,vis60down,'k+',...
    shear40up,vis40up,'mx',shear40down,vis40down,'m+',...
    ,'LineWidth',1,'MarkerSize',8)
grid on
legend('native PDMS upward sweep','native PDMS downward sweep',...
    '50/50wt% PTFE-PDMS upward sweep','50/50wt% PTFE-PDMS downward
    sweep',...
    '40/60wt% PTFE-PDMS upward sweep','40/60wt% PTFE-PDMS downward
    sweep',...
    '60/40wt% PTFE-PDMS upward sweep','60/40wt% PTFE-PDMS downward
    sweep'...
    )
ylabel('Viscosity [Pa\cdots]')
xlabel('Shear rate [1/s]')

```

H.2. Temperature Influence

```

% Stan Otte 4488407
% written for the Msc. thesis at TU Delft, PME department
% goal: Determine mean and standard deviation of droplet radii with
    heated
% and room temperature substrate
clear all; close all; clc;

%% establishing radius vectors

rPDMSshot = [1244,1444,1393,1123,1340,1313,1189];
rGLASSshot = [1408,1517,1453,1500];

rPDMSroom = [2421,2167,2632,2258,1907,2027];
rGLASSroom = [2730,3592,1970,2252];

%% calculation
rPDMSshotmean = mean(rPDMSshot);
rPDMSshotstd = std(rPDMSshot);
rGLASSshotmean = mean(rGLASSshot);
rGLASSshotstd = std(rGLASSshot);

```

```

rPDMSroommean = mean(rPDMSroom);
rPDMSroomstd = std(rPDMSroom);
rGLASSroommean = mean(rGLASSroom);
rGLASSroomstd = std(rGLASSroom);

%making matrix with all values
rmean = [rPDMSshotmean,rGLASSshotmean;rPDMSroommean,rGLASSroommean];
rstd = [rPDMSshotstd,rGLASSshotstd;rPDMSroomstd,rGLASSroomstd];

%% plot

bar(rmean,0.3) %setting bar thickness
set(gca,'XTickLabel',{'150~{\circ}C','room temperature'}); %label
hold on
ngroups = size(rmean,1);
nbars = size(rmean,2);
groupwidth = min(0.8, nbars/(nbars + 1.5));

for i = 1:nbars %manual bar+error graph creation
    x = (1:ngroups) - groupwidth/2 + (2*i-1) * groupwidth / (2*nbars);
    er = errorbar(x, rmean(:,i), rstd(:,i), '.');
    er.Color = [0 0 0];
    er.LineStyle = 'none';
    er.LineWidth = 1;
end
ylabel('mean radius of droplets [\mu m]');
legend('PDMS substrate','Glass substrate','location','northwest')
title('Spreading behaviour of 5 \mu L PDMS droplets')
hold off

```

H.3. Influence of Snap-off Height and Number of Squeegee Passes

```

% Stan Otte 4488407
% written for the Msc. thesis at TU Delft, PME department
% goal: Determine mean and standard deviation of the width for PTFE-
      PDMS
% mix stencil print lines
clear all; close all; clc;

%% establishing width vectors
w_snap = [660,631,597,670,586];
w_nosnap = [704,684,697,650,682];
w_snapmulstro = [816,581,582,590,722];

%% calculation

mean_nosnap = mean(w_nosnap);
std_nosnap = std(w_nosnap);

mean_snap = mean(w_snap);
std_snap = std(w_snap);

mean_snapmulstro = mean(w_snapmulstro);
std_snapmulstro = std(w_snapmulstro);

rmean = [mean_nosnap,mean_snap,mean_snapmulstro];
rstd = [std_nosnap,std_snap,std_snapmulstro];

```

```

%% plot

bar(rmean,0.3)
set(gca,'XTickLabel',{'no snap-off','snap-off','snap-off multiple pulls
  '});
hold on
er = errorbar(rmean,rstd);
er.Color = [0 0 0];
er.LineStyle = 'none';
er.LineWidth = 2.0;
ylabel('mean width of lines [\mum]');

hold off

```

H.4. Stencil Geometry

```

% Stan Otte 4488407
% written for the Msc. thesis at TU Delft, PME department
% goal: determine influence of the stencil geometry
clear all; close all; clc;
%% parameters
syms eta nu a
% l = 1e-3; % [m] Length of holes in stencil
% w = 0.5e-3; % [m] Width of holes in stencil
l = (0.05:0.01:1)*1e-3; % [m] Length of holes in stencil
w = (0.05:0.01:1)*1e-3; % [m] Width of holes in stencil
r = (0.05:0.01:1)*1e-3; % [m] radius of a circular aperture
t = 0.10e-3; % [m] thickness stencil
% t = (0.05:0.01:0.2)*1e-3;
%% equations
%related geomtry parameters
% Awall = 2*t.*(l+w); % [m^2] area of the sidewalls of hole
% Apad = l.*w; % [m^2] area of hole
Fd = 6*pi*eta*nu*a*0.67; % [N] average drag force of stencil on
print material
Fp = 6*pi*eta*nu*a*3.92; % [N] average pull force of subrate on
print material
% ArRat = Apad./Awall; % [m^2] area ratio: ratio between side
wall area and hole area
% AsRat = w./t; % [m^2] aspect ratio: ratio between
width of hole and thickness
% w_optAAR = w(find(ArRat>1.5,1))
% w_optAR = w(find(AsRat>0.6,1))
for i=1:length(l)
    for j=1:length(w)
        Awall(i,j) = 2*t*(l(i)+w(j)); % [m^2] area of the sidewalls of
hole
        Apad(i,j) = l(i)*w(j); % [m^2] area of hole
        ArRat(i,j) = Apad(i,j)/Awall(i,j); % [m^2] area ratio: ratio between
side wall area and hole area
        AsRat(i,j) = w(j)/t; % [m^2] aspect ratio: ratio
between width of hole and thickness
    end
end
end

for k=1:length(r)

```

```

        ArRatCirc(k) = r(k)/(2*t);
    end
    r_opt = r(find(ArRatCirc>0.6,1))
    %% R (for different variable parameters)
    % R = NaN(length(l),length(w),length(t));
    % R = NaN(length(w),length(t));
    % R = NaN(length(l),length(t));
    R = NaN(length(l), length(w));
    % for i=1:length(l)
    %     for j=1:length(w)
    %         for k=1:length(t)
    % Awall(i,j,k) = 2*t(k)*(l(i)+w(j));
    % Apad(i,j,k) = l(i)*w(j);
    % R(i,j,k) = (Awall(i,j)*Fd)/(Apad(i,j)*Fp);
    %         end
    %     end
    % end
    for i=1:length(l)
        for j=1:length(w)
            Awall(i,j) = 2*t*(l(i)+w(j));
            Apad(i,j) = l(i)*w(j);
            R(i,j) = (Awall(i,j)*Fd)/(Apad(i,j)*Fp);
        end
    end
    % for i=1:length(l)
    %     for k=1:length(t)
    % Awall(i,k) = 2*t(k)*(l(i)+w);
    % Apad(i,k) = l(i)*w;
    % R(i,k) = (Awall(i)*Fd)/(Apad(i)*Fp);
    %     end
    % end
    %     for j=1:length(w)
    %         for k=1:length(t)
    % Awall(j,k) = 2*t(k)*(l+w(j));
    % Apad(j,k) = l*w(j);
    % R(j,k) = (Awall(j,k)*Fd)/(Apad(j,k)*Fp);
    %         end
    %     end
    % R = double(R);
    %% graph2
    grid on

    figure(1)
    grid on
    surf(l,w,R)
    ylabel('length of aperture [m]')
    xlabel('width of aperture [m]')
    zlabel('R ratio between drag and pull [-]')
    %colorbar

    figure(2)
    hold on
    grid on
    surf(l,w,ArRat)
    Ar = ones(length(l),length(w))*0.6;
    surf(l,w,Ar,'FaceColor','red','LineStyle','none','EdgeColor','none')

```



```
ylabel('length of aperture [m]')
xlabel('width of aperture [m]')
zlabel('Area Aspect Ratio [-]')
%legend('relation','minimum ratio value')
%colorbar
hold off

figure(3)
hold on
grid on
surf(l,w,AsRat)
As = ones(length(l),length(w))*1.5;
surf(l,w,As,'FaceColor','red','LineStyle','none','EdgeColor','none')
ylabel('length of aperture [m]')
xlabel('width of aperture [m]')
zlabel('Aspect Ratio [-]')
%legend('relation','minimum ratio value')
%colorbar
hold off

figure(4)
hold on
grid on
ArC = 0.6*ones(length(r));
plot(r,ArRatCirc,'b.')
plot(r,ArC,'r')
xlabel('aperture radius [m]')
ylabel('Area Aspect Ratio [-]')
hold off
```

Bibliography

- [1] N. Chidambaram, R. Kirchner, M. Altana, and H. Schiff, “High fidelity 3D thermal nanoimprint with UV curable polydimethyl siloxane stamps,” *Journal of Vacuum Science & Technology B, Nanotechnology and Microelectronics: Materials, Processing, Measurement, and Phenomena*, vol. 34, no. 6, p. 06K401, 11 2016. [Online]. Available: <http://dx.doi.org/10.1116/1.4961250>
- [2] M. Lewińska, J. van Dommelen, V. Kouznetsova, and M. Geers, “Towards acoustic metafoams: The enhanced performance of a poroelastic material with local resonators,” *Journal of the Mechanics and Physics of Solids*, vol. 124, pp. 189–205, 3 2019. [Online]. Available: <https://doi.org/10.1016/j.jmps.2018.10.006>
- [3] R. Zheng, Y. Chen, H. Chi, H. Qiu, H. Xue, and H. Bai, “3D Printing of a Polydimethylsiloxane/Polytetrafluoroethylene Composite Elastomer and its Application in a Triboelectric Nanogenerator,” *ACS Applied Materials and Interfaces*, vol. 12, no. 51, pp. 57441–57449, 12 2020. [Online]. Available: <https://pubs.acs.org/doi/10.1021/acsmi.0c18201>
- [4] S. Bhattacharya, A. Datta, J. Berg, and S. Gangopadhyay, “Studies on surface wettability of poly(dimethyl) siloxane (PDMS) and glass under oxygen-plasma treatment and correlation with bond strength,” *Journal of Microelectromechanical Systems*, vol. 14, no. 3, pp. 590–597, 6 2005. [Online]. Available: <http://ieeexplore.ieee.org/document/1438429/>
- [5] R. Durairaj, T. Nguty, and N. Ekere, “Critical factors affecting paste flow during the stencil printing of solder paste,” *Soldering & Surface Mount Technology*, vol. 13, no. 2, pp. 30–34, 8 2001. [Online]. Available: <https://www.emerald.com/insight/content/doi/10.1108/09540910110385239/full/html>
- [6] J. Pan, G. Tonkay, R. Storer, R. Sallade, and D. Leandri, “Critical Variables of Solder Paste Stencil Printing for Micro-BGA and Fine-Pitch QFP,” *IEEE Transactions on Electronics Packaging Manufacturing*, vol. 27, no. 2, pp. 125–132, 4 2004. [Online]. Available: <http://ieeexplore.ieee.org/document/1366496/>
- [7] C. Jin, C. Ma, Z. Yang, and H. Lin, “A force measurement method based on flexible PDMS grating,” *Applied Sciences (Switzerland)*, vol. 10, no. 7, 2020.
- [8] X. Zheng, H. Lee, T. H. Weisgraber, M. Shusteff, J. DeOtte, E. B. Duoss, J. D. Kuntz, M. M. Biener, Q. Ge, J. A. Jackson, S. O. Kucheyev, N. X. Fang, and C. M. Spadaccini, “Ultralight, ultrastiff mechanical metamaterials,” *Science*, vol. 344, no. 6190, pp. 1373–1377, 6 2014. [Online]. Available: <https://www.sciencemag.org/lookup/doi/10.1126/science.1252291>
- [9] T. Frenzel, M. Kadic, and M. Wegener, “Three-dimensional mechanical metamaterials with a twist,” *Science*, vol. 358, no. 6366, pp. 1072–1074, 11 2017. [Online]. Available: <https://www.sciencemag.org/lookup/doi/10.1126/science.aao4640>
- [10] S. C. L. Fischer, L. Hillen, and C. Eberl, “Mechanical Metamaterials on the Way from Laboratory Scale to Industrial Applications: Challenges for Characterization and Scalability,” *Materials*, vol. 13, no. 16, p. 3605, 8 2020. [Online]. Available: <https://www.mdpi.com/1996-1944/13/16/3605>
- [11] X. Ren, R. Das, P. Tran, T. D. Ngo, and Y. M. Xie, “Auxetic metamaterials and structures: a review,” *Smart Materials and Structures*, vol. 27, no. 2, p. 023001, 2 2018. [Online]. Available: <https://iopscience.iop.org/article/10.1088/1361-665X/aaa61c>
- [12] W. Wu, Z. Yu, S.-Y. Wang, R. S. Williams, Y. Liu, C. Sun, X. Zhang, E. Kim, Y. R. Shen, and N. X. Fang, “Midinfrared metamaterials fabricated by nanoimprint lithography,” *Applied Physics Letters*, vol. 90, no. 6, p. 063107, 2 2007. [Online]. Available: <http://aip.scitation.org/doi/10.1063/1.2450651>

- [13] I. Bergmair, B. Dastmalchi, M. Bergmair, A. Saeed, W. Hilber, G. Hesser, C. Helgert, E. Pshenay-Severin, T. Pertsch, E. B. Kley, U. Hübner, N. H. Shen, R. Penciu, M. Kafesaki, C. M. Soukoulis, K. Hingerl, M. Muehlberger, and R. Schoeftner, "Single and multilayer metamaterials fabricated by nanoimprint lithography," *Nanotechnology*, vol. 22, no. 32, 2011.
- [14] I. Bergmair, M. Mühlberger, K. Hingerl, E. Pshenay-Severin, T. Pertsch, E. B. Kley, H. Schmidt, and R. Schöftner, "3D materials made of gold using Nanoimprint Lithography," *Microelectronic Engineering*, vol. 87, no. 5-8, pp. 1008–1010, 5 2010. [Online]. Available: <http://dx.doi.org/10.1016/j.mee.2009.11.109>
- [15] L. M. Cox, A. M. Martinez, A. K. Blevins, N. Sowan, Y. Ding, and C. N. Bowman, "Nanoimprint lithography: Emergent materials and methods of actuation," *Nano Today*, vol. 31, p. 100838, 4 2020. [Online]. Available: <https://doi.org/10.1016/j.nantod.2019.100838>
- [16] C. C. H. Otte, "High Throughput Fabrication of Micromechanical Metamaterials - Literature Survey," Delft University of Technology, Delft, Tech. Rep., 2021.
- [17] J.-H. Lee, J. P. Singer, and E. L. Thomas, "Micro-/Nanostructured Mechanical Metamaterials," *Advanced Materials*, vol. 24, no. 36, pp. 4782–4810, 9 2012. [Online]. Available: <http://doi.wiley.com/10.1002/adma.201201644>
- [18] J. U. Surjadi, L. Gao, H. Du, X. Li, X. Xiong, N. X. Fang, and Y. Lu, "Mechanical Metamaterials and Their Engineering Applications," *Advanced Engineering Materials*, vol. 21, no. 3, p. 1800864, 3 2019. [Online]. Available: <https://onlinelibrary.wiley.com/doi/abs/10.1002/adem.201800864>
- [19] K. Bertoldi, V. Vitelli, J. Christensen, and M. van Hecke, "Flexible mechanical metamaterials," *Nature Reviews Materials*, vol. 2, no. 11, p. 17066, 11 2017. [Online]. Available: <http://www.nature.com/articles/natrevmats201766>
- [20] W. Wu, W. Hu, G. Qian, H. Liao, X. Xu, and F. Berto, "Mechanical design and multifunctional applications of chiral mechanical metamaterials: A review," *Materials & Design*, vol. 180, no. June, p. 107950, 10 2019. [Online]. Available: <https://doi.org/10.1016/j.matdes.2019.107950>
- [21] Z. Wang, C. Luan, G. Liao, J. Liu, X. Yao, and J. Fu, "Progress in Auxetic Mechanical Metamaterials: Structures, Characteristics, Manufacturing Methods, and Applications," *Advanced Engineering Materials*, vol. 22, no. 10, p. 2000312, 10 2020. [Online]. Available: <https://onlinelibrary.wiley.com/doi/10.1002/adem.202000312>
- [22] X. Yu, J. Zhou, H. Liang, Z. Jiang, and L. Wu, "Mechanical metamaterials associated with stiffness, rigidity and compressibility: A brief review," *Progress in Materials Science*, vol. 94, pp. 114–173, 5 2018. [Online]. Available: <https://doi.org/10.1016/j.pmatsci.2017.12.003>
- [23] E. Barchiesi, M. Spagnuolo, and L. Placidi, "Mechanical metamaterials: a state of the art," *Mathematics and Mechanics of Solids*, vol. 24, no. 1, pp. 212–234, 1 2019. [Online]. Available: <http://journals.sagepub.com/doi/10.1177/1081286517735695>
- [24] T. Frenzel, C. Findeisen, M. Kadic, P. Gumbsch, and M. Wegener, "Tailored Buckling Microlattices as Reusable Light-Weight Shock Absorbers," *Advanced Materials*, vol. 28, no. 28, pp. 5865–5870, 7 2016. [Online]. Available: <http://doi.wiley.com/10.1002/adma.201600610>
- [25] A. Rafsanjani, A. Akbarzadeh, and D. Pasini, "Snapping Mechanical Metamaterials under Tension," *Advanced Materials*, vol. 27, no. 39, pp. 5931–5935, 10 2015. [Online]. Available: <http://doi.wiley.com/10.1002/adma.201502809>
- [26] D. M. Kochmann and K. Bertoldi, "Exploiting Microstructural Instabilities in Solids and Structures: From Metamaterials to Structural Transitions," *Applied Mechanics Reviews*, vol. 69, no. 5, 9 2017. [Online]. Available: <https://asmedigitalcollection.asme.org/appliedmechanicsreviews/article/doi/10.1115/1.4037966/366831/Exploiting-Microstructural-Instabilities-in-Solids>
- [27] M. Kadic, T. Bückmann, N. Stenger, M. Thiel, and M. Wegener, "On the practicability of pentamode mechanical metamaterials," *Applied Physics Letters*, vol. 100, no. 19, p. 191901, 5 2012. [Online]. Available: <http://aip.scitation.org/doi/10.1063/1.4709436>

- [28] H. Schiff, "Nanoimprint lithography: An old story in modern times? A review," *Journal of Vacuum Science & Technology B: Microelectronics and Nanometer Structures*, vol. 26, no. 2, p. 458, 2008. [Online]. Available: <http://scitation.aip.org/content/avs/journal/jvstb/26/2/10.1116/1.2890972>
- [29] C. Thibault, C. Severac, E. Trévisiol, and C. Vieu, "Microtransfer molding of hydrophobic dendrimer," *Microelectronic Engineering*, vol. 83, no. 4-9 SPEC. ISS., pp. 1513–1516, 4 2006. [Online]. Available: <https://linkinghub.elsevier.com/retrieve/pii/S0167931706002334>
- [30] X.-m. Zhao, Y. Xia, and G. M. Whitesides, "Fabrication of three-dimensional micro-structures: Microtransfer molding," *Advanced Materials*, vol. 8, no. 10, pp. 837–840, 10 1996. [Online]. Available: <http://doi.wiley.com/10.1002/adma.19960081016>
- [31] M. E. Deagen, L. S. Schadler, and C. K. Ullal, "Wetting Regimes for Residual-Layer-Free Transfer Molding at Micro- and Nanoscales," *ACS Applied Materials & Interfaces*, vol. 9, no. 41, pp. 36 385–36 391, 10 2017. [Online]. Available: <https://pubs.acs.org/doi/10.1021/acsami.7b09402>
- [32] S. Y. Chou, P. R. Krauss, and P. J. Renstrom, "Imprint of sub-25 nm vias and trenches in polymers," *Applied Physics Letters*, vol. 67, no. 21, pp. 3114–3116, 11 1995. [Online]. Available: <http://aip.scitation.org/doi/10.1063/1.114851>
- [33] O. Sahin, M. Ashokkumar, and P. M. Ajayan, "Micro- and nanopatterning of biomaterial surfaces," in *Fundamental Biomaterials: Metals*. Elsevier, 2018, no. 1, pp. 67–78. [Online]. Available: <http://dx.doi.org/10.1016/B978-0-08-102205-4.00003-9>
- [34] E. P. Yalcintas, K. B. Ozutemiz, T. Cetinkaya, L. Dalloro, C. Majidi, and O. B. Ozdoganlar, "Soft Electronics Manufacturing Using Microcontact Printing," *Advanced Functional Materials*, vol. 29, no. 51, p. 1906551, 12 2019. [Online]. Available: <https://onlinelibrary.wiley.com/doi/abs/10.1002/adfm.201906551>
- [35] A. Alderson, J. Rasburn, S. Ameer-Beg, P. G. Mullarkey, W. Perrie, and K. E. Evans, "An auxetic filter: A tuneable filter displaying enhanced size selectivity or defouling properties," *Industrial and Engineering Chemistry Research*, vol. 39, no. 3, pp. 654–665, 2000.
- [36] N. Khader, S. W. Yoon, and D. Li, "Stencil Printing Optimization using a Hybrid of Support Vector Regression and Mixed-integer Linear Programming," *Procedia Manufacturing*, vol. 11, no. June, pp. 1809–1817, 2017. [Online]. Available: <https://linkinghub.elsevier.com/retrieve/pii/S2351978917305267>
- [37] R. W. Kay, S. Stoyanov, G. P. Glinski, C. Bailey, and M. P. Y. Desmulliez, "Ultra-fine pitch stencil printing for a low cost and low temperature flip-chip assembly process," *IEEE Transactions on Components and Packaging Technologies*, vol. 30, no. 2, pp. 359–359, 6 2007. [Online]. Available: <http://ieeexplore.ieee.org/document/4214943/>
- [38] V. Cadarso, G. Smolik, V. Auzelyte, L. Jacot-Descombes, and J. Brugger, "Heterogeneous material micro-transfer by ink-jet print assisted mould filling," *Microelectronic Engineering*, vol. 98, pp. 619–622, 10 2012. [Online]. Available: <http://dx.doi.org/10.1016/j.mee.2012.04.025>
- [39] B.-J. de Gans, P. C. Duineveld, and U. S. Schubert, "Inkjet Printing of Polymers: State of the Art and Future Developments," *Advanced Materials*, vol. 16, no. 3, pp. 203–213, 2 2004. [Online]. Available: <https://onlinelibrary.wiley.com/doi/10.1002/adma.200300385>
- [40] P. Sundriyal, M. Pandey, and S. Bhattacharya, "Plasma-assisted surface alteration of industrial polymers for improved adhesive bonding," *International Journal of Adhesion and Adhesives*, vol. 101, no. April, p. 102626, 9 2020. [Online]. Available: <https://doi.org/10.1016/j.ijadhadh.2020.102626>
- [41] S. Chou, "Optical Lithography," in *Nanofabrication Handbook*. CRC Press, 2 2012, vol. 106, no. 1, pp. 143–156. [Online]. Available: <https://www.taylorfrancis.com/books/9781420090536/chapters/10.1201/b11626-12>
- [42] B. J. Kim and E. Meng, "Review of polymer MEMS micromachining," *Journal of Micromechanics and Microengineering*, vol. 26, no. 013001, 2016.

- [43] J. J. Dumond and H. Yee Low, "Recent developments and design challenges in continuous roller micro- and nanoimprinting," *Journal of Vacuum Science & Technology B, Nanotechnology and Microelectronics: Materials, Processing, Measurement, and Phenomena*, vol. 30, no. 1, p. 010801, 1 2012. [Online]. Available: <http://avs.scitation.org/doi/10.1116/1.3661355>
- [44] P. Mariani, L. Vesce, and A. Di Carlo, "The role of printing techniques for large-area dye sensitized solar cells," *Semiconductor Science and Technology*, vol. 30, no. 10, p. 104003, 10 2015. [Online]. Available: <https://iopscience.iop.org/article/10.1088/0268-1242/30/10/104003>
- [45] T. Pang, T. S. Aye Chan, Y. A. C. Jande, and J. Shen, "Removal of fluoride from water using activated carbon fibres modified with zirconium by a drop-coating method," *Chemosphere*, vol. 255, p. 126950, 9 2020. [Online]. Available: <https://linkinghub.elsevier.com/retrieve/pii/S0045653520311437>
- [46] J.-H. Lee, C.-H. Kim, K.-M. Ho, and K. Constant, "Two-Polymer Microtransfer Molding for Highly Layered Microstructures," *Advanced Materials*, vol. 17, no. 20, pp. 2481–2485, 10 2005. [Online]. Available: <http://doi.wiley.com/10.1002/adma.200500721>
- [47] X. Ye, D. Cai, X. Ruan, and A. Cai, "Research on the selective adhesion characteristics of polydimethylsiloxane layer," *AIP Advances*, vol. 8, no. 9, p. 095004, 9 2018. [Online]. Available: <http://aip.scitation.org/doi/10.1063/1.5041867>
- [48] P.-C. Chen, R.-H. Zhang, and L.-T. Chen, "Using Micromachined Molds, Partial-curing PDMS Bonding Technique, and Multiple Casting to Create Hybrid Microfluidic Chip for Microlens Array," *Micromachines*, vol. 10, no. 9, p. 572, 8 2019. [Online]. Available: <https://www.mdpi.com/2072-666X/10/9/572>
- [49] M. Lewińska, J. van Dommelen, V. Kouznetsova, and M. Geers, "Broadening the attenuation range of acoustic metafoams through graded microstructures," *Journal of Sound and Vibration*, vol. 483, p. 115472, 9 2020. [Online]. Available: <https://linkinghub.elsevier.com/retrieve/pii/S0022460X20303047>
- [50] H. Schiff, "Nanoimprint lithography: 2D or not 2D? A review," *Applied Physics A*, vol. 121, no. 2, pp. 415–435, 11 2015. [Online]. Available: <http://dx.doi.org/10.1007/s00339-015-9106-3>
- [51] H. Schiff, J. Ahopelto, and N. Consortium, *Library of Processes*, 3rd ed. NaPANIL Consortium, 2008, no. March. [Online]. Available: <http://www.psi.ch/lmn/helmut-schiff>
- [52] J. Li, W. Wang, Y. Li, N. Zhou, G. Wang, Z. Kong, J. Fu, X. Yin, C. Li, X. Wang, H. Yang, X. Ma, J. Han, J. Zhang, Y. Wei, T. Hu, T. Yang, J. Li, H. Yin, H. Zhu, and H. H. Radamson, "Study of selective isotropic etching Si1-xGe_x in process of nanowire transistors," *Journal of Materials Science: Materials in Electronics*, vol. 31, no. 1, pp. 134–143, 1 2020. [Online]. Available: <http://link.springer.com/10.1007/s10854-019-02269-x>
- [53] C. N. LaFratta, T. Baldacchini, R. A. Farrer, J. T. Fourkas, M. C. Teich, B. E. A. Saleh, and M. J. Naughton, "Replication of Two-Photon-Polymerized Structures with Extremely High Aspect Ratios and Large Overhangs," *The Journal of Physical Chemistry B*, vol. 108, no. 31, pp. 11 256–11 258, 8 2004. [Online]. Available: <https://pubs.acs.org/doi/10.1021/jp048525r>
- [54] H. Wickström, R. Koppolu, E. Mäkilä, M. Toivakka, and N. Sandler, "Stencil Printing—A Novel Manufacturing Platform for Orodispersible Discs," *Pharmaceutics*, vol. 12, no. 1, p. 33, 1 2020. [Online]. Available: <https://www.mdpi.com/1999-4923/12/1/33>
- [55] T. A. Nguty and N. N. Ekere, "The rheological properties of solder and solar pastes and the effect on stencil printing," *Rheologica Acta*, vol. 39, no. 6, pp. 607–612, 11 2000. [Online]. Available: <http://link.springer.com/10.1007/s003970000117>
- [56] S. Mallik, N. Ekere, R. Durairaj, and A. Marks, "An investigation into the rheological properties of different lead-free solder pastes for surface mount applications," *Soldering & Surface Mount Technology*, vol. 20, no. 2, pp. 3–10, 4 2008. [Online]. Available: <https://www.emerald.com/insight/content/doi/10.1108/09540910810871511/full/html>

- [57] M. Desmulliez, R. Kay, E. Abraham, E. Gourcuff, G. Jackson, H. H. Steen, C. Liu, and P. Conway, "Sub-100 micron pitch stencil printing for wafer scale bumping," in *2005 Conference on High Density Microsystem Design and Packaging and Component Failure Analysis*. IEEE, 6 2005, pp. 1–7. [Online]. Available: <http://ieeexplore.ieee.org/document/4017419/>
- [58] R. Durairaj, G. Jackson, N. Ekere, G. Glinski, and C. Bailey, "Correlation of solder paste rheology with computational simulations of the stencil printing process," *Soldering & Surface Mount Technology*, vol. 14, no. 1, pp. 11–17, 4 2002. [Online]. Available: <https://www.emerald.com/insight/content/doi/10.1108/09540910210416422/full/html>
- [59] J. B. Hopkins and M. L. Culpepper, "Synthesis of multi-degree of freedom, parallel flexure system concepts via Freedom and Constraint Topology (FACT) – Part I: Principles," *Precision Engineering*, vol. 34, no. 2, pp. 259–270, 4 2010. [Online]. Available: <http://dx.doi.org/10.1016/j.precisioneng.2009.06.008><https://linkinghub.elsevier.com/retrieve/pii/S0141635909000920>
- [60] A. O. Olanrewaju, A. Robillard, M. Dagher, and D. Juncker, "Autonomous microfluidic capillary circuits replicated from 3D-printed molds," *Lab on a Chip*, vol. 16, no. 19, pp. 3804–3814, 2016. [Online]. Available: <http://xlink.rsc.org/?DOI=C6LC00764C>
- [61] M. P. Wolf, G. B. Salieb-Beugelaar, and P. Hunziker, "PDMS with designer functionalities—Properties, modifications strategies, and applications," *Progress in Polymer Science*, vol. 83, pp. 97–134, 2018. [Online]. Available: <https://doi.org/10.1016/j.progpolymsci.2018.06.001>
- [62] F. Schneider, J. Draheim, R. Kamberger, and U. Wallrabe, "Process and material properties of polydimethylsiloxane (PDMS) for Optical MEMS," *Sensors and Actuators A: Physical*, vol. 151, no. 2, pp. 95–99, 4 2009. [Online]. Available: <https://linkinghub.elsevier.com/retrieve/pii/S0924424709000466>
- [63] J. J. Dumond, K. A. Mahabadi, Y. S. Yee, C. Tan, J. Y. H. Fuh, H. P. Lee, and H. Y. Low, "High resolution UV roll-to-roll nanoimprinting of resin moulds and subsequent replication via thermal nanoimprint lithography," *Nanotechnology*, vol. 23, no. 48, p. 485310, 12 2012. [Online]. Available: <https://iopscience.iop.org/article/10.1088/0957-4484/23/48/485310>
- [64] R. Ji, M. Hornung, M. A. Verschuuren, R. van de Laar, J. van Eekelen, U. Plachetka, M. Moeller, and C. Moormann, "UV enhanced substrate conformal imprint lithography (UV-SCIL) technique for photonic crystals patterning in LED manufacturing," *Microelectronic Engineering*, vol. 87, no. 5-8, pp. 963–967, 5 2010. [Online]. Available: <http://dx.doi.org/10.1016/j.mee.2009.11.134>
- [65] A. A. S. Bhagat, P. Jothimuthu, and I. Papautsky, "Photodefinable polydimethylsiloxane (PDMS) for rapid lab-on-a-chip prototyping," *Lab on a Chip*, vol. 7, no. 9, p. 1192, 2007. [Online]. Available: <http://xlink.rsc.org/?DOI=b704946c>
- [66] R. Anastasio, W. Peerbooms, R. Cardinaels, and L. C. A. van Breemen, "Characterization of Ultraviolet-Cured Methacrylate Networks: From Photopolymerization to Ultimate Mechanical Properties," *Macromolecules*, vol. 52, no. 23, pp. 9220–9231, 12 2019. [Online]. Available: <https://pubs.acs.org/doi/10.1021/acs.macromol.9b01439>
- [67] A. Dobie, "Flexible PET Substrate for High-Definition Printing of Polymer Thick-Film Conductive Pastes," *Journal of Microelectronics and Electronic Packaging*, vol. 16, no. 2, pp. 103–116, 4 2019. [Online]. Available: <http://meridian.allenpress.com/jmep/article/16/2/103/420338/Flexible-PET-Substrate-for-HighDefinition-Printing>
- [68] T. N. Tsai, "Modeling and optimization of stencil printing operations: A comparison study," *Computers and Industrial Engineering*, vol. 54, no. 3, pp. 374–389, 2008.
- [69] N. N. Ekere and M. A. Currie, "for SMT assembly," *Journal of Materials Science*, vol. 6, no. Materials in electronics, pp. 34–42, 1995.
- [70] A. Pietrikova and M. Kravcik, "Boundary value of rheological properties of solder paste," in *Proceedings of the 2011 34th International Spring Seminar on Electronics Technology (ISSE)*. IEEE, 5 2011, pp. 94–97. [Online]. Available: <http://ieeexplore.ieee.org/document/6053557/>

- [71] The Dow Company Chemical., "SYLGARD™ 184 Silicone Elastomer Technical Datasheet," pp. 1–4, 2017. [Online]. Available: <https://consumer.dow.com/en-us/document-viewer.html?randomVar=3835418757322904567&docPath=/documents/en-us/productdatasheet/11/11-31/11-3184-sylgard-184-elastomer.pdf>
- [72] M. A. Eddings, M. A. Johnson, and B. K. Gale, "Determining the optimal PDMS–PDMS bonding technique for microfluidic devices," *Journal of Micromechanics and Microengineering*, vol. 18, no. 6, p. 067001, 6 2008. [Online]. Available: <https://iopscience.iop.org/article/10.1088/0960-1317/18/6/067001>
- [73] D. Helmer, A. Voigt, S. Wagner, N. Keller, K. Sachsenheimer, F. Kotz, T. M. Nargang, and B. E. Rapp, "Suspended Liquid Subtractive Lithography: One-step generation of 3D channel geometries in viscous curable polymer matrices," *Scientific Reports*, vol. 7, no. 1, p. 7387, 12 2017. [Online]. Available: <http://www.nature.com/articles/s41598-017-07630-w>
- [74] R. Ariati, F. Sales, A. Souza, R. A. Lima, and J. Ribeiro, "Polydimethylsiloxane Composites Characterization and Its Applications: A Review," *Polymers*, vol. 13, no. 23, p. 4258, 12 2021. [Online]. Available: <https://www.mdpi.com/2073-4360/13/23/4258>
- [75] J. Lv, Z. Gong, Z. He, J. Yang, Y. Chen, C. Tang, Y. Liu, M. Fan, and W.-M. Lau, "3D printing of a mechanically durable superhydrophobic porous membrane for oil–water separation," *Journal of Materials Chemistry A*, vol. 5, no. 24, pp. 12435–12444, 2017. [Online]. Available: <http://xlink.rsc.org/?DOI=C7TA02202F>
- [76] L. Wu, J. Qian, J. Peng, K. Wang, Z. Liu, T. Ma, Y. Zhou, G. Wang, and S. Ye, "Screen-printed flexible temperature sensor based on FG/CNT/PDMS composite with constant TCR," *Journal of Materials Science: Materials in Electronics*, vol. 30, no. 10, pp. 9593–9601, 5 2019. [Online]. Available: <https://doi.org/10.1007/s10854-019-01293-1>
- [77] J. Suriboot, A. C. Marmo, B. K. D. Ngo, A. Nigam, D. Ortiz-Acosta, B. L. Tai, and M. A. Grunlan, "Amphiphilic, thixotropic additives for extrusion-based 3D printing of silica-reinforced silicone," *Soft Matter*, vol. 17, no. 15, pp. 4133–4142, 2021. [Online]. Available: <https://pubs.rsc.org/en/content/articlehtml/2021/sm/d1sm00288k#cit18http://xlink.rsc.org/?DOI=D1SM00288K>
- [78] J. A. Smith, S. Li, E. Mele, A. Goulas, D. Engstrøm, and V. V. Silberschmidt, "Printability and mechanical performance of biomedical PDMS-PEEK composites developed for material extrusion," *Journal of the Mechanical Behavior of Biomedical Materials*, vol. 115, no. October 2020, p. 104291, 3 2021. [Online]. Available: <https://linkinghub.elsevier.com/retrieve/pii/S1751616120308274>
- [79] S. Roh, D. P. Parekh, B. Bharti, S. D. Stoyanov, and O. D. Velev, "3D Printing by Multiphase Silicone/Water Capillary Inks," *Advanced Materials*, vol. 29, no. 30, p. 1701554, 8 2017. [Online]. Available: <https://onlinelibrary.wiley.com/doi/10.1002/adma.201701554>
- [80] A. Carré and F. Eustache, "Spreading Kinetics of Shear-Thinning Fluids in Wetting and Dewetting Modes," *Langmuir*, vol. 16, no. 6, pp. 2936–2941, 3 2000. [Online]. Available: <https://pubs.acs.org/doi/10.1021/la991021d>
- [81] R. Ziegelbaur and J. Caruthers, "Rheological properties of poly(dimethylsiloxane) filled with fumed silica: I. Hysteresis behaviour," *Journal of Non-Newtonian Fluid Mechanics*, vol. 17, no. 1, pp. 45–68, 1 1985. [Online]. Available: <https://linkinghub.elsevier.com/retrieve/pii/0377025785800057>
- [82] H. Kim, H.-G. Kim, S. Kim, and S. S. Kim, "PDMS–silica composite membranes with silane coupling for propylene separation," *Journal of Membrane Science*, vol. 344, no. 1-2, pp. 211–218, 11 2009. [Online]. Available: <https://linkinghub.elsevier.com/retrieve/pii/S0376738809005882>
- [83] T. Ma, R. Yang, Z. Zheng, and Y. Song, "Rheology of fumed silica/polydimethylsiloxane suspensions," *Journal of Rheology*, vol. 61, no. 2, pp. 205–215, 3 2017. [Online]. Available: <http://dx.doi.org/10.1122/1.4973974http://aip.scitation.org/doi/10.1122/1.4973974>
- [84] A. M. Kansara, P. K. Prajapati, V. K. Aswal, and P. S. Singh, "Structure-property interplay of asymmetric membranes comprising of soft polydimethylsiloxane chains and hard silica nanomaterials," *Polymer*, vol. 160, no. July 2018, pp. 30–42, 1 2019. [Online]. Available: <https://linkinghub.elsevier.com/retrieve/pii/S003238611831067X>

- [85] X. Xu, C. Gao, and Q. Zheng, "Rheological characterization of room temperature vulcanized silicone sealant: Effect of filler particle size," *Polymer Engineering & Science*, vol. 48, no. 4, pp. 656–661, 4 2008. [Online]. Available: <https://onlinelibrary.wiley.com/doi/10.1002/pen.20992>
- [86] Dow, "SYLGARD™ 186 Silicone Elastomer Technical Data Sheet," pp. 1–5, 2021. [Online]. Available: <https://www.dow.com/pt-br/document-viewer.html?randomVar=6785447089567248209&docPath=/content/dam/dcc/documents/en-us/productdatasheet/11/11-12/11-1253-sylgard-186-silicone-elastomer.pdf%5CSI>
- [87] J. Stieghorst, D. Majaura, H. Wevering, and T. Doll, "Toward 3D Printing of Medical Implants: Reduced Lateral Droplet Spreading of Silicone Rubber under Intense IR Curing," *ACS Applied Materials & Interfaces*, vol. 8, no. 12, pp. 8239–8246, 3 2016. [Online]. Available: <https://pubs.acs.org/doi/10.1021/acsami.5b12728>
- [88] C. Gonçalves, H. Leitão, C. S. Lau, J. C. Teixeira, L. Ribas, S. Teixeira, M. F. Cerqueira, F. Macedo, and D. Soares, "Wetting behaviour of SAC305 solder on different substrates in high vacuum and inert atmosphere," *Journal of Materials Science: Materials in Electronics*, vol. 26, no. 7, pp. 5106–5112, 7 2015. [Online]. Available: <http://link.springer.com/10.1007/s10854-015-3037-9>
- [89] T. Trantidou, Y. Elani, E. Parsons, and O. Ces, "Hydrophilic surface modification of PDMS for droplet microfluidics using a simple, quick, and robust method via PVA deposition," *Microsystems & Nanoengineering*, vol. 3, no. 1, p. 16091, 12 2017. [Online]. Available: <http://www.nature.com/articles/micronano201691>
- [90] V. Thakur, S. Mallik, and V. Vuppala, "CFD Simulation of Solder Paste Flow and Deformation Behaviours during Stencil Printing Process," *International Journal of Recent advances in Mechanical Engineering*, vol. 4, no. 1, pp. 1–13, 2 2015. [Online]. Available: <http://www.wireilla.com/engg/ijmech/papers/4115ijmech01.pdf>
- [91] L. Kosinski and J. Caruthers, "Rheological properties of poly(dimethylsiloxane) filled with fumed silica: II. Stress relaxation and stress growth," *Journal of Non-Newtonian Fluid Mechanics*, vol. 17, no. 1, pp. 69–89, 1 1985. [Online]. Available: <https://linkinghub.elsevier.com/retrieve/pii/0377025785800069>
- [92] D. Manassis, R. Patzelt, and A. Ostmann, "Stencil printing technology for 100 μ m flip chip bumping," *Global SMT and Packaging*, vol. 4, no. 2, pp. 10–14, 2004.
- [93] E. Amalu, N. Ekere, and S. Mallik, "Evaluation of rheological properties of lead-free solder pastes and their relationship with transfer efficiency during stencil printing process," *Materials & Design*, vol. 32, no. 6, pp. 3189–3197, 6 2011. [Online]. Available: <https://linkinghub.elsevier.com/retrieve/pii/S0261306911001245>
- [94] K. Haubert, T. Drier, and D. Beebe, "PDMS bonding by means of a portable, low-cost corona system," *Lab on a Chip*, vol. 6, no. 12, p. 1548, 2006. [Online]. Available: <http://xlink.rsc.org/?DOI=b610567j>
- [95] K. T. L. Trinh and N. Y. Lee, "Fabrication of Wearable PDMS Device for Rapid Detection of Nucleic Acids via Recombinase Polymerase Amplification Operated by Human Body Heat," *Biosensors*, vol. 12, no. 2, p. 72, 1 2022. [Online]. Available: <https://www.mdpi.com/2079-6374/12/2/72>
- [96] P. Soman, J. W. Lee, A. Phadke, S. Varghese, and S. Chen, "Spatial tuning of negative and positive Poisson's ratio in a multi-layer scaffold," *Acta Biomaterialia*, vol. 8, no. 7, pp. 2587–2594, 7 2012. [Online]. Available: <http://dx.doi.org/10.1016/j.actbio.2012.03.035>
- [97] J. Matthews, T. Klatt, C. Morris, C. C. Seepersad, M. Haberman, and D. Shahan, "Hierarchical Design of Negative Stiffness Metamaterials Using a Bayesian Network Classifier1," *Journal of Mechanical Design*, vol. 138, no. 4, pp. 1–12, 4 2016. [Online]. Available: <https://asmedigitalcollection.asme.org/mechanicaldesign/article/doi/10.1115/1.4032774/474837/Hierarchical-Design-of-Negative-Stiffness>
- [98] H. Yang and L. Ma, "Multi-stable mechanical metamaterials by elastic buckling instability," *Journal of Materials Science*, vol. 54, no. 4, pp. 3509–3526, 2 2019. [Online]. Available: <http://link.springer.com/10.1007/s10853-018-3065-y>

-
- [99] Y. Pennec, B. Djafari-Rouhani, H. Larabi, J. Vasseur, and A.-C. Hladky-Hennion, "Phononic crystals and manipulation of sound," *physica status solidi (c)*, vol. 6, no. 9, pp. 2080–2085, 9 2009. [Online]. Available: <http://doi.wiley.com/10.1002/pssc.200881760>